2842-9-T

THE UNIVERSITY OF MICHIGAN

COLLEGE OF LITERATURE, SCIENCE, AND THE ARTS

DEPARTMENT OF PHYSICS

*Technical Report*

# *Theory of (d,p) Reactions*

C. R LUBITZ

*Under Contract With:*

U. S Atomic Energy Commission
Chicago Operations Office
Contract No AT(11-1)-275
Lemont, Illinois

*Administered by:*

*June 1960*

THE UNIVERSITY OF MICHIGAN RESEARCH INSTITUTE • ANN ARBOR

THE UNIVERSITY OF MICHIGAN
COLLEGE OF LITERATURE, SCIENCE, AND THE ARTS
Department of Physics

Technical Report

# THEORY OF (d,p) REACTIONS

C. R. Lubitz

UMRI Project 2842

under contract with:

U. S. ATOMIC ENERGY COMMISSION
CHICAGO OPERATIONS OFFICE
CONTRACT NO. AT(11-1)-275
LEMONT, ILLINOIS

administered by:

THE UNIVERSITY OF MICHIGAN RESEARCH INSTITUTE ANN ARBOR

June 1960

This report has also been submitted as a dissertation in partial fulfillment of the requirements for the degree of Doctor of Philosophy in The University of Michigan, 1960.

TABLE OF CONTENTS

APPENDIX Page

LIST OF FIGURES

ABSTRACT

The differential cross section for the deuteron stripping reaction to a particular state in the residual nucleus (target plus captured neutron) is evaluated subject to the following approximations:

1. The interaction between the outgoing proton and the residual nucleus is divided into a central, non-spin-dependent potential $V_{np}$ between the proton and the neutron in the incident deuteron, plus an optical potential $V_{tp}$ between the proton and the target nucleus. Both potentials are treated as source terms in the transition matrix element.

2. The exact wave function is approximated by a modified plane (incident) wave. The modification consists of phenomenological cutoff functions which decrease the amplitude of the wave when either the neutron or the proton approaches the nucleus. This attenuation represents absorption in the sense of the optical model.

Compared to the Butler theory, the present work involves three principal differences:

1. If the Butler cutoff is regarded as absorption of the incident wave then additional proton-induced absorption has been added.

2. The radius at which the incident wave falls to half its asymptotic intensity (the cutoff radius) is regarded as an adjustable parameter, essentially independent of the nuclear radius.

3. The interaction between the proton and the target nucleus is taken into account. Because it is treated as a source term in the matrix element, and scattering or refraction of the incident wave is neglected, the complexity of the distorted wave treatment is avoided.

As a result of the above three points, certain features of the stripping reaction seem more physically reasonable than hitherto:

1. By allowing the cutoff radius to vary with energy, the angular distribution can in principle be fitted with an energy-independent nuclear radius and reduced width. (On the other hand, when the Butler radius is chosen to fit a particular stripping peak at different energies, its value generally varies, so that it is effectively energy-dependent, and causes a similar energy-dependence of the reduced width.)

2. By divorcing the nuclear radius from the larger cutoff radii, the former's value is reduced from that required by the Butler theory. A second factor tending in the same direction is the removal of the inner proton region by the additional cutoff. In the Butler theory, this region pushes the stripping peak to large angles, and bringing it forward requires a fictitious enhancement of the neutron cutoff radius.

3. The proton cutoff reduces the single-particle cross section by an order-of-magnitude, with a corresponding increase of the reduced width relative to the Butler theory value. Because the modified matrix element is roughly proportional to Butler's, the reduced width ratios are not drastically affected.

4. Quantitatively reasonable results are obtained by including as a source term an optical potential interaction between the target nucleus and the stripped proton. A similar procedure in the Butler theory leads to incorrect results, because the proton "overlaps" too strongly with this potential. The imaginary part of the potential produces qualitatively new results, eliminating the nodes in the Butler angular distribution, and causing a polarization of the outgoing proton. Of special interest is the prediction of a correlation between the capture j-value and the sign of the polarization, the latter being in agreement with experiment.

The same formalism is applied to the deuteron elastic scattering reaction, and it is shown how a (d,d) analysis can in principle determine the cutoff radii, so that the (d,p) parameters are essentially specified in advance. The practical application of this procedure is however hampered by a lack of uniqueness in the shapes of the cutoff functions and in the absorptive potential representing deuteron dissociation. [The proton-nucleus potential, itself not unique, is supposed for simplicity to be determined by the (p,p) reaction].

# CHAPTER I

# INTRODUCTION

## A. SUMMARY AND RESULTS OF THE PRESENT WORK

From the standpoint of nuclear spectroscopy, deuteron stripping theories fall roughly into two classes: plane wave theories and distorted wave theories. The former, in particular the theories of Butler (1) and Bhatia, et al.,(2), have served as the basis for the analysis of a great number of nuclear levels, although they possess some puzzling features. Generalizations of the plane wave theories have invariably been in the direction of adding scattered or distorted waves to the ingoing and outgoing plane waves, a technique which greatly complicates the formalism (3).

In the present work an approach is adopted which retains the essential simplicity of the plane wave theories, while minimizing certain of their difficulties. Following a suggestion by Francis and Watson (4), the neutron cutoff in the Butler theory, as formulated by Daitch and French (5), is regarded as an absorption of the incident wave. From this, two consequences are then drawn:

1. Absorption must be induced also by the approach of the proton to the nucleus, i.e., a proton cutoff must occur.

2. It is not correct to identify the nuclear radius (an energy-

independent size parameter) with the cutoff radius. The latter measures the extent of penetration of the incident wave into the nucleus and can reasonably be expected to decrease as the incident energy increases.

Both of these points can be readily included in a plane wave theory, distortion and scattering of the incident and outgoing waves not being essential to their description. Accordingly, in the present work the differential cross section for stripping to a particular final state is evaluated subject to the following approximations:

1. The interaction between the outgoing proton and the residual nucleus is divided into a central, non-spin-dependent potential $V_{np}$ between the proton and the neutron in the incident deuteron, plus an optical potential $V_{tp}$ between the proton and the target nucleus. Both potentials are treated as source terms in the transition matrix element. Compound nucleus processes (6), exchange reactions (7), and heavy particle stripping (8) are neglected.

2. The exact wave function is approximated by a modified plane (incident) wave. The modification consists of phenomenological cutoff functions which decrease the amplitude of the wave when either the neutron or the proton approaches the nucleus. This attenuation represents absorption in the sense of the optical model, due to excitation of the target nucleus, and in the present case, also dissociation of the incident deuterons.

Compared to the Butler theory (1,5), the present work involves three principal differences:

1. If the Butler cutoff is regarded as absorption of the incident wave when the neutron reaches the nuclear surface (4), then additional proton-induced absorption has been added.

2. The radius at which the incident wave falls to half its asymptotic intensity (the cutoff radius) is regarded as an adjustable parameter, essentially independent of the nuclear radius.

3. The interaction between the proton and the target nucleus is taken into account. Because it is treated as a source term in the matrix element, and scattering and distortion of the incident wave is neglected, the complexity of the distorted wave treatment (3) is avoided.

As a result of the above three points, certain features of the stripping reaction seem more physically reasonable than hitherto:

1. By allowing the cutoff radius to vary with energy, the angular distribution can in principle be fitted with an energy-independent nuclear radius and reduced width. (On the other hand, when the Butler radius is chosen to fit a particular stripping peak at different energies, its value generally varies, so that it is effectively energy-dependent, and causes a similar energy-dependence of the reduced width.)

2. The peculiarly large size of the Butler radius is in part explained by its hybrid nature—a cross between a true nuclear radius and an absorption or cutoff radius, the latter being quite large at low energies ($\lesssim$ 10 Mev). As a corollary, it follows that the Butler radius

is not intrinsically large, but will tend to a small value at high energy.

A second factor tending to fictitiously enlarge the Butler radius is the tendency of stripping from small radial distances, $r_n$ or $r_p$, to peak at large angles and vice-versa. By removing the interior proton region, the present theory moves the peak forward so that this effect need not be accomplished, as in the Butler theory, by a fictitous enlargement of the neutron cutoff radius.

3. Elimination of the interior proton region reduces the low-energy single-particle cross section by roughly a factor of ten. (This refers to the neutron-proton interaction term which occurs in the Butler theory.) As a result, the neutron reduced widths fall in the intermediate coupling theory range instead of having the puzzlingly small values predicted by the Butler theory (9,10). Since the size of the cross section is roughly proportional to the square of the volume of configuration space over which the transition amplitude is non-negligible, and the same region is removed in the matrix elements leading to different levels in the same nucleus, the reduced width ratios will not be drastically affected. In principle, however, their presumably incorrect energy-dependence is eliminated.

4. Elimination of the interior proton region permits a simple evaluation of the transition amplitude resulting from the interaction of the proton with the target nucleus. If this interaction is approximated by an optical potential (assumed the same as that operative in

(p,p) reactions), and inserted into the Butler matrix element as a source term, it results in an amplitude larger than the n-p interaction term (11). This is paradoxical in view of the fact that it is neglected as small in the Butler theory. The proton cutoff, which produces the afore-mentioned order-of-magnitude reduction in the n-p interaction term, reduces the optical potential terms even more drastically so that they become more nearly "correction terms" to the main n-p interaction. This unequal reduction in size results from the relatively good overlap between the excised region at small $r_p$ and the proton optical potential, as compared to this region's overlap with the n-p potential, the latter being strongest along the "diagonal" region $\vec{R}_n \approx \vec{R}_p$.

This possibility, of evaluating the nuclear contribution as a source term, rather than in the guise of a distorted outgoing wave, makes the present formulation much simpler than the distorted wave treatment.

The result of including a real nuclear potential and a Coulomb repulsion, which interfere with the real n-p potential, is mainly to change the height of the stripping peak. The extent of this effect is sensitive to the amount of cancellation between the attractive nuclear and repulsive Coulomb potentials. With present-day diffuse wells, this cancellation tends to be rather complete, the usual Coulomb barrier estimate, $Z/A^{\frac{1}{3}}$ Mev, being a considerable overestimate for light nuclei.

On the other hand, the imaginary (absorptive) component of the optical potential produces qualitatively new results. Being incoherent

with the real amplitudes, it provides a "background" to the angular distribution and eliminates the nodes which are characteristic of the Butler theory. More importantly, it provides a non-zero polarization of the emitted protons. A result of special interest is the fact that for $\ell$=1 capture, a correlation is predicted between the value of $j=\ell\pm\frac{1}{2}$, and the sign of the polarization. Such a correlation is suggested by the experimental data (12) but has not been successfully explained by the distorted wave theories. The cases of capture with $\ell$ greater than one are a little more complicated and the question of a correlation must await further numerical work with the present theory. (The semi-classical arguments (13) which originally predicted such a correlation make no distinction between different $\ell$-values, but it is not certain that they can be trusted in this respect.)

B. PARAMETER DETERMINATION IN THE PRESENT THEORY

If the view is taken that the n-p interaction and the proton optical potential are known quantities, then the unknown parameters in the (d,p) reaction are the cutoff radii and the nuclear radius. However, it can be shown (Chapter 5) that precisely the same formalism must apply to the deuteron elastic scattering reaction, in which only the cutoff parameters are unknown. The (d,d) reaction therefore in principle determines these parameters, leaving only the nuclear radius adjustable in the (d,p) reaction. Indeed, since the nuclear radius is energy-independent, its determination at any energy reduces the (d,p) analysis at any other energy (where (d,d) results are available) to a completely predictive

procedure (within the framework of the present method).

The principal difficulty in realizing this program is the uniqueness question. Just as in phase-shift analyses of nucleon-nucleus scattering the optical potentials are not uniquely defined, so in the present case it is not possible to completely fix the shape of the cutoff functions (for a set of assumed potentials). In addition, the absorptive potential which represents the effects of deuteron dissociation is unknown. One might hope that the deuteron-induced reactions will eventually provide another set of conditions to be met by the optical potentials, but the theoretical and experimental accuracy will need improvement for this goal to be realized.

## C. PHYSICAL INTERPRETATION OF DEUTERON-INDUCED DIRECT REACTIONS

The fact that introducing the physically reasonable proton absorption, and recognizing the distinction between the nuclear radius and the cutoff radius remedies many of the previous difficulties with plane wave theories leads to the following picture of deuteron-induced direct reactions:

Because of specifically nuclear absorption (target nucleus excitation) and deuteron dissociation (projectile excitation), the projection of the total wave function onto the product of the target and deuteron ground states (the elastic component of the total wave function) exhibits very strong absorption. The success of the plane wave approximation, however, suggests that this absorption can occur without entirely

distorting the incident wave. The simplest explanation of this is that a strong interaction, which would distort the wave function of a tightly bound particle, succeeds mainly in breaking up the easily dissociated deuteron, so that the distortion is transmuted into an apparent absorption. Plane wave theories, which can give a reasonable account of absorption while completely ignoring distortion and scattering, can therefore succeed despite the fact that perturbation theory is not applicable.

Essential to this interpretation is the assumption that, once the target nucleus has been excited (4) or the deuteron dissociated, the (d,d) and (d,p) reactions will be strongly inhibited, and this is very reasonable.

It is probable that the inner regions which are "cut off" in the present formulation contribute primarily a large-angle component to the (d,d) and (d,p) reactions. The plane wave theories handle accurately only those events involving deuterons moving directly forward. The elastically scattered deuterons, which are largely moving in other directions, will provide back-angle scattering and stripping, and this is the principal improvement obtainable by including (as in distorted wave theories) elastically scattered deuterons in the approximation to the exact wave function. An important point however, is that a plane wave theory, even though valid only at forward angles, is adequate for the purposes of nuclear spectroscopy.

D. TECHNIQUE OF EVALUATING THE TRANSITION AMPLITUDES

Concerning the actual evaluation of the transition matrix elements, the handling of the n-p interaction term is not very different from the method employed by Daitch and French (5). In fact, by a suitable approximation, (3.26) and (3.27), the results can be evaluated with the help of the tabulated Butler cross section (14), avoiding the explicit handling of spherical Bessel functions.

The proton optical potential terms are more difficult, but relatively simple closed formulas are still obtained. The essential point in splitting the original six-dimensional integral (in $\vec{R}_n$ and $\vec{R}_p$) is the observation that the proton coordinate is a relative coordinate with respect to the neutron coordinate and the n-p separation, i.e., $\vec{R}_p=\vec{R}_n-\vec{R}_{np}$. If the dependence of the integrand on $\vec{R}_n$ and $\vec{R}_{np}$ is expressed (as is possible) in terms of harmonic oscillator eigenfunctions, then a "center-of-mass" transformation in $\vec{R}_n$ and $\vec{R}_{np}$ succeeds in splitting the integral into simple three-dimensional ones. Since the oscillator frequencies are unequal, this requires a generalization of the transformation originally employed by Talmi (15) in a different context. However, as in Talmi's application, the result is a short sum of terms rather than the infinite series which results from expanding the proton potential or the deuteron wave function (16).

# CHAPTER II

## DISCUSSION

The purpose of this chapter is to discuss qualitatively certain points concerning the interpretation of plane wave theories. The element which these topics have in common is the localization of the stripping process in the surface region of the nucleus.

### A. TRANSITION MATRIX ELEMENTS FOR THE PLANE WAVE THEORIES (1,2,5)

The (d,p) cross sections predicted by these theories are derivable from matrix elements exhibiting a close similarity in structure. Neglecting the proton-target interaction, they are:

(a) Butler (1):

$$M_{BU} = \langle \vec{K}_p ; \ell m \,|\, V_{np} \,|\, \phi_d \; H(r_n - r_{BU}) \rangle \qquad (2.1)$$

(b) Bhatia, et al. (2):

$$M_{BH} = \langle \vec{K}_p ; \ell m \,|\, V_{np} \,|\, \phi_d \; \delta(r_n - r_{BH}) \rangle \qquad (2.2)$$

(c) Born approximation (5):

$$M_{BO} = \langle \vec{K}_p ; \ell m \,|\, V_{np} \,|\, \phi_d \rangle \qquad (2.3)$$

The various symbols are:

$\delta(x)$ = Dirac delta function.

$H(x)$ = Heaviside step function.

$|K_p\rangle$ = an outgoing proton plane wave.

$|\ell,m\rangle$ = the component of the captured neutron's wave function with angular momentum $\ell$, z-projection m.

$V_{np}$ = the neutron-proton interaction.

$|\phi_d\rangle$ = an incident plane wave of deuterons.

These expressions differ in appearance from the forms originally given. The equivalence of (2.1) to Butler's method has been shown in (4,5,17) among others. The use in (2,5) of the neutron-target interaction $V_{tn}$ involves the post-prior ambiguity or equivalence (18, p.233). In Born approximation the (prior) deuteron-target interaction $V_{tn}+V_{tp}$ is equivalent to the (post) proton-residual nucleus interaction $V_{np}$ + $V_{tp}$. Since $V_{tp}$ is neglected, $V_{tn}$ and $V_{np}$ are interchangeable in Born approximation.

The distinguishing feature of these matrix elements is the real function which modulates the incident plane wave, H, δ, and 1 (one), respectively. Since in these integrals regions of small $r_n$ or $r_p$ contribute most heavily to stripping at large angles (and vice-versa), it is a simple matter to understand certain regularities in their behavior.

## B. LOCALIZATION OF THE STRIPPING PROCESS IN THE PLANE WAVE THEORIES AND ITS INFLUENCE ON STRIPPING RADII AND REDUCED WIDTHS

In the Butler matrix element (2.1) the reaction is confined to $r_n > r_{Bu}$ and the proton integration is unrestricted. For given $r_{Bu}$, the peak in the angular distribution occurs at some angle $\vartheta_{Bu}$ with a height

$\sigma_{Bu}$ that implies a reduced width $\theta^2_{Bu}$. (Throughout this section $\sigma$ will mean the intrinsic or single-particle cross section which must be multiplied by the reduced width to give the actual cross section.)

In the Bhatia, et al., version (2.2), the proton integration is still unrestricted but the neutron integration is confined to the surface $r_n = r_{Bh}$. The interior is therefore eliminated as in (2.1) but the exterior is also. If $r_{Bh}=r_{Bu}$, this means a relative weakening of the large $r_n$ contributions and a reduction in the small-angle stripping. As a result the peak angle is at $\vartheta_{Bh}>\vartheta_{Bu}$. It can be brought into coincidence with $\vartheta_{Bu}$ by taking $r_{Bh}>r_{Bu}$.

In the Born approximation (2.3) there are no restrictions at all. However, the largersize of the neutron wave function inside the nuclear radius $r_{Bo}$ than outside weights the integrand to small $r_n$ compared with (2.2). This throws the peak out so that if $r_{Bo}=r_{Bh}$, $\vartheta_{Bo}>\vartheta_{Bh}$. To bring them into coincidence requires $r_{Bo}> r_{Bh}$. Relative to the Butler theory, there is a contribution to the peak height from $r_n < r_{Bu}$ which increases $\sigma_{Bo}$ over $\sigma_{Bu}$ with the result that $\theta^2_{Bo}< \theta^2_{Bu}$. This explains the regularities (assuming peak locations and heights equalized):

$$r_{BO} > r_{BH} > r_{BU} \tag{2.4}$$

$$\theta^2_{BO} < \theta^2_{BU} \tag{2.5}$$

Since $r_{Bu}$ is larger than conventional radii at low energy while $\theta^2_{Bu}$ is too small, the necessary modification is clear. To increase $\theta^2$

above $\theta^2_{Bu}$ (i.e., reduce $\sigma_{Bu}$) the integration in (2.1) must be further restricted. If at the same time $r_{Bu}$ is to be reduced, the interior (small $r_n$ or $r_p$) contribution must be reduced more than the exterior (large $r_n$ or $r_p$) one. Interpreting the Butler cutoff as absorption due to neutron-induced excitation of the target nucleus implies the necessity for a proton cutoff at small $r_p$ and this is precisely what is needed.

This "optical" interpretation of the Butler cutoff seems first to have been suggested by Francis and Watson (4), their equation (20). The absorption is the same as that encountered in optical model analyses of elastic nucleon scattering where only the projection of the total wave function on the target ground state is considered. Target excitation then appears as absorption of this incomplete wave function by the optical potential. For deuteron scattering the projection is onto the target ground state and the deuteron ground state. In addition to target excitation there occurs deuteron dissociation, so that the deuteron absorptive potential will not be merely the sum of the nucleon optical potentials.

Indeed, this "extra" absorption representing deuteron breakup would appear to play a role in understanding the accuracy of the plane wave stripping theories. Compared to elastic nucleon scattering, the deuteron scattering results (Chapter 5, Section E), exhibit considerably more absorption and a better fit to experiment. These effects are consistent with the view that the interactions which distort the incident

nucleon wave function and spoil the agreement with the plane wave theory, will to a large extent merely dissociate the deuteron and therefore appear, not as distortion but as absorption, which can be handled rather simply. It is necessary that the broken up deuterons not contribute appreciably to either the (d,d) or (d,p) reactions and this is quite plausible (4).

C. A W.K.B.-TYPE OF APPROXIMATION

Although the present work employs only phenomenological cutoff functions which are spherically symmetric in $r_n$ and $r_p$, it is illuminating to consider the form which these functions might take in a more exact theory. The following approximate treatment exhibits a number of interesting features which are duplicated by the cutoff functions of the present work (independent, real cutoffs in $r_n$ and $r_p$, approximately related to the nucleon scattering results at half the deuteron energy). The main feature not duplicated is the shadow region behind the nucleus.

As the previous discussion has indicated, the plane wave theories are characterized by the following approximation to the exact wave function,

$$\psi \approx f \phi \tag{2.6}$$

where $\phi$ is the incident wave, and f is a real function. A similar approximation is well-known for the nucleon scattering case (19), namely,

$$\psi \approx e^{ikz} \exp\left\{-\frac{i}{\hbar v}\int_{-\infty}^{z} V(x,y,z')\,dz'\right\} \tag{2.7}$$

While this expression is derivable as an approximate solution to the Schrödinger equation, a closely related one can be obtained as an exact solution to the continuity equation:

$$\nabla \cdot \vec{J} = \frac{2}{\hbar} U \rho \tag{2.8}$$

This equation, where $\vec{J}$ is the current and $\rho$ the probability density, involves only the imaginary part of the potential, U. In a sense, therefore, the real potential is neglected in (2.8) while the absorption is taken into account, and this is similar to the viewpoint of the plane wave theories. It is not difficult to show that (2.6) defines an exact, unique solution to (2.8), namely

$$\psi = e^{ikz} \exp\left\{ \frac{1}{\hbar v} \int_{-\infty}^{z} U(x, y, z')\, dz' \right\} \tag{2.9}$$

In (2.9), the envelope function is real, as desired.

In a similar manner, the Schrödinger equation describing the interaction of a neutron and proton with a complex potential well and each other,

$$\left( T_n + V_n + i U_n + T_p + V_p + V_c + i U_p + V_{np} - E \right) \psi = 0 \tag{2.10}$$

leads to the continuity equation,

$$\nabla_6 \cdot \vec{J}_6 = \frac{2}{\hbar} \left( U_n + U_p \right) \rho \tag{2.11}$$

In this equation $\rho$ is $\psi^* \psi$; $\nabla_6$ is the six-dimensional gradient operator, $\nabla_n + \nabla_p$; and $\vec{J}_6$ is the current $(\hbar/m)\ \mathrm{Im}\psi^* \nabla_6 \psi$. If the relative and

center-of-mass coordinates are denoted by $\vec{R}_{np}=\vec{R}_n-\vec{R}_p$ and $\vec{R}_d=\frac{1}{2}(\vec{R}_n+\vec{R}_p)$, then $\nabla_e = \nabla_d$.

For the cutoff plane wave we take

$$\psi = f(\vec{R}_n, \vec{R}_p)\,\psi_{np}\, e^{i\vec{K}_d\cdot\vec{R}_d} \tag{2.12}$$

where $\psi_{np}$ is the deuteron ground state. Using this expression to evaluate $\vec{J}_e$ and $\rho$ in (2.11) leads to

$$\vec{K}_d\cdot\nabla_d s = 2m_d\,(U_n+U_p)/\hbar^2 \tag{2.13}$$

where $s = \ln f^2$ and $m_d = 2m$ is the deuteron mass. The solution to this equation is

$$\ln f = \frac{1}{\hbar v_d}\int_{-\infty}^{z_d}\left[U_n(\ldots z_d')+U_p(\ldots z_d')\right]dz_d' \tag{2.14}$$

uniqueness being obtained by the boundary condition $f \to 1$ as $z \to -\infty$. The term involving $U_n(\vec{R}_n) = U_n(\vec{R}_d + \frac{1}{2}\vec{R}_{np})$ is explicitly

$$\frac{1}{\hbar v_d}\int_{-\infty}^{z_d} U_n\left(x_d+\tfrac{1}{2}x_{np},\, y_d+\tfrac{1}{2}y_{np},\, z_d'+\tfrac{1}{2}z_{np}\right)dz_d' \tag{2.15}$$

A change of variable to $z_n' = z_d' + \frac{1}{2}z_{np}$ (and the corresponding translation in the proton integral) yields

$$\ln f = \frac{1}{\hbar v_d}\int_{-\infty}^{z_n} U_n(x_n y_n z_n')dz_n' + \frac{1}{\hbar v_d}\int_{-\infty}^{z_p} U_p(x_p y_p z_p')dz_p' \tag{2.16}$$

The absorption induced by each nucleon contributes additively to the logarithm in (2.16), so that f is a product of independent nucleon

cutoffs. These will be formally identical to (2.9) if the nucleon velocity in the latter equation is taken equal to the deuteron velocity $v_d = \hbar k_d/m_d$ in (2.16). This suggests that the optical potentials in (2.16) should be taken as those for nucleon scattering at half the deuteron energy. The physical meaning of this choice is that under deuteron bombardment the nuclear excitation is the same as that due to two independent nucleons each with half the deuteron energy. The weak binding of the deuteron makes this not unreasonable, at least at deuteron energies well above the deuteron binding energy.

On the other hand, the same weak binding complicates the situation as follows. The potentials $U_n$ and $U_p$ determined from elastic nucleon scattering are a measure of the absorption due to two processes, nuclear excitation and spin-flip of the incident nucleon. (At much higher energies, meson processes would also enter.) However, when the projectile is a deuteron, the entirely new process of deuteron dissociation also contributes to the absorption. This means that the nucleon scattering absorptive potentials must be augmented by additional terms to account for this new effect.

## D. SCATTERING OF LARGER AGGREGATES

The formal procedure of the preceding paragraphs can be applied to the scattering of an aggregate of A nucleons, an essential point being that the internal wave function cancels from the flux equation. The analog of (2.16) is:

$$\ln f = \frac{1}{\hbar v_A} \sum_{j=1}^{A} \int_{-\infty}^{z_j} U_j(x_j y_j z_j') \, dz_j' \qquad (2.17)$$

where $v_A$ is the center-of-mass velocity and $U_j$ is the absorptive potential felt by the $j^{th}$ nucleon. The remarks of the preceding section concerning the difference between the absorptive potentials of (2.9) and those of (2.16) apply with equal force here. (As an example of a tightly bound particle for which projectile excitation might be negligible, one thinks immediately of the $\alpha$-particle.) The content of (2.17) is expressible in terms of absorption coefficients in hypothetical uniformly absorbing nuclear matter. If the intensity of a beam of A-nucleon aggregates is

$$I_A = I_{A0} e^{-\kappa_A z} \qquad (2.18)$$

(with corresponding equations for nucleon beams), then

$$\kappa_A = \sum_{j=1}^{A} \kappa_j \approx A \kappa_{NUCLEON} \qquad (2.19)$$

For an alpha particle this predicts an absorption four times the nucleon value (20), suggestive of the "black nucleus" model (21) which has had some success in the interpretation of elastic alpha scattering.

## E. RESONANCES IN STRIPPING REACTIONS

The present theory, like all direct reaction theories, does not apply to compound nucleus processes. However, according to the resonance theory of nuclear reactions, increased penetration of the in-

cident wave occurs on resonance and it is possible that this can cause an enhancement of the direct process. Insofar as the localization argument applies to a single partial wave (the usual resonant situation), the increased penetration should result in a shift of the stripping peak to larger angles on resonance. According to the Butler theory, this would reflect as a decrease in the Butler radius. An example of this type of behavior appears to occur in reference (22).

F. EFFECT OF THE ZERO-RANGE APPROXIMATION

In a theory without proton-absorption (1,2,5), the zero-range approximation, $V_{np} \propto \delta(\vec{R}_n - \vec{R}_p)$, will be quite accurate. The contribution to the stripping reaction arises in a sphere surrounding the neutron, with a radius equal to the n-p force range. If the proton density over that sphere is uniform, then the zero-range approximation, which replaces the density by its value at the center of the sphere, will be correct. In distorted-wave theories, or the present type, the proton density decreases inwardly over that sphere, so the delta-function produces an (incorrect) enhancement of the small-$r_p$ stripping. This in turn will lead to an overly large nuclear radius.

## CHAPTER III

## DEUTERON STRIPPING: THE PROTON-NEUTRON INTERACTION AMPLITUDE

### A. SUMMARY

In this and the following chapter the cutoff Born approximation will be applied to the deuteron stripping reaction, using (d,p) nomenclature throughtout. For (d,n) reactions the Coulomb part of the proton-target optical interaction is omitted and if necessary, the correction described in Ref. 23, Chapter 5, Section 2,is made.

Starting from the exact transition matrix element (3.1), the use of an optical potential as an approximation to the proton-target interaction and the particular form of the cutoff Born approximation (3.2) permits a relatively simple evaluation of all integrals. By a suitable choice of approximations, (3.26) and (3.27), the $V_{np}$-amplitude can be expressed in terms of the tabulated Butler cross section (14).

Spin-dependent forces are neglected for the reason that they do not play an essential role in the (d,p) problem. In the $V_{np}$-amplitude they result in the appearance of the D-state part of the deuteron wave function in an unimportant manner (24, 25). In the $V_{tp}$-amplitude they have a small effect on the polarization in the vicinity of the stripping peak, but serve mainly to provide polarizations greater than 1/3 at larger angles. (With spin-independent forces the maximum polarization

is 1/3 (26)). Since observed polarizations appear to be less than 1/3 on the stripping peak, spin-dependent forces are not required for their explanation. The present work is not concerned with the large-angle stripping (Chapter 1, Section C).

A partial reduction of the matrix element is carried out in Section B, while Section C gives some details of the remaining evaluation. The results for the $V_{np}$-amplitude are summarized in Section D, while Section E is intended as a guide to the use of the formulas. The results for the proton-target interaction amplitudes are given in Chapter 4, together with the polarization formulas.

## B. THE (d,p) STRIPPING CROSS SECTION

In this section the transition matrix element will be expressed in terms of an integral over spatial functions, (3.6). This is accomplished by introducing an appropriate angular momentum coupling scheme and integrating out the spin coordinates. The procedure is standard and is only sketched here. For details see Refs. (23, 27, 28).

The exact matrix element may be written in the form:

$$A^{m_i m_d}_{m_f m_p}(\vec{K}_p, \vec{K}_d) = -\int e^{-i\vec{K}_p\cdot\vec{R}_{pf}}\, \chi^{*}_{\frac{1}{2}m_p}(\sigma_p)\, \psi^{*}_{J_f m_f}(t, \vec{R}_n, \sigma_n)$$
$$\times \left[V_{np} + \sum_{i=1}^{A} V_{ip}\right] \Psi(t, \vec{R}_n, \sigma_n, \vec{R}_p, \sigma_p)\, dt\, d\vec{R}_n\, d\sigma_n\, d\vec{R}_p\, d\sigma_p \qquad (3.1)$$

In this equation the factors are, from left to right, the final proton plane wave, $\vec{R}_{pf}$ being its separation from the center-of-mass of the final nucleus (target plus neutron); the proton spin function; the final

nucleus wave function; the interaction between the proton and all the other nucleons; and the exact wave function. The integration is extended over the coordinates of the neutron, the proton, and the target nucleons "t," including all spins.

To simplify (3.1), the interaction between the proton and the target nucleons is replaced by an average potential $V_{tp}$, and the exact wave function by a cutoff plane wave:

$$\Psi \approx e^{i \vec{K}_d \cdot \vec{R}_d} \psi_{np}(\vec{R}_{np}) \chi_{1 m_d}(\sigma_n, \sigma_p) \mathcal{C}_{J_t m_t}(t) f_n(r_n) f_p(r_p) \qquad (3.2)$$

The factors here are the deuteron c.m. wave function, its internal wave function, the triplet spin function, the target ground state wave function, and two Gaussian-type cutoff functions,

$$f_n(r_n) = 1 - b_n e^{-\frac{1}{2} \Omega_n^2 r_n^2} \qquad (3.3a)$$

$$f_p(r_p) = 1 - b_p e^{-\frac{1}{2} \Omega_p^2 r_p^2} \qquad (3.3b)$$

Next the final nucleus wave function is expanded in the target eigenfunctions, the coefficients depending on $\vec{R}_n$ and $\sigma_n$. Only the term corresponding to the target ground state survives the integration over the target coordinates and the coefficient (the neutron wave function) can be expanded in a complete set of spin-angle functions for the neutron. These are taken in a representation which diagonalizes the neutron's total and orbital angular momenta, j and $\ell$. This is convenient for expressing the polarization results (Chapter 4).

Carrying out the spin integrations yields:

$$A^{m_t m_b}_{m_f m_p} = \sum_{jl} C^{\frac{1}{2}\ \frac{1}{2}\ 1}_{m_p \cdot m_d} C^{\frac{1}{2}\ l\ j}_{m_d - m_p \cdot m_f - m_i} C^{J_t\ j\ J_f}_{m_t \cdot m_f} X^{jlm} \qquad (3.4)$$

where $X^{jlm}$ is the spatial integral:

$$X^{jlm} = -\int e^{i(\vec{K}_d \vec{R}_d - \vec{K}_p \vec{R}_{pf})} w^*_{jl}(r_n) Y^*_{lm}(\hat{R}_n) [V_{np} + V_{tp}] \psi_{m_f}(\vec{r}_{np}) f_n f_p \, d\vec{R}_n \, d\vec{R}_p \qquad (3.5)$$

The quantum number m stands for $m_f+m_p-m_i-m_d$ and $w_{jl}(r_n)$ is the neutron radial wave function, i.e., the radial coefficient in the spin-angle expansion mentioned above. The large set of quantum numbers needed to specify the target and final nucleus wave functions, implicit in the symbols $J_t$ and $J_f$ (which have the restricted significance of angular momenta in the Clebsch-Gordan coefficients), and which label $w_{jl}(r_n)$, have been suppressed. The Clebsch-Gordan coefficient $C^{ABC}_{abc}$ expresses the coupling of angular momenta A and B to a resultant C. The relation a+b=c permits suppressing any one magnetic quantum number, indicated by a dot above.

The symbol A for the matrix element has been chosen to agree with Ref. (25). The integral $X^{jlm}$ above corresponds to Tobocman's $\sqrt{\gamma^{FI}_{lj}}\ B^{lm}$. In the present work a slightly different definition is employed (see eq. (3.25):

$$X^{jlm} = i^l \theta_{jl} B^{lm} \qquad (3.6)$$

The differential cross section,

$$\sigma_{dp}(\vartheta_p) = \frac{m_{pf}\, m_{dt}}{(2\pi\hbar^2)^2} \frac{k_p}{k_d} \frac{1}{3(2J_t+1)} \sum_{\substack{m_t m_f \\ m_p m_d}} \left| A^{m_t m_d}_{m_f m_p} \right|^2 \tag{3.7}$$

has the well-known form of an incoherent sum:

$$\sigma_{dp}(\vartheta_p) = \sum_{j\ell} \sigma_{j\ell}(\vartheta_p) \tag{3.8}$$

The cross section for neutron capture to a state with definite j and $\ell$ is:

$$\sigma_{j\ell}(\vartheta_p) = \frac{m_{pf}\, m_{dt}}{8\pi^2\hbar^4} \frac{k_p}{k_d} \frac{2J_f+1}{2J_t+1} \frac{1}{2\ell+1} \sum_m \left| X^{j\ell m} \right|^2 \tag{3.9}$$

The remaining sum can be performed once the amplitude $X^{j\ell m}$ is expressed in terms of spherical harmonics, as in this and the following chapter.

Because of the particular form chosen for the cutoff functions (3.3), the total amplitude $X^{j\ell m}$ contains four partial amplitudes:

$$X^{j\ell m} = X_0^{j\ell m} - b_n X_n^{j\ell m} - b_p X_p^{j\ell m} + b_n b_p X_{np}^{j\ell m} \tag{3.10}$$

From the explicit evaluation of $X_{np}^{j\ell m}$ the others are obtained as follows: $X_n^{j\ell m}$ by setting $\Omega_p = 0$, $X_p^{j\ell m}$ by setting $\Omega_n = 0$, and the Born approximation amplitude $X_0^{j\ell m}$ by setting both equal to zero. The partial amplitude $X_{np}^{j\ell m}$ itself contains two terms,

$$X_{np}^{j\ell m} = -\int e^{i(\vec{K}_d \vec{R}_d - \vec{K}_p \vec{R}_p)} w^*_{j\ell}(r_n)\, Y^*_{\ell m}(\hat{R}_n) \times \tag{3.11}$$

$$\times \left[ V_{np} + V_{tp} \right] \psi_{np}\, e^{-\frac{1}{2}\left(\Omega_n^2 r_n^2 + \Omega_p^2 r_p^2\right)} d\vec{R}_n d\vec{R}_p$$

$$\equiv X_{np}^{jlm}(V_{np}) + X_{np}^{jlm}(V_{tp}) \qquad (3.12)$$

the second of which will be treated in the next chapter.

C. DERIVATION OF THE $V_{np}$-AMPLITUDE

The usual procedure of eliminating the potential $V_{np}$ by means of the Schrödinger equation for the deuteron ground state, $(T_{np} + V_{np} + 2.226)\ \psi_{np} = 0$, is not used here because the presence of the proton cutoff complicates the subsequent integration by parts. It is also possible to avoid the zero-range approximation which is somewhat inaccurate in the presence of proton absorption (Chapter 2, Section F and Ref. 29). Instead, the product $V_{np}\psi_{np}$ is approximated as follows:

The Schrödinger equation for the potential,

$$V_{np} = -86.4\, e^{-(r_{np}/1.332)^2} \ \text{Mev} \qquad (3.13)$$

has been numerically integrated (30) and the results for $\psi_{np}$ exhibited as a sum of three gaussian terms. However, the product $V_{np}\psi_{np}$ is accurately given by one such term,

$$V_{np}\psi_{np} \approx -C_1 e^{-\frac{1}{2}\mu^2 r_{np}^2} \quad (C_1 = 16.2\ \text{Mev}/f^{3/2};\ \mu^2 = 1.703 f^{-2}) \qquad (3.14)$$

When (3.14) is introduced into the first term of (3.12), the resulting integral can be split by the following transformation: Replace $\vec{R}_p$ by the vector $\vec{W}_{np} = \vec{R}_p - (\mu^2/f_{np}^2)\vec{R}_n$, with

$$f_{np}^2 = \mu^2 + \Omega_p^2 \tag{3.15}$$

Then the exponential terms transform as follows:

$$\mu^2 r_{np}^2 + \Omega_n^2 r_n^2 + \Omega_p^2 r_p^2 = d_{np}^2 r_n^2 + f_{np}^2 W_{np}^2$$

$$\vec{K}_d \cdot \vec{R}_d - \vec{K}_p \cdot \vec{R}_{pf} = \vec{T}_{np} \cdot \vec{R}_n + \vec{K} \cdot \vec{W}_{np} \tag{3.16}$$

The new constants and wave vectors are given by

$$d_{np}^2 = \Omega_n^2 + \mu^2 \Omega_p^2 / f_{np}^2 \tag{3.17}$$

$$\vec{K} = \tfrac{1}{2}\vec{K}_d - \vec{K}_p \tag{3.18}$$

$$\vec{T}_{np} = (1 - \Omega_p^2/2f_{np}^2)\vec{K}_d - (\mu^2/f_{np}^2 - m_n/m_f)\vec{K}_p \tag{3.19}$$

Carrying out the integration over $d\vec{W}_{np}$ and the directions $d\hat{R}_n$ yields

$$I_{np}^{jlm}(V_{np}) = 4\pi(2\pi)^{3/2} i^l C_1 f_{np}^{-3} e^{-k^2/2f_{np}^2} Y_{lm}^*(\hat{T}_{np}) G_{np}^{jl}(V_{np}) \tag{3.20}$$

It is now necessary to choose a form for the neutron radial wave function in the remaining integral,

$$G_{np}^{jl}(V_{np}) = \int_0^\infty w_{jl}(r_n) j_l(t_{np} r_n) e^{-\frac{1}{2} d_{np}^2 r_n^2} r_n^2 dr_n \tag{3.21}$$

This will be taken as a square well wave function, with the dimensionless reduced width $\theta^2_{j\ell}$ serving to normalize it,

$$w_{j\ell}(r_n) = (3/a^3)^{1/2}\theta_{j\ell}\, j_\ell(\kappa r_n)/j_\ell(\kappa a) \qquad r_n < a \qquad (3.22)$$

$$= (3/a^3)^{1/2}\theta_{j\ell}\, h_\ell(\kappa r_n)/h_\ell(\kappa a) \qquad r_n > a \qquad (3.23)$$

The function $h_\ell(\kappa r_n)$ in (3.23) is defined in terms of the spherical Hankel function (18, p.79),

$$h_\ell(x) = -i^\ell h_\ell^{(1)}(ix) \qquad (3.24)$$

For states of positive binding energy it is a real, positive function.

The reduced width $\theta^2$ is defined in terms of the Wigner-Teichmann reduced width (31) according to the usage in Ajzenberg and Lauritsen (32),

$$\theta_{j\ell} = \left(\frac{2m_{nt}a}{3\hbar^2}\right)^{1/2}\gamma_{j\ell} \qquad (3.25)$$

The explicit use of an "inside" wave function (3.22) permits, as the penetration parameters in (3.3) are varied, a continuous transition between the Born approximation (complete transparency, $\Omega_n$ and $\Omega_p \to \infty$) and a situation in which the capture is nearly all outside of the radius a, similar to Butler's approach. A steeper cutoff than (3.3) would be desirable in exploring this question. (cf. Appendix F, Section 2, and remarks in Chapter 4, Section H.)

The use of (3.22) and (3.23) splits (3.21) into an inner part ($r_n < a$) and an outer part ($r_n > a$). The integrals cannot be performed as they stand, so that if numerical integration is to be avoided some approximation is required. A convenient choice is:

$$\text{Inner: } j_\ell(\gamma r_n)\, e^{-\frac{1}{2}d_{np}^2 r_n^2} \approx j_\ell(\gamma a)\, e^{-\frac{1}{2}d_{np}^2 a^2}\, j_\ell(\gamma_{np} r_n)/j_\ell(\gamma_{np} a) \quad (3.26)$$

$$\text{Outer: } h_\ell(\kappa r_n)\, e^{-\frac{1}{2}d_{np}^2 r_n^2} \approx h_\ell(\kappa a)\, e^{-\frac{1}{2}d_{np}^2 a^2}\, h_\ell(\xi_{np} r_n)/h_\ell(\xi_{np} a) \quad (3.27)$$

A discussion of these approximations, some numerical examples, and formulas for determining the effective wave numbers $\gamma_{np}$ and $\xi_{np}$ are contained in Appendix C. The subscripts "np" on $\gamma_{np}$ and $\xi_{np}$ indicate their dependence on $d_{np}$ and therefore on the particular partial amplitude of (3.10).

The approximation (3.27) is suitable only for bound states (real $\kappa$). The problem of stripping to virtual states would require a different treatment and is not considered here.

The integrations are now straightforward and lead to the following expressions, in which the derivatives of the cylindrical functions have been eliminated in favor of functions of order $\ell$-1:

$$\text{Inner: } \frac{\sqrt{3a^3\theta_{j\ell}^2}\, e^{-\frac{1}{2}d_{np}^2 a^2}}{\gamma_{np}^2 a^2 - t_{np}^2 a^2} \left[ t_{np} a\, j_{\ell-1}(t_{np} a) - \gamma_{np} a\, \frac{j_{\ell-1}(\gamma_{np} a)}{j_\ell(\gamma_{np} a)}\, j_\ell(t_{np} a) \right] \quad (3.28)$$

$$\frac{\sqrt{3a^3\theta_{jl}^2}\, e^{-\frac{1}{2}d_{np}^2 a^2}}{\xi_{np}^2 a^2 + t_{np}^2 a^2}\left[t_{np}a\, j_{l-1}(t_{np}a)\right.$$

Outer:

$$\left. + \xi_{np}a\, \frac{h_{l-1}(\xi_{np}a)}{h_l(\xi_{np}a)}\, j_l(t_{np}a)\right] \qquad (3.29)$$

The square bracket in (3.28) can be brought to the same form as in (3.29) by the substitution.

$$\gamma_{np}a\, \frac{j_{l-1}(\gamma_{np}a)}{j_l(\gamma_{np}a)} = -\kappa_{np}a\, \frac{h_{l-1}(\kappa_{np}a)}{h_l(\kappa_{np}a)} \qquad (3.30)$$

This represents the condition for matching square well wave functions at the radius a, with the usual derivatives eliminated. The wave number $\kappa_{np}$ can be found from the curves of Appendix G.

Both (3.28) and (3.29) are now expressible in terms of the tabulated Butler cross section (14),

$$\sigma_{TAB}^{l}(x,y) = \left[\frac{G_l(y)\, j_l(x) + x\, j_{l-1}(x)}{(x^2+y^2)\left[1+(x^2+y^2)/125\right]}\right]^2 \qquad (3.31)$$

where

$$G_l(y) \equiv -iy\, \frac{h_{l-1}^{(1)}(iy)}{h_l^{(1)}(iy)} \equiv y\, \frac{h_{l-1}(y)}{h_l(y)} \qquad (3.32)$$

Introducing the "outside," "inside," and Born amplitudes, $O_l(x,y)$, $I_l(x,y)$, and $B_l(x,y)$, (the definitions of these amplitudes are given in Appendix G, where their evaluation is discussed), (3.21) becomes

$$G_{np}^{j\ell}(V_{np}) = (3a^3\theta_{j\ell}^2)^{1/2} e^{-\frac{1}{2}d_{np}^2 a^2}\left[I_\ell(t_{np}a, \kappa_{np}a) + O_\ell(t_{np}a, \zeta_{np}a)\right] \tag{3.33}$$

As a practical matter, the vector $\vec{T}_{np}$ is very closely equal to $\vec{Q} = \vec{K}_d - m_i\vec{K}_p/m_f$, the momentum transfer vector occurring in the Butler theory. This stems from the fact that the n-p force range is much smaller than the usual cutoff radius,

$$\mu^2 >> \Omega_p^2 \tag{3.34}$$

Henceforth, we will put $t_{np} = q$, and $\hat{T}_{np} = \hat{Q}$ in the spherical harmonic.

$X^{j\ell m}(V_{np})$ appears as follows, with $x = qa$,

$$\begin{aligned} X^{j\ell m}(V_{np}) = {} & 4\pi(2\pi)^{3/2} i^\ell C_1 (3a^3\theta_{j\ell}^2)^{1/2} Y_{\ell m}^*(\hat{Q}) \cdot \\ & \cdot \Big\{ \mu^{-3} e^{-k^2/2\mu^2} B_\ell(x, \kappa a) \\ & - b_n \mu^{-3} e^{-\frac{1}{2}\Omega_n^2 a^2 - k^2/2\mu^2}\left[I_\ell(x, \kappa_n a) + O_\ell(x, \zeta_n a)\right] \\ & - b_p f_{np}^{-3} e^{-\frac{1}{2}d_{np}^2 a^2 - k^2/2f_{np}^2}\left[I_\ell(x, \kappa_p a) + O_\ell(x, \zeta_p a)\right] \\ & + b_n b_p f_{np}^{-3} e^{-\frac{1}{2}d_{np}^2 a^2 - k^2/2f_{np}^2}\left[I_\ell(x, \kappa_{np} a) + O_\ell(x, \zeta_{np} a)\right] \Big\} \end{aligned} \tag{3.35}$$

$$\approx 4\pi(2\pi)^{3/2} i^{\ell} C_1 (3a^3\theta_{j\ell}^2)^{1/2} e^{-k^2/2\mu^2} Y_{\ell m}^*(\hat{\varphi}) \cdot$$

$$\cdot \Big\{ \mu^{-3} B_\ell(x,\kappa a) - \Big[ b_n \mu^{-3} e^{-\frac{1}{2}\Omega_n^2 a^2} +$$

$$+ b_p f_{np}^{-3} e^{-\frac{1}{2} d_{np}^2 a^2} \Big] \Big[ I_\ell(x,\tilde{\kappa}a) + O_\ell(x,\tilde{\xi}a) \Big]$$

$$+ b_n b_p f_{np}^{-3} e^{-\frac{1}{2} d_{np}^2 a^2} \Big[ I_\ell(x,\kappa_{np}a) + O_\ell(x,\xi_{np}a) \Big] \Big\}$$

(3.36)

In (3.35) some of the redundant symbols have been eliminated by the relations: $f_p = f_{np}$; $f_n = f_o = \mu$; $d_n = \Omega_n$; $d_o = 0$; $\xi_o = \kappa$; $\kappa_o = \kappa$; $\gamma_o = \gamma$; and in the Born term, $B_\ell = I_\ell + O_\ell$. The reduction from seven amplitudes in (3.35) to five in (3.36) is the result of approximating $\kappa_n \approx \kappa_p \approx \tilde{\kappa}$, $\xi_n \approx \xi_p \approx \tilde{\xi}$. The quantities $\tilde{\gamma}$ and $\tilde{\xi}$ are computed (Appendix C) from the average value $\tilde{d}^2 = \frac{1}{2}(d_n^2 + d_p^2) = \frac{1}{2} d_{np}^2$. The quantity $\tilde{\kappa}$ then follows from $\tilde{\gamma}$ according to (3.30). This approximation is accurate when (3.34) holds and also $\Omega_n^2 \approx \Omega_p^2$. The same relations permit taking the slowly varying exponentials $\exp(-k^2/2f_{np}^2) \approx \exp(-k^2/2f_p^2) \approx \exp(-k^2/2\mu^2)$ as a common factor in (3.36).

The symbols $f_o$, $f_n$, $f_p$; $d_o$, $d_n$, $d_p$; $\gamma_o, \gamma_n$, $\gamma_p$; $\xi_o$, $\xi_n$, $\xi_p$; and $\kappa_o$, $\kappa_n$, $\kappa_p$, are the analogs of $f_{np}$ (3.15); $d_{np}$(3.17); $\gamma_{np}$(3.26); $\xi_{np}$

(3.27); and $\kappa_{np}$ (3.30), but appropriate to the other partial amplitudes occurring in (3.10) and therefore obtainable as stated following that equation. The derivation of Section C concerns explicitly the partial amplitude $X_{np}^{\ell m}$ ($V_{np}$) of (3.10), up to and including the sentence following (3.34), while all four amplitudes are included in (3.35) and (3.36).

D. DIFFERENTIAL CROSS SECTION WITHOUT PROTON-TARGET INTERACTION

If the proton-target term in (3.5) is temporarily ignored, the result is a "cutoff-proton" version of the Butler formula. This is useful for estimating reduced widths without the refinement of the additional proton-interaction terms of Chapter 4. For finding the capture $\ell$-value, the Butler formula (with the large radius) is simpler and usually perfectly adequate.

Because of (3.34), a single spherical harmonic occurs in (3.35) and (3.36), so that there are no interference terms in the m-sum of (3.9). In the following "summed" form of (3.9), all quantities are to be evaluated in nuclear units, Appendix A, the cross section itself being in units of $f^2/sr$:

$$\sigma_{j\ell}(\vartheta_p) = 36.1 \frac{m_f^2}{(m+m_d)^2} \frac{2J_f+1}{2J_t+1} ta^3 \theta_j^2 \exp[-.014Q - .294\left(\frac{m+1}{m}\right)q^2]\{M\} \qquad (3.37)$$

Notation: (All quantities in c.m. system except $E_d$.)

$a$ = nuclear radius.

$E_d$ = deuteron laboratory energy.

$J_t$, $J_f$ = target and final nuclear spins.

$k_p$, $k_d$ = proton and deuteron wave numbers.

$k_d^2 = 0.09567\ m^2 E_d/(m+m_d)^2$.

$m$, $m_f$, $m_d$ = target, final nucleus, and deuteron masses.

$m_{pf}$, $m_{dt}$ = reduced masses.

$Q$ = reaction Q-value.

$q^2 = (t^2+1)k_d^2 - 2tk_d^2 \cos\theta_p$ = square of momentum transfer.

$$t^2 = \left(\frac{m}{m+1}\frac{k_p}{k_d}\right)^2 = \frac{1}{2}\left(\frac{m}{m+1} + \frac{m+2}{m+1}\frac{Q}{E_d}\right).$$

$\{M\}$ = curly bracket in (3.35) or (3.36).

The wave number of the captured neutron is

$$\kappa^2 = 0.04827m\ [Q+2.226]/(m+1).$$

The factor $\exp(-k^2/\mu^2)$ occurring in (3.36) has been re-written using the relation,

$$k^2 = |\tfrac{1}{2}\vec{K}_d - \vec{K}_p|^2 = \tfrac{1}{2}(m+1)\,q^2/m + 0.02395Q.$$

The cross section for the (p,d) pickup reaction can be found by reciprocity,

$$\sigma_{j\ell}(\theta_d) = 54.12\ (m^2/(m+2)^2)\ t^{-1}\ a^3\theta_{j\ell}^2\ e^{-0.0141Q_e - 0.2937(\frac{m+1}{m})q^2}\ \{M\}^2\ f^2/sr. \qquad (3.38)$$

In this formula, equivalent (d,p) quantities must be used. Thus m is the target mass for the (d,p) reaction, or final nucleus mass for (p,d). Q means $Q_{dp} = -Q_{pd}$, and $E_d$ is obtained from the incident proton laboratory energy in the (p,d) reaction using

$$E_d = \frac{m+1}{m} E_p - \frac{m+2}{m} Q \qquad (3.39)$$

This permits using the formulas of the above tabulation as they are written.

E. OUTLINE OF PROCEDURE

1. The energies, masses, and spins multiplying the curly bracket in (3.37) are supposed known. The reduced width $\theta_{j\ell}^2$ is to be determined by comparison with the absolute cross section.

2. If the penetration parameters $\Omega_n$ and $\Omega_p$ have been determined by a (d,d) analysis at the same energy, as described in Chapter 5, then only the nuclear radius a is adjustable. Otherwise, all three may be varied. The criterion for a correct choice is agreement in peak position between theory and experiment. In what follows it is assumed that $\Omega_n \cong \Omega_p$, and $b_n = b_p = 1$.

3. The numbers $k_d$, $k_p$, t, $\kappa$, and $q^2$ (the latter as a function of the scattering angle) can be found from the formulas in Section D. In order to eliminate interpolation in x = qa in the stripping tables, the cross section should be evaluated at even tenths in x, converting to angle via $\cos \theta_p = (t^2+1)/2t - x^2/2tk_d^2a^2$.

Interpolation in y = $\kappa$a can be partially avoided by taking a value for the radius a that makes y an even tenth.

4. With y = $\kappa$a, enter Fig. G-2 (Appendix G, Section 2(a)) and read out $x_o^2$, observing the translated ordinate scale. Then the internal wave number is $\gamma = x_o/a$.

5. Compute $f_{np}^2 = \mu^2+\Omega_p^2$ and $d_{np}^2 = \Omega_n^2+\mu^2\Omega_p^2/f_{np}^2$. Then $\gamma$, $d_{np}$, and a determine $\gamma_{np}$ via Appendix C, Section 2. Then use $\gamma_{np}$ and a as in-

puts to Appendix G, Section 2(b), to find $\kappa_{np}$.

6. Use $\tilde{d}^2 = \frac{1}{2}d_{np}^2$, $\gamma$, and a, to find $\tilde{\gamma}$ via Appendix C, Section 2. Then use $\tilde{\gamma}$ and a as inputs to Appendix G, Section 2(b), to find $\tilde{\kappa}$.

7. Use $d_{np}$, $\kappa$, and a, to find $\xi_{np}$ from Appendix C, Section 4.

8. Use $\tilde{d}$, $\kappa$, and a, to find $\tilde{\xi}$ from Appendix C, Section 4.

9. The five amplitudes in (3.36) can now be computed as functions of x as described in Appendix G, Section 1. This completes the specification of the quantities occurring in the curly bracket of (3.36) and (3.37).

F. THE BUTLER THEORY WITH A PROTON CUTOFF ADDED

A simpler formula than (3.36) results from grafting a proton cutoff of the form (3.3b) onto the Butler theory with its sharp neutron cutoff. Only two stripping amplitudes occur in the result, one of them the Butler amplitude itself, so it displays directly the way in which the excised proton region makes itself felt. Equation (3.1) is unchanged, but (3.2) becomes:

$$\Psi \approx e^{i\vec{K}_d\cdot\vec{R}_d}\psi_{np}(\vec{R}_{np})\,\chi_{1m_d}(\sigma_n\sigma_p)\,\mathcal{L}_{J_t m_t}(t)\,H(r_n-a)\,f_p(r_p) \qquad (3.40)$$

where H(x) is the unit step function.

The procedure is the same as in Section C, the result being

$$\sigma_{j\ell}(\vartheta_p) = 7.31\left(\frac{m+1}{m+2}\right)^2 t a^3 \theta_{j\ell}^2 \left(\frac{2J_f+1}{2J_t+1}\right) e^{-k^2/\mu^2} \cdot \left[O_\ell(x,y) - b_p e^{-\frac{1}{2}\bar{a}^2\bar{a}^2} O_\ell(x,3a)\right]^2 \qquad (3.41)$$

The wave number $\xi$ is determined by the analog to (3.27),

$$h_\ell(\kappa r_m) e^{-\frac{1}{2}\bar{d}^2 r_m^2} \approx h_\ell(\kappa a) e^{-\frac{1}{2}\bar{d}^2 a^2} h_\ell(\xi r_m) / h_\ell(\xi a) \qquad (3.42)$$

so that the inputs to Appendix C, Section 4, are $\kappa$, a, and $\bar{d}^2 = \mu^2\Omega_p^2/(\mu^2+\Omega_p^2) \approx \Omega_p^2$.

For the (p,d) reaction, the factors $7.313((m+1)/(m+2))^2 t(2J_f+1)/(2J_t+1)$ in (3.41) are replaced by $10.96(m/(m+2))^{2t-1}$, equivalent (d,p) quantities being understood.

# CHAPTER IV

## DEUTERON STRIPPING: THE PROTON-TARGET INTERACTION AMPLITUDE

### A. SUMMARY AND CONCLUSIONS

In this chapter the (d,p) stripping amplitude due to the smoothed interaction between the proton and the target nucleus will be evaluated. In previous plane wave theories (1, 2, 5) this interaction was neglected, while in distorted wave theories (3, 4, 28) it is included in the construction of the Green's function by adding to the outgoing proton plane wave the scattered waves appropriate to the distorting potential (34). The method employed here is to include the proton optical potential as a source term in the cutoff Born approximation, a compromise between the above two methods in respect to simplicity of treatment and potentially attainable accuracy. The introduction of a proton cutoff is essential for obtaining quantitatively reasonable results (Chapter 1, Section A).

Since the optical potential does not involve any reference to the coordinates of the target nucleons, the resulting amplitude is subject to the usual stripping selection rules.

In Section B it is shown that by approximating the nuclear (non-electrical) potential and the deuteron ground state by Gaussian type expressions (Appendix F), and using the Coulomb potential due to a Gaussian charge distribution, the integrals reduce to the one evaluated

in the previous chapter, or are derivable from it. However, a great simplification occurs if the neutron square well wave function (3.22) and (3.23), is replaced by an harmonic oscillator eigenfunction. The accuracy of such a procedure is discussed and the evaluation of the integrals sketched in Section C.

A final simplification occurs if the neutron cutoff function is expanded as in eq. (4.7). Explicit formulas for this caseare derived in Section D, and summarized in Section E, where the results are also specialized for capture to the low single-particle states 1s, 1p, 1d, and 2s. An approximate, extremely simple formula for the polarization is derived and discussed in Section F, while the last two Sections, G and H, concern the analysis of the reactions $Be^9(p,d)Be^8$ and $Be^9(d,p)Be^{10}$.

## B. PROTON-TARGET INTERACTION AMPLITUDE WITH A SQUARE WELL NEUTRON WAVE FUNCTION

The integral whose value is required was given in eq. (3.11):

$$\int e^{i(\vec{K}_d\vec{R}_d - \vec{K}_p\vec{R}_{pf})} w^*_{jl}(r_n)\, Y^*_{lm}(\hat{R}_n)\, V_{tp}\, \psi_{np}\, e^{-\frac{1}{2}(\Omega_n^2 r_n^2 + \Omega_p^2 r_p^2)} \qquad (4.1)$$

In the present section it is assumed that the radial neutron function is described by eqs. (3.22) and (3.23). This integral can be evaluated if the nuclear potentials (real and imaginary) in $V_{tp}$ and the deuteron ground state are approximated by series of terms of the form $r_p^{2n} \exp(-ar_p^2)$ and $r_{np}^{2m} \exp(-br_{np}^2)$, while the Coulomb potential is that due to a Gaussian charge distribution,

$$\rho(r_p) = Z\epsilon\gamma^3(2\pi)^{-3/2} e^{-\frac{1}{2}\gamma^2 r_p^2} \tag{4.2}$$

with an r.m.s. charge radius $\langle r^2 \rangle = 3/\gamma^2$.

Denoting the error function by $\phi(x) = (2/\pi^{\frac{1}{2}}) \int_0^x e^{-t^2} dt$, the latter potential is

$$V_c = \frac{Z\epsilon^2}{r_p} \phi\left(\frac{\gamma r_p}{2^{1/2}}\right) \tag{4.3}$$

with the convenient integral representation,

$$V_c = \sqrt{\frac{2}{\pi}}\, Z\epsilon^2 \int_0^\gamma e^{-\frac{1}{2}x^2 r_p^2} dx \tag{4.4}$$

The basic integral is one with n = m = 0. Employing the coordinate transformation (3.15) - (3.19) and trivial changes in notation, the result is the same as for the $V_{np}$-amplitude of the preceding chapter. The integrals with n and m $\neq$ 0 can then be obtained by differentiating this result with respect to the parameters a and b. The Coulomb amplitude can be gotten analogously by (numerically) integrating with respect to the parameter a.

The complicated nature of the above procedure makes it suitable only for machine computation.

## C. PROTON-TARGET INTERACTION AMPLITUDE WITH AN OSCILLATOR NEUTRON WAVE FUNCTION

Much simpler expressions for the amplitude than those suggested above can be obtained by using an harmonic oscillator eigenfunction (Appendix D) in place of the previous square well function. This de-

vice permits use of the generalized center-of-mass transformation (GCMT) described in Appendix D to split the six-fold integral with coupled variables into a short sum of independent, easily evaluated, three-fold integrals.

The use of oscillator functions to represent independent particle motion in the nucleus is so widespread that it might be thought no justification was required. However, the stripping reaction is sensitive to the tail of the captured particle wave function, and it is precisely here that the oscillator is at its worst viz-a-viz the free particle Hankel functions. In particular, the oscillator functions would be a poor choice in the $V_{np}$-amplitude of the previous chapter, since the characteristic dependence on binding energy would be lost.

However, the proton-target interaction amplitudes of the present chapter are less sensitive to the exact shape of the neutron wave function. The reason for this is that they are smoother functions of angle than the $V_{np}$-amplitude, and more nearly isotropic. A change in the neutron wave function which would alter the location of the $V_{np}$-peak has no such effect on the $V_{tp}$ terms. It is only important to get the magnitude of the latter correctly and this can be done by a suitable choice of oscillator parameter.

Concerning the deuteron ground state wave function, the results of Ref. (30) are expressible as a combination of three Gaussians. A fair approximation to the Hulthén function can be had with two such terms (Appendix F, Section 3). In the remainder of this chapter, the

results will be given for a single term of this type, expressed as the 1s harmonic oscillator eigenfunction, $v_{100}(p_d,\vec{R}_{np})$. In the actual calculations, $p_d$ is chosen so that the mean inter-particle distance agrees with that in the Hulthén function, $\propto(e^{-ar_{np}} - e^{-br_{np}})$. With $b = 6.2a$, $\langle r_{np}\rangle = 3.11f$ and $p_d = .363f^{-1}$.

The basic approximation is therefore the introduction of the oscillator function with normalization and parameter value left temporarily unspecified:

$$w_{jl}(r_n)\,Y_{lm}(\hat{R}_n) = N_1(3/a^3)^{1/2}\,\theta_{jl}\,v_{nlm}(p_n,\vec{R}_n) \qquad (4.5)$$

The remaining steps are exact:

(a) Combine $v_{nlm}(p_n,\vec{R}_n)$ and $\exp(-\frac{1}{2}\Omega_n^2 r_n^2)$ according to

$$v_{nlm}(p_n,\vec{R}_n)\,e^{-\frac{1}{2}\Omega_n^2 r_n^2} = \sum_{k=1}^{m} D_{knl}\,v_{klm}(\xi_n,\vec{R}_n) \qquad (4.6)$$

(b) Subject the two oscillator functions $v_{klm}(\xi_n,\vec{R}_n)$ and $v_{100}(p_d,\vec{R}_{np})$ to the generalized center-of-mass transformation to split off the dependence on the relative coordinate, $\vec{R}_n - \vec{R}_{np} \equiv \vec{R}_p$.

The remaining integrals are independent and easily evaluated if the potentials are approximated as suggested in Section B. This completes the algebra for the partial amplitude $x_{np}^{jlm}(V_{tp})$, and the others may be found by setting one or both of $\Omega_n$ and $\Omega_p$ equal to zero.

## D. THE LOW PENETRATION APPROXIMATION: DERIVATION OF FORMULAS

Further simplification can be obtained by noting that the deuteron penetration is usually low enough to permit the expansion, when $b_n = 1$,

(eq. (3.3a))

$$f_n(r_n) = 1 - e^{-\frac{1}{2}\Omega_n^2 r_n^2} = \tfrac{1}{2}\Omega_n^2 r_n^2 + \cdots \qquad (4.7)$$

with retention of only the leading term. The rapid diminution of the neutron radial wave function at large $r_n$ provides the justification for (4.7).

As a preliminary step to the use of the GCMT, the factor $r_n^2$ and the neutron radial function (Appendix D) are combined,

$$r_n^2 R_{n\ell}(p_n, r_n) = \sum_{k=n}^{n+1} C_{kn\ell}(p_n) R_{k\ell}(p_n, r_n) \qquad (4.8)$$

While (4.8) is exact, it doubles the number of terms to be handled, so that an approximate relation is more convenient. Temporarily inserting the factor of $r_n^2$ occurring in the volume element $d\vec{R}_n$, (4.8) is replaced by,

$$r_n^4 R_{n\ell}(p_n, r_n) \approx N_2 r_n^2 R_{n\ell}(\rho, r_n) \qquad (4.9)$$

The criterion for the choice of the two normalization constants $N_1$ and $N_2$ (which occur as a single number $N_1N_2$) and the new oscillator parameter $\rho$ occurring in (4.5) and (4.9), can now be given. Taken together, the equations (4.5), (4.7), and (4.9) imply that the function

$$(a^3/3)^{1/2}\theta_{j\ell}^{-1} r_n^2 w_{j\ell}(r_n)\left(1 - e^{-\frac{1}{2}\Omega_n^2 r_n^2}\right) \qquad (4.10)$$

which in the previous chapter was given by,

$$r_n^2\left(1 - e^{-\frac{1}{2}\Omega_n^2 r_n^2}\right) j_\ell(\gamma r_n)/j_\ell(\gamma a) \qquad r_n < a \qquad (4.11)$$

$$r_n^2\left(1-e^{-\frac{1}{2}\Omega_n^2 r_n^2}\right) h_\ell(\kappa r_n)/h_\ell(\kappa a) \qquad r_n > a \tag{4.12}$$

is now to be approximated by the expression,

$$\tfrac{1}{2}\Omega_n^2 N_1 N_2 r_n^2 R_{n\ell}(\rho, r_n) \tag{4.13}$$

The simplest way to fix the unknown constants in (4.13) is to sketch the function (4.11)-(4.12) and then adjust (4.13) to agree with it near the outermost peak. The peak height determines $N_1N_2$, while its position determines $\rho_.$. The relevant information concerning $r^2R_{n\ell}(p,r)$ is in Appendix D, Section 2.

Using (4.13) in (4.1), combining $R_{n\ell}(\rho,r_n)$ with $Y^*_{\ell m}(\hat{R}_n)$ to form $v^*_{n\ell m}(\rho,\vec{R}_n)$, the total $V_{tp}$-amplitude (i.e., the partial "np" term of (4.1) plus the other three partial amplitudes (cf. eq. (3.10) with $b_n=b_p=1$) takes the form:

$$X^{j\ell m}(V_{tp}) = -\tilde{G}\,\theta_{j\ell}\int e^{i(\vec{K}_d\vec{R}_d - \vec{K}_p\vec{R}_{pf})}\,\tilde{V}_{tp}\cdot \\ \cdot v^*_{n\ell m}(\rho,\vec{R}_n)\,v_{100}(p_d,\vec{R}_{np})\,d\vec{R}_n\,d\vec{R}_p \tag{4.14}$$

In (4.14), $\tilde{G} = \frac{1}{2}\Omega_n^2 N_1 N_2 (3/a^3)^{\frac{1}{2}}$, and $\tilde{V}_{tp} \equiv (1-e^{-\frac{1}{2}\Omega_p^2 r_p^2})\,V_{tp}$.

The GCM transformation is defined by:

$$\vec{R}_p = \vec{R}_n - \vec{R}_{np} \qquad \vec{R}_c = (\rho^2\vec{R}_n + p_d^2\vec{R}_{np})/(\rho^2+p_d^2)$$

$$p_c^2 = \rho^2 + p_d^2 \qquad \rho^2 = \rho^2 p_d^2/p_c^2 \qquad d\vec{R}_n\,d\vec{R}_p \to d\vec{R}_c\,d\vec{R}_p \tag{4.15}$$

The new wave vectors,

$$\vec{\varphi}_2 = \tfrac{1}{2}\vec{K}_d + \frac{1}{m+1}\vec{K}_p \approx \tfrac{1}{2}\vec{K}_d$$

$$\vec{\varphi}_3 = \left(\frac{p_d^2 + p_c^2}{2p_c^2}\right)\vec{K}_d - \left(\frac{\rho^2}{p_c^2} + \frac{m p_d^2}{(m+1)p_c^2}\right)\vec{K}_p \qquad (4.16)$$

are associated with the plane wave transformation,

$$\vec{K}_d\cdot\vec{R}_d - \vec{K}_p\cdot\vec{R}_{pf} = \vec{\varphi}_3\cdot\vec{R}_p + \vec{\varphi}_2\cdot\vec{R}_c \qquad (4.17)$$

The eigenfunctions in (4.14) transform according to:

$$v_\beta^*(\rho,\vec{R}_m)\,v_\gamma(p_d,\vec{R}_{mp}) = \sum_{\alpha\alpha_c} A_{\beta\gamma}^{\alpha_c\alpha}\, v_{\alpha_c}^*(p_c,\vec{R}_c)\,v_\alpha^*(p,\vec{R}_p) \qquad (4.18)$$

where the four sets of oscillator quantum numbers have been abbreviated as

$$nlm \equiv \beta \qquad 100 \equiv \gamma \qquad n_c l_c m_c \equiv \alpha_c \qquad \nu\lambda\mu \equiv \alpha \qquad (4.19)$$

The five-fold integral over $d\vec{R}_c d\hat{R}_p$ can be performed explicitly and yields the final formula:

$$X^{jlm}(V_{tp}) = -N_1 N_2 \Omega_m^2\,\theta_{jl}\,(96\pi^5/a^3)^{1/2}\cdot$$

$$\cdot \sum_{\alpha\alpha_c} (-1)^{n_c+1} i^{l_c+\lambda} A_{\beta\gamma}^{\alpha_c\alpha}\, I^{\nu\lambda}(\tilde{V}_{tp})\, Y_{\lambda\mu}^*(\hat{\varphi}_3)\, v_{\alpha_c}^*\left(\frac{1}{p_c},\vec{\varphi}_2\right) \qquad (4.20)$$

The remaining radial integrals in (4.20) are defined as:

$$I^{\nu\lambda}(q) \equiv \int_0^\infty j_\lambda(q_3 r_p)\, R_{\nu\lambda}(p, r_p)\, g(r_p)\, r_p^2\, dr_p \qquad (4.21)$$

These may be done numerically for any potential shapes or, as in Appendix E, by approximating the potential by Gaussian type expressions and using the Weber-Sonine formula (35, p.35 and Appendix E, eq. 2).

E. THE LOW PENETRATION APPROXIMATION: SUMMARY OF FORMULAS

By expressing the single-particle amplitude $B^{\ell m}$, eq. (3.6) as a sum of spherical harmonics of different arguments,

$$B^{\ell m} = \sum_{i=1}^{N} \omega_i^{\ell}\, Y_{\ell m}^*(\hat{q}_i) \qquad (4.22)$$

the cross section and polarization formulas can be given in summed form. The general formulas for these quantities are: (25, 26, 23, p.88).

Differential Cross Section for Capture to a State With Definite $\ell$-Value and Mixed j-Values

$$\sigma_\ell = \sum_{j=\ell\pm\frac{1}{2}} \sigma_{j\ell}$$

$$= \left(\theta^2_{j_+,\ell} + \theta^2_{j_-,\ell}\right) \frac{m_{pf}\, m_{at}}{8\pi^2\hbar^4} \frac{k_p}{k_d} \frac{2J_f+1}{(2J_t+1)(2\ell+1)} \sum_m |B^{\ell m}|^2 \qquad (4.23)$$

This equation refers to the usual situation with protons of different $\ell$-value well separated in angle, so that only the mixing of j-values need be considered.

Polarization for Capture to a State With Definite $\ell$-Value and Mixed j-Values

$$P_z = \frac{2}{3}\left(\theta^2_{j_+,\ell} + \theta^2_{j_-,\ell}\right)^{-1}\left[\frac{\theta^2_{j_+,\ell}}{2j_+ + 1} - \frac{\theta^2_{j_-,\ell}}{2j_- + 1}\right]\frac{\sum_m m\,|B^{\ell m}|^2}{\sum_m |B^{\ell m}|^2} \qquad (4.24)$$

The usual definition of polarization P is the value of (4.24) when the z-axis of the coordinate system is oriented along the direction of the polarization vector $\vec{P}$. Since only the polar vectors $\vec{K}_d$ and $\vec{K}_p$ occur in the matrix element, $\vec{P}$ is necessarily along the direction $\vec{K}_d \times \vec{K}_p$. This comes out automatically when the sums in (4.24) are carried out.

Explicit Formulas for the B-Sums

The fact that $B^{\ell m}$ can be given the form (4.22), which is not obvious from (4.20), permits the m-sums to be carried out:

$$\sum_m |B^{\ell m}|^2 = \frac{2\ell+1}{4\pi}\left\{\sum_{i=1}^N |\omega_i^\ell|^2 + 2\,\mathrm{Re}\sum_{i<j=1}^N \omega_i^\ell \omega_j^{\ell *} P_\ell(\hat{\varphi}_i \cdot \hat{\varphi}_j)\right\} \qquad (4.25)$$

$$\sum_m m\,|B^{\ell m}|^2 = -\frac{2\ell+1}{2\pi}\,\mathrm{Im}\sum_{i<j=1}^N \omega_i^\ell \omega_j^{\ell *} P_\ell'(\hat{\varphi}_i \hat{\varphi}_j)\left[\hat{\varphi}_i \times \hat{\varphi}_j\right]_z \qquad (4.26)$$

For the case $\ell=0$, these are simply $\frac{1}{4\pi}\left|\sum_{i=1}^N \omega_i^0\right|^2$ and zero respectively.

Summary of the Coefficients $\omega_i^\ell$

The coefficient of $Y^*_{\ell m}(\hat{Q}_1)$ in (4.22), $\omega_1^\ell$, can be given by an expression valid for all n- and $\ell$-values. This is simply eq. (3.35) or (3.36), omitting the factors $i^\ell \theta_{j\ell}\, Y^*_{\ell m}(\hat{Q})$, where for the present section it is convenient to put

$$\vec{Q} \equiv \vec{Q}_1 \tag{4.27}$$

The coefficients $\omega_i^{\ell}$ for $i > 1$ require separate specification for the different single-particle capture states. In the following,

$$G \equiv 2\pi^2 (6/a^3)^{1/2} N_1 N_2 \Omega_n^2$$

$$I^{\nu\lambda} \equiv I^{\nu\lambda}(\tilde{V}_{tp}) \qquad \text{(see Appendix E)} \tag{4.28}$$

$$\vec{Q}_4 \equiv \vec{Q}_2 + \vec{Q}_3$$

$$R_{\nu\lambda} \equiv R_{\nu\lambda}\left(\frac{1}{p_c}, q_2\right)$$ = the harmonic oscillator radial function of the indicated arguments, (Appendix D).

n=1, $\ell$=0: 1s-capture

There are three terms in the sum (4.22). In view of the form which (4.25) takes for $\ell$=0, it suffices to give the sum, ($\omega_1^0$ is given above)

$$\omega_1^0 + \omega_2^0 + \omega_3^0 = \omega_1^0 - G R_{10} I^{10} \tag{4.29}$$

n=1, $\ell$=1: 1p-capture

There are three terms in the sum (4.22). ($\omega_1^1$ is given above)

$$\omega_2' = -G(p/p_c) R_{11} I^{10} \tag{4.30}$$

$$\omega_3' = -G(p_d/p_c) R_{10} I^{11} \tag{4.31}$$

n=1, $\ell$=2: 1d-capture

There are four terms in the sum (4.22). ($\omega_1^2$ is given above)

$$\omega_2^2 = -G\left(\rho^2/p_c^2\right) R_{12}\, I^{10} + G\left(p/p_c\right)\sqrt{\frac{3}{5}}\,\frac{q_2}{q_3}\, R_{11}\, I^{11} \qquad (4.32)$$

$$\omega_3^2 = -G\left(p_d^2/p_c^2\right) R_{10}\, I^{12} + G\left(p/p_c\right)\sqrt{\frac{3}{5}}\,\frac{q_3}{q_2}\, R_{11}\, I^{11} \qquad (4.33)$$

$$\omega_4^2 = -G\left(p/p_c\right)\sqrt{\frac{3}{5}}\;\frac{q_4^2}{q_2 q_3} \qquad (4.34)$$

In order to go from the form involving vector-coupled first degree harmonics (see Appendix D, Section 3) which facilitates the integration in (4.14), to the form (4.22) involving only second degree harmonics, the identity is used:

$$\sum_k C^{112}_{k,m}\; Y_{1k}(\hat{B})\; Y_{1m-k}(\hat{C}) = \sqrt{\frac{3}{40\pi}}\;\frac{1}{bc}\;\times$$

$$\times\left\{(\vec{B}+\vec{C})^2\, Y_{2m}(\widehat{B+C}) - b^2 Y_{2m}(\hat{B}) - c^2 Y_{2m}(\hat{C})\right\} \qquad (4.35)$$

This can be derived by expressing $Y_{2m}(\hat{A})$ as the vector coupling of two first degree harmonics, putting $\vec{A} = \vec{B} + \vec{C}$, and suitably grouping the terms.

n=2, $\ell$=0: 2s-capture

There are four terms in the sum (4.22). ($\omega_1^0$ is given above). Again, only the sum need be given:

$$\sum_{i=1}^{4} \omega_i^0 = \omega_1^0 + G\left(p^2/p_c^2\right) R_{20} I^{10} - G\left(p_d^2/p_c^2\right) R_{10} I^{20}$$
$$- G\sqrt{6}\left(p/p_c\right)\left(\hat{Q}_2 \cdot \hat{Q}_3\right) R_{11} I^{11} \qquad (4.36)$$

As in the preceding case, a vector-coupling identity was employed:

$$\sum_m C^{110}_{m\,\cdot\,0}\, Y_{1m}(\hat{B})\, Y_{1-m}(\hat{C}) = -\sqrt{\frac{3}{16\pi^2}}\ \hat{B}\cdot\hat{C} \qquad (4.37)$$

## F. AN APPROXIMATE POLARIZATION FORMULA FOR 1p-CAPTURE

Eq. (4.26) shows that the imaginary part of the optical potential interferes with the real amplitudes to produce the polarization. An interesting formula can be derived from (4.26) by neglecting the real amplitudes resulting from the proton-target interaction, since these are small in comparison with the real neutron-proton interaction term $\omega_1^1$ .

Calculation shows that the contribution of $\omega_3^1$ to the polarization is much less than that of $\omega_2^1$ . This is true for two reasons. One is that $\omega_3^1$ is smaller than $\omega_2^1$ , the other that $\hat{Q}_1$ and $\hat{Q}_3$ are nearly parallel, so that their cross product is small. For capture to a state with definite $j = l \pm \frac{1}{2}$ , the polarization is,

$$P_z = \pm \frac{2}{3(2j+1)} \quad \frac{\sum_m m\,|B^{1m}|^2}{\sum_m |B^{1m}|^2} \qquad (4.38)$$

and according to the above approximations, $B^{1m}$ has the simple form,

$$B^{1m} = a\, Y^*_{1m}\left(\widehat{K_d - K_p}\right) + i\, b\, Y^*_{1m}\left(\hat{K}_d\right) \qquad (4.39)$$

In this equation, finite mass corrections have been neglected so that $\hat{Q}_2 \approx \hat{K}_d$, and $\hat{Q}_1 \approx \hat{K_d - K_p}$. Also, the quantities $a \equiv \omega_1^1$ and $b \equiv -i\omega_2^1$ are real and positive near the stripping peak. $(I^{lo}(\tilde{V}_{tp})$ in (4.30) is negative imaginary due to the absorptive potential.)

Using (4.38) in (4.39), it is a simple matter to derive the following formula:

$$\vec{P} = \pm \frac{4}{3(2j+1)} \frac{k_p}{q_1} \sin\vartheta_p \left[\frac{ab}{a^2+b^2}\right] \hat{n} \qquad (4.40)$$

In this equation, $k_p$ is the proton wave number, $\theta_p$ the scattering angle, and $\hat{n}$ a unit vector in the direction $\vec{K}_d \times \vec{K}_p$. Eq. (4.40) has a number of consequences which appear to be borne out by the experimental results (12):

1. On the stripping peak, where a and b are positive, the sign of the polarization is determined by the capture j-value, being ± when $j = l \pm \frac{1}{2}$.

2. The polarization is a relative minimum on the stripping peak, where a/b is greatest and $ab/(a^2+b^2)$ is least.

3. The polarization rises to a relative maximum as a and b approach equality, and $ab/(a^2+b^2)$ approaches its maximum value of $\frac{1}{2}$.

4. The polarization changes sign when either a or b changes sign, thus giving information about the amplitudes rather than merely their squares. (This bears on the shape of the absorption pattern, as discussed in the next section.)

5. The factors multiplying the square bracket in (4.40) form an envelope limiting the maximum excursions of P regardless of how the stripping amplitudes a and b may vary.

The explanation of the dip in P on the stripping peak and its sign change were given earlier by Newns and Refai (36) on the basis of qualitative arguments.

Because of the two terms of opposite signs occurring in (4.32), the correlation between the sign of the polarization and the j-value for 2d-capture is not as definite as it was above. In addition, the distribution of polarization may exhibit more structure than above.

## G. $Be^9(p,d)Be^8$(GROUND STATE) AT Ep = 12.0 AND 16.5 MEV (37)

The analysis of the $Be^9(d,d)$ reaction described in the next chapter yields the cutoff parameters appropriate to 24 Mev deuterons incident on $Be^9$. In the same sequence of experiments (38), the angular distribution of the beryllium pickup reaction, to which stripping theory is applicable by reciprocity, was also measured. Since the absolute cross section was determined, and the experimental data appear to show a dip near zero degrees (so that the peak position is at least roughly defined), it seemed worthwhile to neglect the fact that in this reaction the deuterons "see" $Be^8$ rather than $Be^9$ and use the $Be^9$ cutoff parameters.

The results of such a calculation are shown in Fig. 4-1. As can be seen, the theory predicts no dip in the forward direction (nor does the Butler formula—the theoretical curve of Fig. 6 in Ref. 38 is

apparently in error). The ambiguity in the small-angle experimental data makes it difficult to determine a unique fit, as the two curves in Fig. 4-1 indicate. The second set of experimental points, taken at 16.5 Mev (39), suggest that the cross section would continue to rise toward zero degrees if the experimental difficulties at small angles could be overcome.

The remarkable tendency of the angular distribution to remain fixed in angle as the deuteron energy varies, remarked in both Refs. 38 and 39, is explained qualitatively by the present theory as follows. An increase in energy tends to throw the peak forward, purely kinematically. On the other hand, the decreasing cutoff radius throws it to larger angles, and the effects approximately cancel. At some higher energy, when "complete" penetration is achieved, the shape should change rapidly but this has not yet occurred at 31 Mev (40).

The two theoretical curves in Fig. 4-1 exhibit the qualitative features expected from the present theory—smaller radii than in the Butler theory and larger reduced widths. The two values of $\theta^2$ indicated in Fig. 4-1 correspond to the predictions of intermediate coupling theory (41) in the jj- and LS-coupling limits, but there is no possibility of distinguishing between them on the basis of the present results. (The LS-coupling reduced width was computed assuming that the ground state of $Be^9$ was pure $^{22}P_{3/2}$ [41] (Ref. 42), while that of $Be^8$ was pure $^{11}S_0$ [4], (43), and using the p-shell, LS-coupling, coefficients of fractional parentage of Ref. 44. The single-particle reduced width was obtained

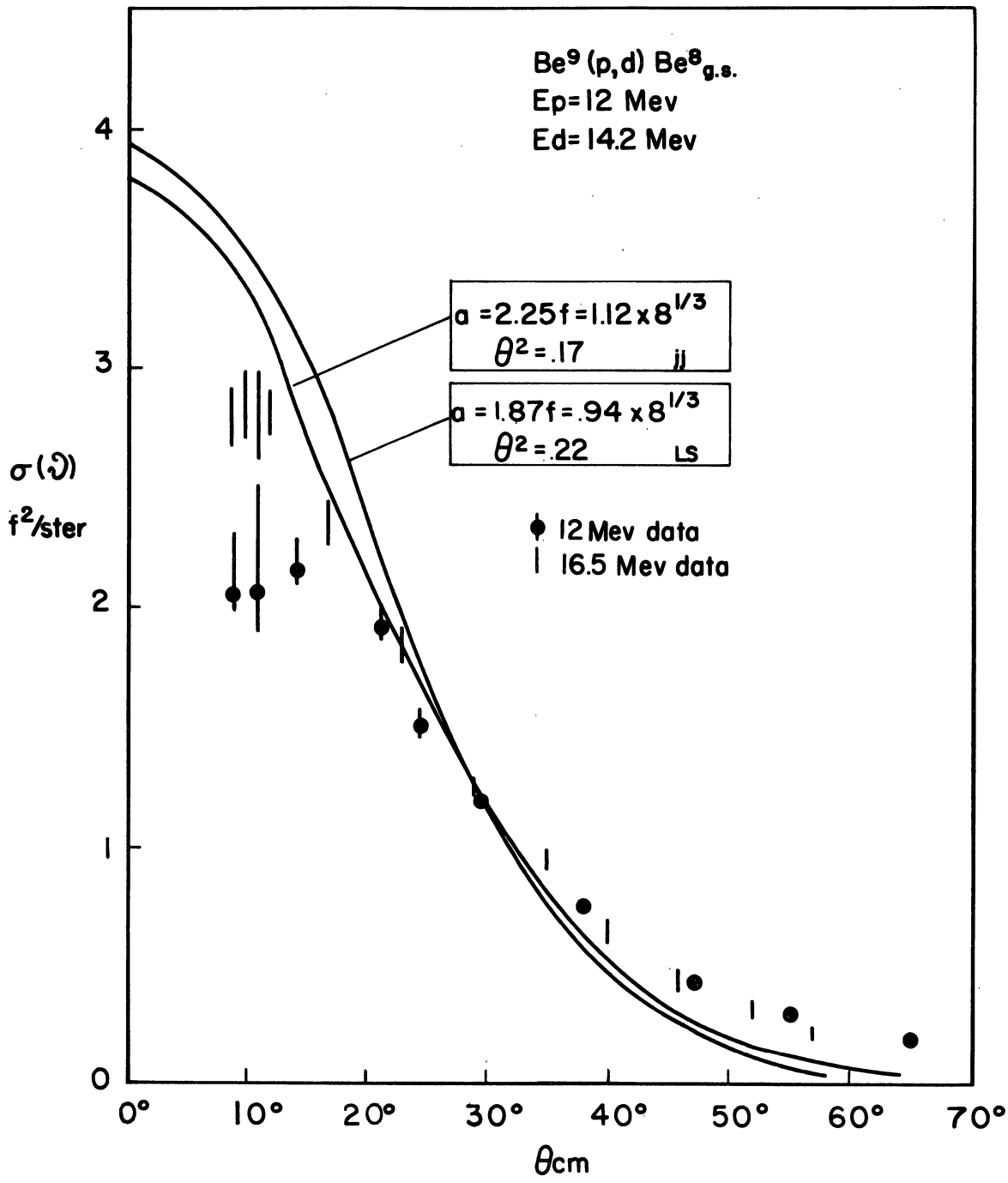


Fig. 4-1. Comparison of theory and experiment for the pickup reaction $Be^9(p,d)Be^8$ (ground state) at 12 Mev. Proton-target interaction has been neglected.

from Ref. 14. In jj-coupling, the $Be^9$ ground state was assumed to have seniority one, $Be^8$ seniority zero. The c.f.p. for this case are given by an explicit formula (45).)

Because of the ambiguity in fitting the curve and the difference in energy between this reaction and the one from which the cutoff parameters were determined, the actual numbers are of only qualitative significance. They do however show that the introduction of a proton cutoff results in a decrease of nuclear radius, and increase of reduced width compared to the Butler theory. For example, the latter theory applied to the 16.5 Mev data (39) gives a radius of 3f, and $\theta^2 = 0.024$, about a factor of ten lower than the intermediate coupling theory values.

The theoretical curves of Fig. 4-1 were computed from eq. (3.36), the proton-target interaction being neglected.

H. $Be^9(d,p)Be^{10}$ (GROUND STATE) AT $E_d = 8.0$ MEV (46)

The deuteron cutoff parameters used in the previous section are not applicable at 8 Mev because the incident wave penetrates much more at the higher energy. The curves described in this section were drawn after adjusting both the radius a and the cutoff parameter, $\Omega_n=\Omega_p=\Omega$. The values used here are a = 4.0f and $\Omega = 0.226f^{-1}$, the latter implying that the incident wave falls to half intensity at either $r_n$ or $r_p = 6.9f$.

The experimental points are from Holt and Marsham (47) at 8.0 Mev. The absolute cross section was not measured, but in determing the re-

duced width, a peak height of $0.40f^2$/ster was assumed determined by interpolating between two absolute cross section measurements at 3.6 Mev (48) and 14.5 Mev (32). This results in a value of about 2.5 for the ratio to the single-particle square well reduced width. This may be compared to the intermediate coupling theory value of approximately 2.2 (49) and the Butler theory value of 0.2(27, p.204).

The solid curve, labelled A in Fig. 4-2, is the prediction of the present theory, including only the $V_{np}$-amplitude (Chapter 3) and the incoherent (absorptive proton-target potential amplitude, Chapter 4). Curve D illustrates the "isotropic" nature of the latter contribution, and the manner in which the $V_{np}$-cross section "rides" on it. The imaginary potential depth used here was 6.4 Mev, obtained by fitting the ratio of the experimental cross sections at the peak and at zero degrees. The agreement of this depth with those encountered in (p,p) elastic scattering analyses is an indication of the overall consistency of the present theory, although its similarity to the value obtained in Chapter 5, Section E, is fortuitous.

The lack of a minimum in the theoretical curve A (following the main peak) is due to the too-gradual cutoff embodied by (3.3). The theoretical curve has a strong "Born approximation component" which has no node (5) and which dominates the overall cross section. To see that this behavior reflects the shape of the neutron cutoff, curve B is the prediction of the formula given in Chapter 3, Section F, which has a

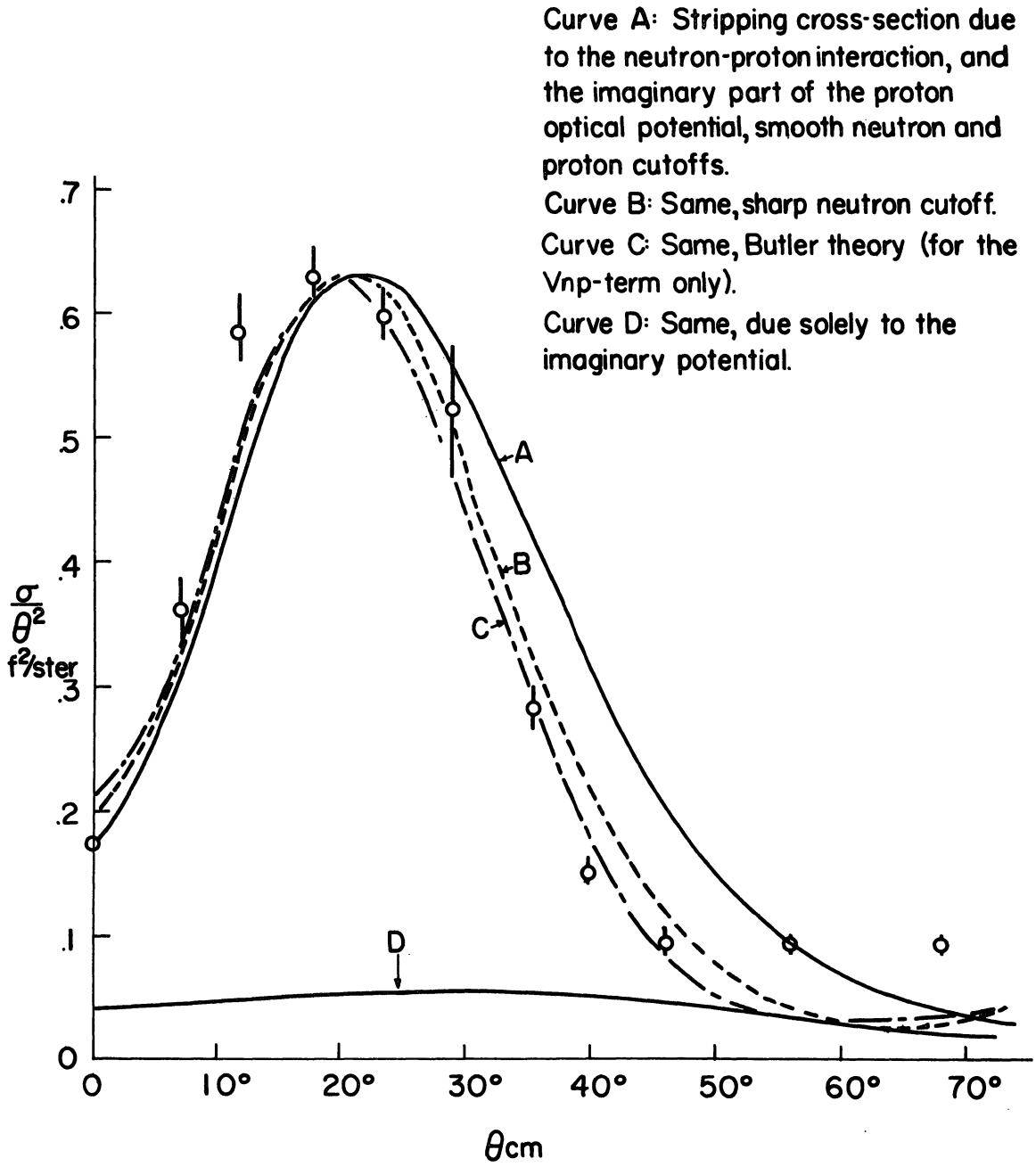


Fig. 4-2. Comparison of theory and experiment for the reaction $Be^{9}(d,p)Be^{10}$ (ground state) at 8 Mev. The theoretical curves illustrate the effect of differently shaped cut-off functions on the angular distribution.

sharp neutron cutoff of the Butler type, plus a smooth proton cutoff (3.3b). The height of this curve has been normalized to agree with Curve A since despite its incorrect shape near the minimum, the latter curve is the most reliable in absolute height.

Finally, Curve C is a simple Butler curve, involving a sharp neutron cutoff and no proton cutoff, normalized in height to Curve A. Evidently the difference in proton cutoffs between Curves B and C makes little difference in the shape of the angular distribution. (The heights of Curves B and C before normalization are of course entirely different.)

The agreement among the three curves forward of the stripping peak is striking, but expected, since this part of the curve is determined by the stripping at large impact parameters, where the three matrix elements are essentially identical.

Figure 4-3 shows the $V_{np}$-amplitudes corresponding to the cross sections in Fig. 4-2. These are labelled A,B, and C, with A supplying the normalization. Curve D is that part of the absorptive potential amplitude which is effective in producing polarization and the curves $P_a$, $P_b$, and $P_c$ show the polarization resulting from the interference of Curve D with each of A, B, and C, according to the simplified formula (4.40). The rather small difference in angular distribution between Curve A on the one hand and Curves B and C on the other (Fig. 4-2) is greatly magnified in the polarization curves. The latter are therefore sensitive to the shape of the neutron cutoff function, and can provide information

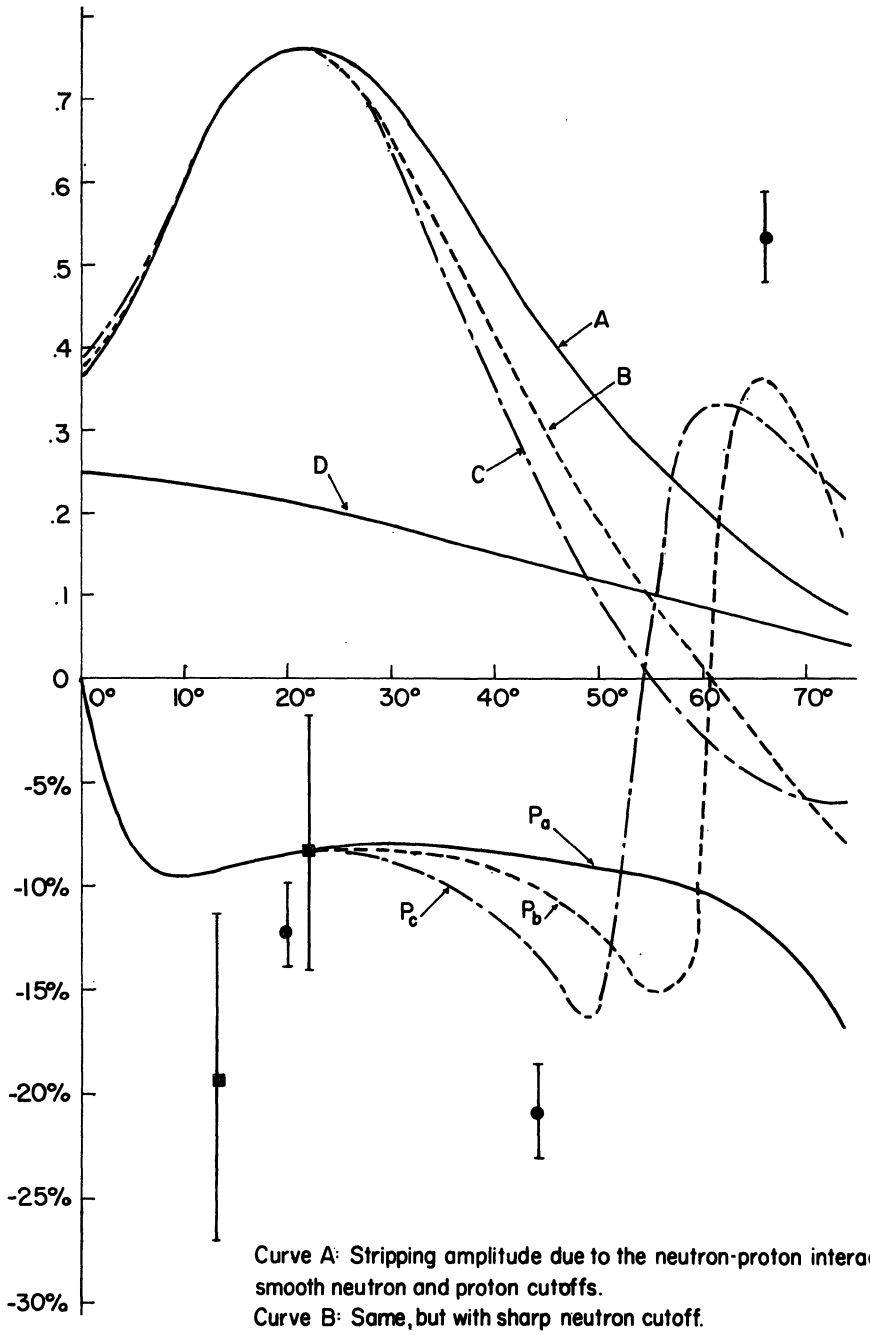


Curve A: Stripping amplitude due to the neutron-proton interaction, smooth neutron and proton cutoffs.
Curve B: Same, but with sharp neutron cutoff.
Curve C: Same, Butler theory.
Curve D: Amplitude due to the imaginary part of the proton optical potential.
Curves $P_a$ $P_b$ $P_c$: Polarizations corresponding to curves A, B, and C.
Experimental (Green and Parkinson)
Experimental (Hird, et al)

Fig. 4-3. Stripping amplitudes and polarizations for the $Be^9$ (d,p) $Be^{10}$ (ground state) reaction at 8 Mev, illustrating the effect of differently shaped cutoff functions.

about the degree of transparency of the nucleus in cases where the angular distributions are ambiguous (50, 51, Fig. 11). A transition from the "opaque nucleus" of the Butler theory, to the "transparent nucleus" of the Born approximation as the energy increases, would not be unexpected, and could be easily analyzed with the present or similar formulas.

The experimental points (52) are in reasonable agreement with either curve $P_b$ or $P_c$. The remaining discrepancies are in part due to the omission of the spin-orbit coupling between the proton and the nucleus. A similar polarization curve, exhibiting the initial rise, the dip on the stripping peak, and the subsequent rapid sign change, is also exhibited by the more extensive measurements on the $C^{12}(d,p)C^{13}_0$ reaction (53). The close similarity between the carbon and beryllium data implies that the present theory will be in agreement with the former also, and this is borne out by preliminary calculations (37).

The effect of the Coulomb potential is illustrated by Fig. 4-4. Curve A is the part of the cross section due solely to the Coulomb potential, curve B is the interference term between the Coulomb amplitude and the $V_{np}$-amplitude, and curve C is the cross section due to both terms, the real and imaginary nuclear potential amplitudes having been omitted. The effect of the Coulomb potential is reduced by the inclusion of the real nuclear attraction. Thus, a Gaussian potential, $V_p = -30 \exp(-0.44r_p^2)$ Mev reduces the interference term to that given by curve D. The latter is negative at small angles, where the repulsive,

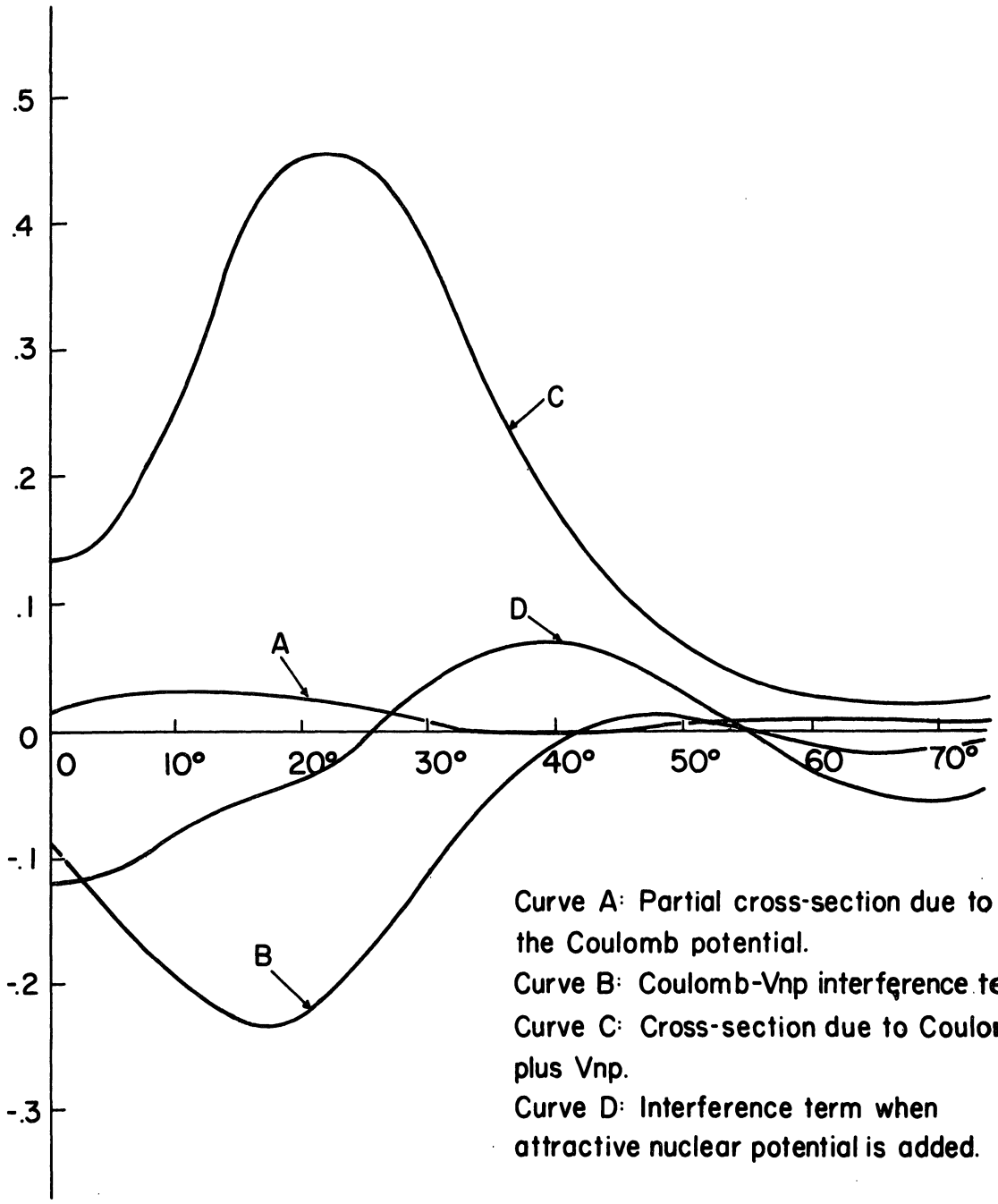


Fig. 4-4. Effect of the Coulomb and real nuclear potentials on the stripping cross section for $Be^{9}(d,p)Be^{10}$ at 8 Mev.

large impact parameter Coulomb potential dominates. At about 25°, the attractive nuclear potential begins to dominate and the curve changes signs.

Apart from the change in peak height in going from Curve A of Fig. 5-2 to Curve C of Fig. 4-4, the Coulomb potential has very little effect on the peak shape or position. This is contrary to the effect sometimes seen in distorted wave calculations, that the Coulomb field broadens the peak and shifts it to larger angles (3 , Figs. 7(a),7(b), 10(a), 10)b); 54). The latter effect probably requires a stronger Coulomb field or lower deuteron energy than in the present reaction.

# CHAPTER V

# ELASTIC SCATTERING OF DEUTERONS BY COMPLEX NUCLEI

## A. SUMMARY AND CONCLUSIONS

In this chapter the cutoff Born approximation will be applied to the elastic scattering of deuterons. This is a logical application of the formalism used in the preceding chapters for the (d,p) reaction and permits in principle a determination of the cutoff parameters indendently of the latter. Starting from the exact matrix element (5.1), use of the cutoff Born expression (3.2) leads to simple formulas for the scattering amplitudes.

Section B discusses the approximations that are employed, while Section C summarizes the final formulas. These are derived in Section D. The $Be^9$(d,d) reaction at 24 Mev is analyzed in Section E and compared with the cutoff Born approximation prediction of $Be^9$(n,n) and (p,p) at corresponding energies (i.e., one half $E_d$.)

The results of this chapter represent an approximate method for treating the (d,d) reaction as a three-body problem. Exact potential scattering analyses have been made for this reaction using a single optical potential and considering the deuteron as a particle of mass two, charge one (3, 55, 56). The present method would appear to be more directly related to the nucleon scattering formalism.

If the optical potentials derived from elastic nucleon scattering are used in the present (d,d) matrix element, then the absorptive potential representing specifically deuteron dissociation is neglected (Chapter 2, Section B). This effect can be approximately allowed for by readjusting the penetration parameters. The $Be^9$(d,d) analysis shows (Section E) that the deuteron cutoff occurs considerably further out (approximately 1.2 to 1.5f) than in the corresponding nucleon reactions. This appears to be a reason why plane wave theories enjoy some success for deuteron induced reactions at 5-10 Mev, when distortion effects are important in nucleon scattering at half these energies.

Consistent with the above remark is the fact that the theoretical deuteron angular distribution (Fig. 5-3) fits the experimental data well past the first minimum, whereas the nucleon curves (Figs. 5-1 and 5-2) begin to diverge at that point. Since the theoretical formulas are identical in physical content, this is evidence that the deuteron reaction is closer to a "plane wave reaction" than are the nucleon reactions at corresponding energies.

B. REDUCTION OF THE SCATTERING CROSS SECTION

The exact matrix element for elastic deuteron scattering may be written in the form

$$A^{m_d}_{m_d'}(\vec{K}_f,\vec{K}_i) = -\int e^{-i\vec{K}_f\cdot\vec{R}_d}\psi^*_{np}(\vec{R}_{np})\,\chi^*_{l m_d'}(\sigma_n\sigma_p)\,\mathcal{L}^*_{J_t m_t}(t)$$
$$\times \sum_{i=1}^{A}\left(V_{in}+V_{ip}\right)\Psi(t,\vec{R}_n\sigma_n,\vec{R}_p\sigma_p)\,d\vec{R}_n\,d\sigma_n\,d\vec{R}_p\,d\sigma_p\,dt \qquad (5.1)$$

In this equation the factors are, from left to right, the center-of-mass wave function of the scattered deuteron; its internal wave function; the triplet spin function; the ground state of the target nucleus; the total interactions between target nucleus and neutron and target and proton; and the exact wave function. The integration is extended over the coordinates of the neutron, the proton, and the target nucleons "t," including all spins.

To simplify (5.1), the many-body interactions are replaced by optical potentials,

$$\sum_{i=1}^{A} (V_{in} + V_{ip}) \rightarrow V_n + iU_n + V_p + iU_p + V_c \qquad (5.2)$$

and $\Psi$ is approximated by (3.2).

The optical potentials on the r.h.s. of (5.2) do not involve the target coordinates t so that, if we imagine the exact wave function $\psi$ to be expanded in the target eigenfunctions, only the term involving the ground state fails to vanish by orthogonality.

If this reaction were being investigated from a more fundamental viewpoint it would be necessary to take into account the excited state contributions which vanish in this manner, and to discuss the validity of the optical potential replacement (5.2) in the ground-state term. The same points arise in the (d,p) problem and have been considered by

Francis and Watson (4). Briefly, they argue that the excited state contributions are negligible because an interaction strong enough to excite the target nucleus will strongly dissociate the deuteron. The neutron and proton then have to "find" each other (their quotation marks) in order to undergo stripping. Here the process is elastic scattering but the idea is the same. They then show that the ground state component of $\psi$ satisfies an equation in which the many-body interactions of (5.1) are replaced by an optical potential independent of t (their eq. 16). This potential is in general non-local, so that the employment of spherically symmetric, local potentials as in (5.2) is a rather drastic approximation. It can be partially justified by the fact that these same simple potentials appear to work well in the nucleon scattering case, where non-local potentials are also required in principle.

It is also assumed that the internal deuteron wave function in $\psi$ can be taken as the undistorted ground state wave function, neglecting the small D-admixture. Since the deuteron has only one bound state, any "internal" distortion results in dissociation. The same argument as before suggests that we may neglect these dissociated deuterons and in effect keep only the projection of the distorted wave function on the ground state. In addition, unpublished numerical estimates of distortion effects suggest they are small (4,57). It will be essential of course to take account of the absorption which this dissociation represents, and this is done by the cutoff factors in (3.2)

The integrals involved may be carried out most simply if the deuteron ground state is given a Gaussian representation. This is taken the same as in Chapter 4 (Section C).

Finally, and for the reason discussed in Chapter 3, Section A, spin-dependent forces are neglected. Carrying out the final sum and initial average over the square of (5.1) yields the differential cross section in terms of a spatial integral.

$$\sigma(\theta) = |\mathcal{I}|^2 \tag{5.3}$$

$$\mathcal{I} = -\frac{m_{dt}}{2\pi\hbar^2}\int e^{i\vec{\varphi}\cdot\vec{R}_d}\,\psi_{np}^2\left[V_n + iU_n + V_p + iU_p + V_c\right]\times$$

$$\times\left(1 - b_n e^{-\frac{1}{2}\alpha_n^2 r_n^2}\right)\left(1 - b_p e^{-\frac{1}{2}\alpha_p^2 r_p^2}\right) d\vec{R}_n\, d\vec{R}_p \tag{5.4}$$

In this equation, $\vec{Q} = \vec{K}_i - \vec{K}_f$, the momentum transfer and $m_{dt}$ is the reduced mass.

Using the methods in Section D, the integrals in (5.4) can be carried out for any potentials having a Gaussian representation. For simplicity, the results will be given in explicit form only for the simple choices:

$$V_n = -V_{no}\exp\left\{-\frac{1}{2}\tau_n^2 r_n^2\right\} \tag{5.5a}$$

$$U_n = -\tfrac{1}{2}\, e\, U_{no}\, \sigma_n^2 r_n^2 \exp\left\{-\tfrac{1}{2}\sigma_n^2 r_n^2\right\} \qquad (5.5b)$$

$$V_p = -V_{po} \exp\left\{-\tfrac{1}{2}\tau_p^2 r_p^2\right\} \qquad (5.6a)$$

$$U_p = -\tfrac{1}{2}\, e\, U_{po}\, \sigma_p^2 r_p^2 \exp\left\{-\tfrac{1}{2}\sigma_p^2 r_p^2\right\} \qquad (5.6b)$$

$$V_c = \text{equations (4.3) - (4.4)} \qquad (5.7)$$

The results involve only exponentials and the function F of Appendix B, and are summarized in the next section.

C. SUMMARY OF DEUTERON SCATTERING FORMULAS

The real and imaginary potentials do not interfere with each other, so that the differential cross section has the form,

$$\sigma_{dd}(\vartheta_d) = \left[X(V_n) + X(V_p) + X(V_c)\right]^2 + \left[X(U_n) + X(U_p)\right]^2 \qquad (5.8)$$

Each potential amplitude consists of four partial amplitudes (cf.(3.10)),

$$X(V_n) = X_o(V_n) - b_n X_n(V_n) - b_p X_p(V_n) + b_n b_p X_{np}(V_n) \qquad (5.9)$$

$$X(V_p) = X_o(V_p) - b_n X_n(V_p) - b_p X_p(V_p) + b_n b_p X_{np}(V_p) \qquad (5.10)$$

There are three similar equations for $X(V_c)$, $X(U_n)$, and $X(U_p)$.

The $V_n$-amplitude

Let $\alpha_1 = (m_{dt}/2\pi\hbar^2)\ 8\pi^{\frac{3}{2}}\ p^3 V_{no}$.

$$f_{np}^2 = 2p^2 + \Omega_p^2$$

$$d_{np}^2 = 2p^2 + \tau_n^2 + \Omega_n^2 - (2p^2)^2/f_{np}^2$$

$$d_n^2 = \tau_n^2 + \Omega_n^2$$

$$d_p^2 = d_{np}^2 - \Omega_n^2$$

$$t_{np} = (4p^2 + \Omega_p^2)\ q/(4p^2 + 2\Omega_p^2)$$

$$q = |\vec{Q}|$$

Then,

$$X_o(V_n) = \frac{\alpha_1}{2^{3/2}\tau_n^3 p^3}\ e^{-\frac{1}{2}\left(\frac{1}{\tau_n^2} + \frac{1}{8p^2}\right)q^2}$$

$$X_n(V_n) = \frac{\alpha_1}{2^{3/2} d_n^3 p^3}\ e^{-\frac{1}{2}\left(\frac{1}{d_n^2} + \frac{1}{8p^2}\right)q^2}$$

$$X_p(V_n) = \frac{\alpha_1}{d_p^3 f_{np}^3}\ e^{-\frac{1}{2}\left(\frac{t_{np}^2}{d_p^2} + \frac{q^2}{4f_{np}^2}\right)}$$

$$X_{np}(V_n) = \frac{\alpha_1}{d_{np}^3 f_{np}^3}\ e^{-\frac{1}{2}\left(\frac{t_{np}^2}{d_{np}^2} + \frac{q^2}{4f_{np}^2}\right)}$$

The $V_p$-amplitude

Let $\alpha_2 = (m_{dt}/2\pi\hbar^2)\ 8\pi^2\ p^3 V_{po}$.

$$\bar{f}_{np}^2 = 2p^2 + \Omega_n^2$$

$$\bar{d}_{np}^2 = 2p^2 + \tau_p^2 + \Omega_p^2 - (2p^2)^2/\bar{f}_{np}^2$$

$$\bar{d}_n^2 = \bar{d}_{np}^2 - \Omega_p^2$$

$$\bar{d}_p^2 = \tau_p^2 + \Omega_p^2$$

$$\bar{\tau}_{np} = (4p^2+\Omega_n^2)\ q/(4p^2+2\Omega_n^2)$$

Then,

$$X_o(V_p) = \frac{\alpha_2}{2^{3/2}\tau_p^3 p^3}\ e^{-\frac{1}{2}\left(\frac{1}{\tau_p^2} + \frac{1}{\beta_p^2}\right) q^2}$$

$$X_n(V_p) = \frac{\alpha_2}{\bar{d}_n^3 \bar{f}_{np}^3}\ e^{-\frac{1}{2}\left(\frac{\bar{\tau}_{np}^2}{\bar{d}_n^2} + \frac{q^2}{4\bar{f}_{np}^2}\right)}$$

$$X_p(V_p) = \frac{\alpha_2}{2^{3/2}\bar{d}_p^3 p^3}\ e^{-\frac{1}{2}\left(\frac{1}{\bar{d}_p^2} + \frac{1}{\beta_p^2}\right) q^2}$$

$$X_{np}(V_p) = \frac{\alpha_2}{\bar{d}_{np}^3 \bar{f}_{np}^3}\ e^{-\frac{1}{2}\left(\frac{\bar{\tau}_{np}^2}{\bar{d}_{np}^2} + \frac{q^2}{4\bar{f}_{np}^2}\right)}$$

The $U_n$-amplitude

Let $\alpha_3 = (m_{dt}/2\pi\hbar^2)\ 4\pi^2\ p^3 e U_{no}\sigma_n^2$.

$$c_{np}^2 = d_{np}^2 + \sigma_n^2 - \tau_n^2$$

$$c_n^2 = \sigma_n^2 + \Omega_n^2$$

$$c_p^2 = d_p^2 + \sigma_n^2 - \tau_n^2$$

Then,

$$X_o(U_n) = \frac{\alpha_3}{2^{3/2}\sigma_n^5 p^3}\left(3 - \frac{q^2}{\sigma_n^2}\right) e^{-\frac{1}{2}\left(\frac{1}{\sigma_n^2} + \frac{1}{8p^2}\right)q^2}$$

$$X_n(U_n) = \frac{\alpha_3}{2^{3/2} c_n^5 p^3}\left(3 - \frac{q^2}{c_n^2}\right) e^{-\frac{1}{2}\left(\frac{1}{c_n^2} + \frac{1}{8p^2}\right)q^2}$$

$$X_p(U_n) = \frac{\alpha_3}{c_p^5 f_{np}^3}\left(3 - \frac{t_{np}^2}{c_p^2}\right) e^{-\frac{1}{2}\left(\frac{t_{np}^2}{c_p^2} + \frac{q^2}{4f_{np}^2}\right)}$$

$$X_{np}(U_n) = \frac{\alpha_3}{c_{np}^5 f_{np}^3}\left(3 - \frac{t_{np}^2}{c_{np}^2}\right) e^{-\frac{1}{2}\left(\frac{t_{np}^2}{c_{np}^2} + \frac{q^2}{4f_{np}^2}\right)}$$

The $U_p$-amplitude

Let $\alpha_4 = (m_{dt}/2\pi\hbar^2)\, 4\pi^2 p^3 e U_{po} \sigma_p^2$

$$\bar{c}_{np}^2 = \bar{d}_{np}^2 + \sigma_p^2 - \tau_p^2$$

$$\bar{c}_n^2 = \bar{d}_n^2 + \sigma_p^2 - \tau_p^2$$

$$\bar{c}_p^2 = \sigma_p^2 + \Omega_p^2$$

Then,

$$X_o(U_p) = \frac{\alpha_4}{2^{3/2}\sigma_p^5 p^3}\left(3 - \frac{q^2}{\sigma_p^2}\right) e^{-\frac{1}{2}\left(\frac{1}{\sigma_p^2} + \frac{1}{8p^2}\right)q^2}$$

$$X_n(U_p) = \frac{\alpha_4}{\bar{c}_n^5 \bar{f}_{np}^3}\left(3 - \frac{\bar{t}_{np}^2}{\bar{c}_n^2}\right) e^{-\frac{1}{2}\left(\frac{\bar{t}_{np}^2}{\bar{c}_n^2} + \frac{q^2}{4\bar{f}_{np}^2}\right)}$$

$$X_p(U_p) = \frac{\alpha_4}{2^{3/2}\bar{c}_p^{\,5} p^3}\left(3 - \frac{q^2}{\bar{c}_p^{\,2}}\right) e^{-\frac{1}{2}\left(\frac{1}{\bar{c}_p^{\,2}} + \frac{1}{8p^2}\right)q^2}$$

$$X_{np}(U_p) = \frac{\alpha_4}{\bar{c}_{np}^{\,5}\,\bar{f}_{np}^{\,3}}\left(3 - \frac{\bar{t}_{np}^{\,2}}{\bar{c}_{np}^{\,2}}\right) e^{-\frac{1}{2}\left(\frac{\bar{t}_{np}^{\,2}}{\bar{c}_{np}^{\,2}} + \frac{q^2}{4\bar{f}_{np}^{\,2}}\right)}$$

The $V_c$-amplitude

Let $\alpha_5 = -(m_{dt}/2\pi\hbar^2)\ 16\pi\ Z\epsilon^2 p^3$.

$$m_{np}^2 = \bar{d}_{np}^2 - \tau_p^2$$

$$m_n^2 = \bar{d}_n^2 - \tau_p^2$$

$$\rho_{np} = \gamma\bar{t}_{np}/[2m_{np}^2(m_{np}^2+\gamma^2)]^{\frac{1}{2}}$$

$$\rho_n = \gamma q/[2m_n^2(m_n^2+\gamma^2)]^{\frac{1}{2}}$$

$$\rho_p = \gamma\bar{t}_{np}/[2\Omega_p^2(\Omega_p^2+\gamma^2)]^{\frac{1}{2}}$$

Then,

$$X_o(V_c) = \frac{\alpha_5}{4p^3 q^2}\, e^{-\frac{1}{2}\left(\frac{1}{\gamma^2} + \frac{1}{8p^2}\right)q^2}$$

$$X_n(V_c) = \frac{\alpha_5}{m_n \bar{f}_{np}^{\,3}\,\bar{t}_{np}}\, e^{-\frac{1}{2}\left(\frac{\bar{t}_{np}^{\,2}}{m_n^2+\gamma^2} + \frac{q^2}{4\bar{f}_{np}^{\,2}}\right)} F(\rho_n)$$

$$X_p(V_c) = \frac{\alpha_5}{2^{3/2} p^3 \Omega_p q}\, e^{-\frac{1}{2}\left(\frac{1}{\Omega_p^2+\gamma^2} + \frac{1}{8p^2}\right)q^2} F(\rho_p)$$

$$X_{np}(V_c) = \frac{\alpha_5}{m_{np}\bar{f}_{np}^3\bar{t}_{np}} e^{-\frac{1}{2}\left(\frac{\bar{t}_{np}^2}{m_{np}^2+\gamma^2} + \frac{q^2}{4\bar{f}_{np}^2}\right)} F(\rho_{np})$$

D. DERIVATION OF THE SCATTERING AMPLITUDES

If the cutoff functions in (5.6) are multiplied out, the integral splits into four partial amplitudes. The one containing both exponentials, $e^{-\frac{1}{2}\Omega_n^2 r_n^2}\, e^{-\frac{1}{2}\Omega_p^2 r_p^2}$, is denoted by indices "np," the one containing only the neutron exponential by index "n," and the other two by "p" and "o," the last-named term being just the Born approximation amplitude. It is only necessary to evaluate the "np"-term since the others follow from it by setting the appropriate $\Omega$'s equal to zero.

The $V_n$-amplitude

$$X_{np}(V_n) = \left(\frac{m_{dt}}{2\pi\hbar^2}\right)\frac{p^3 V_{no}}{\pi^{3/2}} \int d\vec{R}_n d\vec{R}_p\, e^{i\vec{\varphi}\cdot\vec{R}_d} e^{-\frac{1}{2}\left[2p^2 r_{np}^2 + (\Omega_n^2+\tau_n^2) r_n^2 + \Omega_p^2 r_p^2\right]} \tag{5.11}$$

Replace the variable $\vec{R}_p$ by $\vec{W}_{np} = \vec{R}_p - 2p^2\vec{R}_n/(2p^2+\Omega_p^2)$. This coordinate transformation induces the identity

$$2p^2 r_{np}^2 + \Omega_p^2 r_p^2 + (\Omega_n^2+\tau_n^2) r_n^2 = d_{np}^2 r_n^2 + f_{np}^2 w_{np}^2 \tag{5.12}$$

where $d_{np}^2 = 2p^2 + \Omega_n^2 + \tau_n^2 - (2p^2)^2/f_{np}^2$ and $f_{np}^2 = 2p^2 + \Omega_p^2$. In addition, the plane wave splits according to

$$\vec{\varphi}\cdot\vec{R}_d = \vec{T}_{np}\cdot\vec{R}_n + \frac{1}{2}\vec{\varphi}\cdot\vec{W}_{np} \tag{5.13}$$

with $$\vec{T}_{np} = (4p^2 + \Omega_p^2)\vec{\varphi}/(4p^2 + 2\Omega_p^2) \qquad (5.14)$$

The integral (5.11) then separates into easily integrated factors,

$$X_{np}(V_n) = \left(\frac{m\Delta t}{2\pi\hbar^2}\right) \frac{p^3 V_{no}}{\pi^{3/2}} \int e^{i\vec{T}_{np}\cdot\vec{R}_n} e^{-\frac{1}{2}d_{np}^2 r_n^2} d\vec{R}_n \times$$

$$\times \int e^{i\frac{1}{2}\vec{\varphi}\cdot\vec{W}_{np}} e^{-\frac{1}{2}f_{np}^2 W_{np}^2} d\vec{W}_{np}$$

$$= \left(\frac{m\Delta t}{2\pi\hbar^2}\right) \frac{8\pi^{3/2} p^3 V_{no}}{d_{np}^3 f_{np}^3} e^{-\frac{1}{2}\left(\frac{t_{np}^2}{d_{np}^2} + \frac{q^2}{4f_{np}^2}\right)} \qquad (5.15)$$

When $\Omega_n$ or $\Omega_p$ or both are set equal to zero in (5.15), it remains unaltered in form but the constant $d_{np}$ is replaced by $d_p$, $d_n$, or $d_o$, respectively, with similar replacements for $f_{np}$ and $t_{np}$.

The $U_n$-amplitude

The "np" partial amplitude involving $U_n(r_n)$ can be obtained by a coordinate transformation as in the previous paragraph or by differentiating (5.15) with respect to $\tau_n^2$ and suitably relabelling the potential parameters. The results have been summarized in Section C.

The $V_p$- and $U_p$-amplitudes

These may be obtained by interchanging the indices "n" and "p" in the results for the $V_n$- and $U_n$-amplitudes. Those quantities which are not invariant under this exchange have been denoted by a bar in Section C.

The $V_c$-amplitude

Using the integral representation (4.4) for the potential of a Gaussian charge distribution, the "np" amplitude becomes

$$X_{np}(V_c) = -\left(\frac{m dt}{2\pi\hbar^2}\right)\frac{2^{1/2}p^3 Z\epsilon^2}{\pi^2}\int_0^\gamma dx \int e^{i\vec{\varphi}\cdot\vec{R}_d} \times e^{-\frac{1}{2}\left[2p^2 r_{np}^2 + \Omega_n^2 r_n^2 + (\Omega_p^2 + x^2) r_p^2\right]} d\vec{R}_n d\vec{R}_p \tag{5.16}$$

Introduce the same coordinate transformation as in the $V_n$-amplitude, but with n and p interchanged and with x replacing $\tau_n$. The integral over $d\vec{R}_p d\vec{W}_{np}$ is the same as in that case and yields

$$X_{np}(V_c) = -\left(\frac{m dt}{2\pi\hbar^2}\right)\frac{8\sqrt{2}\,\pi Z\epsilon^2 p^3}{f_{np}^3} e^{-\frac{q^2}{2f_{np}^2}} \times \int_0^\gamma (m_{np}^2 + x^2)^{-3/2} e^{-\bar{t}_{np}^2/2(m_{np}^2 + x^2)} dx \tag{5.17}$$

The remaining integral was evaluated in connection with the (d, p) reaction (Appendix B). The results are summarized in Section C, the Born term $X_0(V_c)$ being obtained from the asymptotic form of F(x) given in Appendix B.

Inspection of the Born approximation partial amplitude just mentioned shows that it is simply the Rutherford amplitude for point charge scattering multiplied by an exponential factor involving the finite sizes of the nucleus and deuteron. The latter causes a gentle decrease of the Born amplitude $X_0(V_c)$, below Rutherford as the scattering angle increases. When the cutoff terms are added to give the complete Coulomb amplitude $X(V_c)$, this decrease is greatly enhanced, to the point that $X(V_c)$ may become positive and interfere constructively with the real

nuclear amplitudes $X(V_n)$ and $X(V_p)$. This consequence of the cutoff theory is rather different from Born approximation, the extra oscillation introduced by the cutoff being in close analogy to the different (d,p) angular distributions predicted by the Born approximation and the Butler theory (Chapter 4, Section H).

As is well-known, the Born approximation for point charge scattering gives exactly the Rutherford cross section, when a suitable shielding factor is used at large distances. The result for $X_o(V_c)$ is in precise analogy to this result since it is obtained from $X_p(V_c)$ in the limit as $\Omega_p$ approaches zero. The cutoff exponential $\exp(-\frac{1}{2}\Omega_p^2 r_p^2)$ therefore provides the shielding factor necessary to get a finite result.

In the present theory, as in the point charge case, one has a built-in agreement with experiment at very small angles, where the actual scattering also approaches Rutherford. However, at high values of the Coulomb parameter $Z\epsilon^2/\hbar v$ the agreement is almost completely fortuitious, there being practically no similarity between the plane incident wave, cutoff or not, and the Coulomb wave function. This remark has been slightly qualified since it is true that the reason this mathematical accident occurs for the Coulomb field is a consequence of its long-range, and the approximate validity of the Born approximation at large impact parameters clearly plays a role.

## E. ANALYSIS OF THE REACTIONS $Be^9(n,n)$, (p,p), AND (d,d)

If the neutron and proton optical potential parameters are considered known, then the formulas of Section C involve four adjustable parameters, $b_n$, $b_p$, $\Omega_n$, and $\Omega_p$. As a trial procedure, $b_n$ and $b_p$ can be set equal to one, and $\Omega_n$ set equal to $\Omega_p$. This reduces the problem to the specification (by trial and error) of a single parameter.

On the other hand, it might be thought that the cutoff parameters could themselves be determined from the corresponding nucleon scattering data. According to Chapter 2, these would be at approximately half the deuteron energy. The following paragraphs describe the results of such a procedure, using data on $Be^9(n,n)$ at 14.7 Mev (58), $Be^9(p,p)$ at 12.0 Mev (38) and $Be^9(d,d)$ at 24.0 Mev (38).

### $Be^9(n,n)$ at 14.7 Mev

Nakada, et al., (58) measured the elastic scattering of neutrons from $Be^9$, using as a source the (d,n) reaction on tritium. Because of their scattering geometry, the incident neutron energy varied with the angle of scattering. This was allowed for by employing the correct (variable) energy in the calculation of momentum-transfer versus scattering angle. Any change in the optical parameters over the small energy spread involved was of course neglected.

The total cross section as given by them was $151 \pm 3$ $f^2$. Using the wave number appropriate to zero degrees, the optical theorem gave $[\mathrm{Im}\ f(0°)]^2 = 82.6$ $f^2$/ster, (for $\sigma_t = 150$ $f^2$). The measured forward

cross section extrapolated from their Fig. 5 was 95 $f^2$/ster in the laboratory system, 76.9 center-of-mass. This agrees with the value of about 77 $f^2$/ster extrapolated from their c.m. plot using the theoretical Bjorklund-Fernbach curve as a guide (59). Since this is smaller than the value 82.6 given above, it is incompatible with the total cross section.

The value of the non-elastic cross section which they measured, 57 ± 6 $f^2$, is higher than the value due to MacGregor, et al., (60) which they quote, and also higher than Howerton's (61). Assuming therefore that their value of $\sigma_t$ was too high, the value 77 $f^2$/ster was accepted as the forward cross section. An isotropic component of 1.1 $f^2$/ster, determined from the height of the first experimental minimum, was subtracted and regarded as an incoherent component (62, 63, p. 416). This avoids the necessity for computing the compound nucleus contribution (64) and is sufficiently accurate when the effect is as small as it is here. This gave a coherent zero degree cross section $\sigma_o$ = 75.9 $f^2$/ster. In turn this implied a total cross section of 144 $f^2$, assuming the equality $k\sigma_t = 4\pi(\sigma_o)^{\frac{1}{2}}$, as is implied by the data.

A purely imaginary forward scattering amplitude, as is the case here, implied a purely imaginary potential in the cutoff Born approximation. The interpretation of this is not that the real potential is actually zero, but that it plays a negligible role in the forward scattering, most probably because it is concentrated at smaller radial distances than the absorptive potential.

The cutoff Born approximation transition matrix element,

$$\int e^{-i\vec{K}_f\cdot\vec{R}_n} U_n(r_n)\, e^{i\vec{K}_i\cdot\vec{R}_n}\left(1-b_n e^{-\frac{1}{2}\Omega_n^2 r_n^2}\right) d\vec{R}_n \qquad (5.18)$$

where $U_n(r_n)$ is given by (5.5b), yields the differential cross section:

$$\sigma_{nn}(\vartheta_n) = .0597\, m_{nt}^2 \left(U_{no}/\sigma_n^3\right)^2 \left[\left(1-\frac{2x_\sigma^2}{3}\right) e^{-x_\sigma^2} - b_n p_\sigma^5 \left(1-\frac{2p_\sigma^2 x_\sigma^2}{3}\right) e^{-p_\sigma^2 x_\sigma^2}\right]^2 \qquad (5.19)$$

The notation employed here is: $m_{nt}$= reduced mass of neutron, $X_\sigma^2 = q^2/2\sigma_n^2$, $p_\sigma^2 = (1+\Omega_n^2/\sigma_n^2)^{-1}$, $q^2 = |\vec{K}_i - \vec{K}_f|^2 = .09567\,(\frac{m_{nt}^2}{m_n})\, E_{lab}(1-\cos\Theta)$, and all quantities are to be expressed in nuclear units (Appendix A).

Since the Bjorklund-Fernbach potential radius (65) is too large to fit this experiment (as indicated in Fig. 3 of Ref. 58, the theoretical curve goes through its first minimum at too small an angle), a radius was used which reproduced the node position, although it is not clear that this simple theory should still be accurate at an 80° scattering angle.

While the parameters are not uniquely determined, the set $b_n$=1, $\sigma_n$= 0.619f$^{-1}$, $\Omega_n$= 0.701f$^{-1}$, $U_{no}$ = 10.7 Mev, appear reasonable and fit the forward scattering as indicated in Fig. 5-1. The imaginary potential peaks at 2.28f = 1.1(9)$^{\frac{1}{3}}$, while the incident wave falls to half its asymptotic intensity at 2.24f.

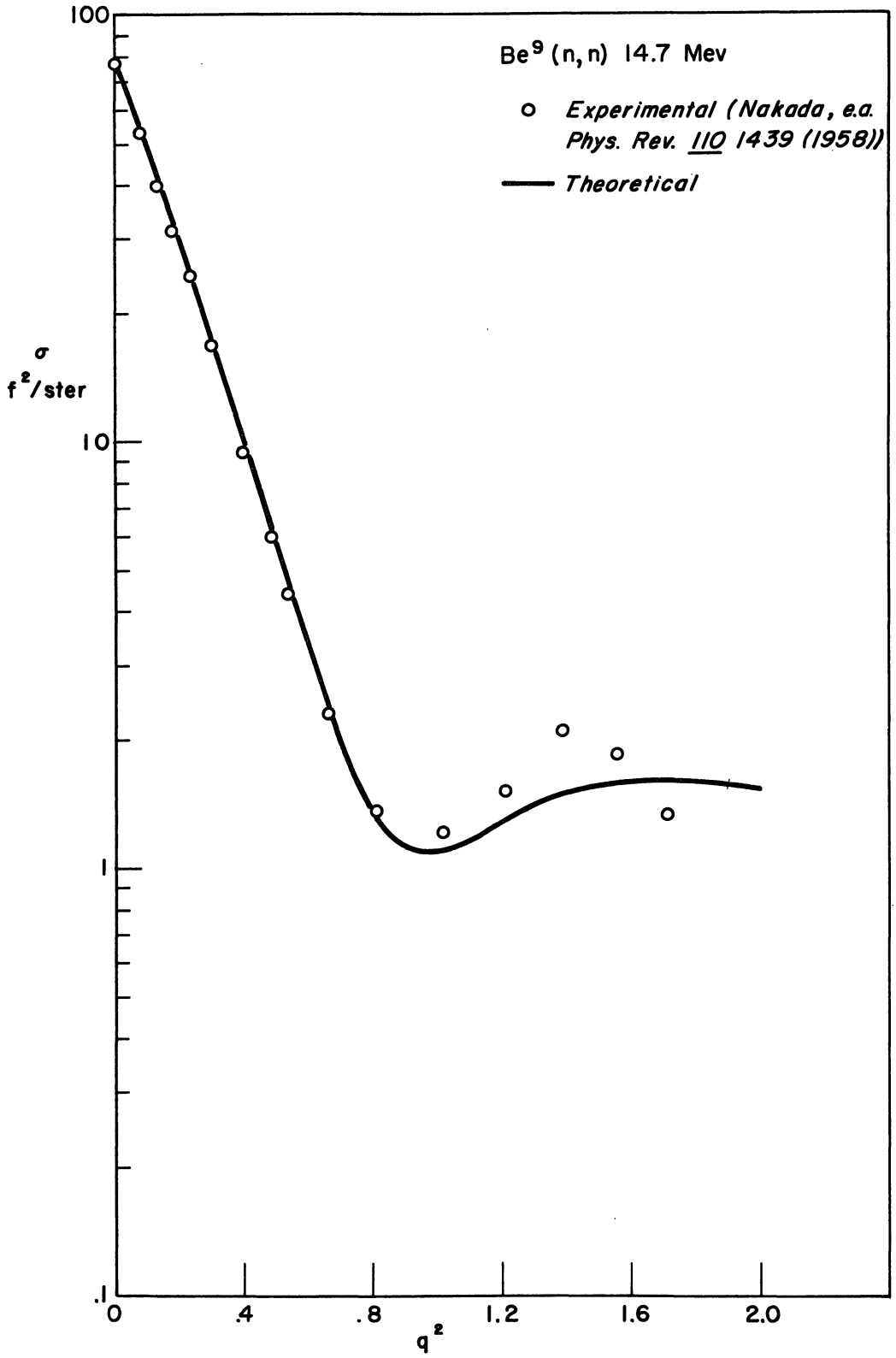


Fig. 5-1. Comparison of theory and experiment for the reaction $Be^9(n,n)$ at 14.7 Mev.

The logarithmic presentation in Fig. 5-1 emphasizes the disagreement past the first minimum, but is helped somewhat by the isotropic component mentioned earlier, which eliminates the true node possessed by (5.19).

Be$^9$(p,p) at 12.0 Mev

The data of R. G. Summers-Gill (38) were taken at nearly the neutron energy of the previous section. The angular distribution was computed using (arbitrarily) the same ratio $\Omega_p/\sigma_p$ as in the neutron case, but readjusting $\sigma_p$ to fit the node position. This could be done with the parameters $b_p$=1, $\sigma_p$ = 0.521f$^{-1}$, $\Omega_p$ = 0.590f$^{-1}$, and $U_{po}$ = 6.2 Mev, resulting in the curve of Fig. 5-2.

The first minimum is at a smaller value of momentum transfer than in the neutron case, suggesting that the beryllium nucleus appears larger to a proton than to a neutron. This phenomenon may be connected with the difference between the electromagnetic radii of the neutron and proton (66). The proton potential in this case peaks at 2.71f, about 0.4f further out than the neutron potential, while the half intensity point of the incident wave is at 2.7f, so that the proton wave penetrates less than the neutron wave in the previous case. The lower incident energy, the Coulomb repulsion, and the wider spread of the absorptive potential all work in this direction, although the lower value of $U_{po}$ than $U_{no}$ favors greater penetration. If $U_{po}$ were to be adjusted upward to around 11 Mev, nearer the neutron value, the pen-

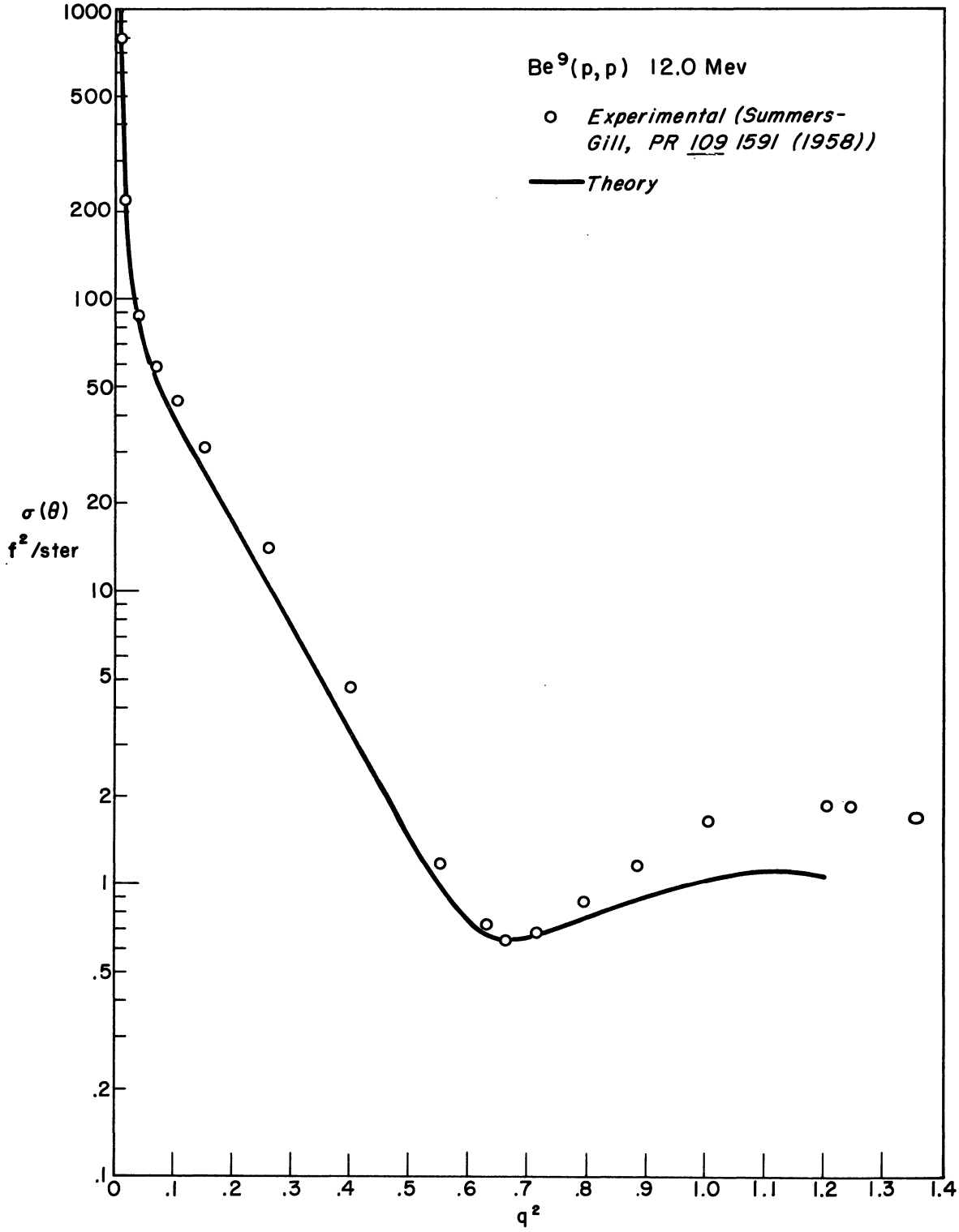


Fig. 5-2. Comparison of theory and experiment for the reaction $Be^9(p,p)$ at 12 Mev.

etration would be even further decreased. (This would have a negligible effect on the angular distribution, which depends on $U_{po}$ and $\Omega_p$ only through the combination $U_{po}\Omega_p^2$.)

In computing the theoretical cross section it was assumed that in this reaction the real nuclear potential could again be neglected. This is a weak application of "charge independence" since the Coulomb repulsion tends to keep the proton away from the inner real potential. In this situation it is only necessary to add (incoherently) the Coulomb cross section to that due to the absorptive potential (5.19). For a Gaussian charge distribution, (4.2) - (4.4), the matrix element,

$$\int e^{-i\vec{K}_f\cdot\vec{R}_p}\left(\frac{Ze^2}{r_p}\right)\phi\left(\frac{\gamma r_p}{\sqrt{2}}\right)\left(1-b_p e^{-\frac{1}{2}\Omega_p^2 r_p^2}\right)e^{i\vec{K}_i\cdot\vec{R}_p} \tag{5.20}$$

yields the differential cross section,

$$\sigma_{COUL}(\vartheta_p) = \left[X(V_c)\right]^2 \tag{5.21}$$

$$X(V_c) = -\left(\frac{m_p t}{2\pi\hbar^2}\right)\left(\frac{2\pi Z e^2}{\gamma^2}\right)\left[e^{-x_\gamma^2}/x_\gamma^2\right.$$

$$\left. - 2p_\gamma b_p \gamma^2 \Omega_p^{-2} e^{-p_\gamma^2 x_\gamma^2} F(\lambda)/\lambda\right] \tag{5.22}$$

The new symbols are:

$$x_\gamma^2 = q^2/2\gamma^2 \qquad p_\gamma^2 = (1 + \Omega_p^2/\gamma^2)^{-1}$$

and

$$\lambda = p_\gamma \gamma x_\gamma / \Omega_p$$

F(x) is defined in Appendix B.

The rms radius <r> = 3.04 for beryllium was obtained from Table VI of Ref. 66. The remarks concerning the Rutherford component of the $V_c$-amplitude (Section D) apply to eq. (5.22) also.

Be$^9$(d,d) at 24.0 Mev

The data of Summers-Gill (38) are at a suitable energy for comparison with the above (n,n) and (p,p) reactions. If the parameters determined there are taken over unchanged, the (d,d) cross section is considerably over-estimated. To obtain agreement, smaller values of $\Omega_n$ and $\Omega_p$ may be employed, and interpreted as reflecting the additional absorption due to deuteron dissociation.

The curve of Fig. 5-3 was obtained using the same $b_n$, $b_p$, $\sigma_n$, $\sigma_p$, $U_{no}$, and $U_{po}$ as in the previous reactions, but with $\Omega_n = \Omega_p = 0.39$. The incident wave falls to half intensity at 4.0f, about 1.5f further out than in the (n,n) and (p,p) cases. The fact that the fit to the experimental points in Fig. 5-3 appears to extend to larger values of momentum transfer than in the nucleon cases may be due to this confinement of the reaction to larger separations where the neglect of distortion is better justified.

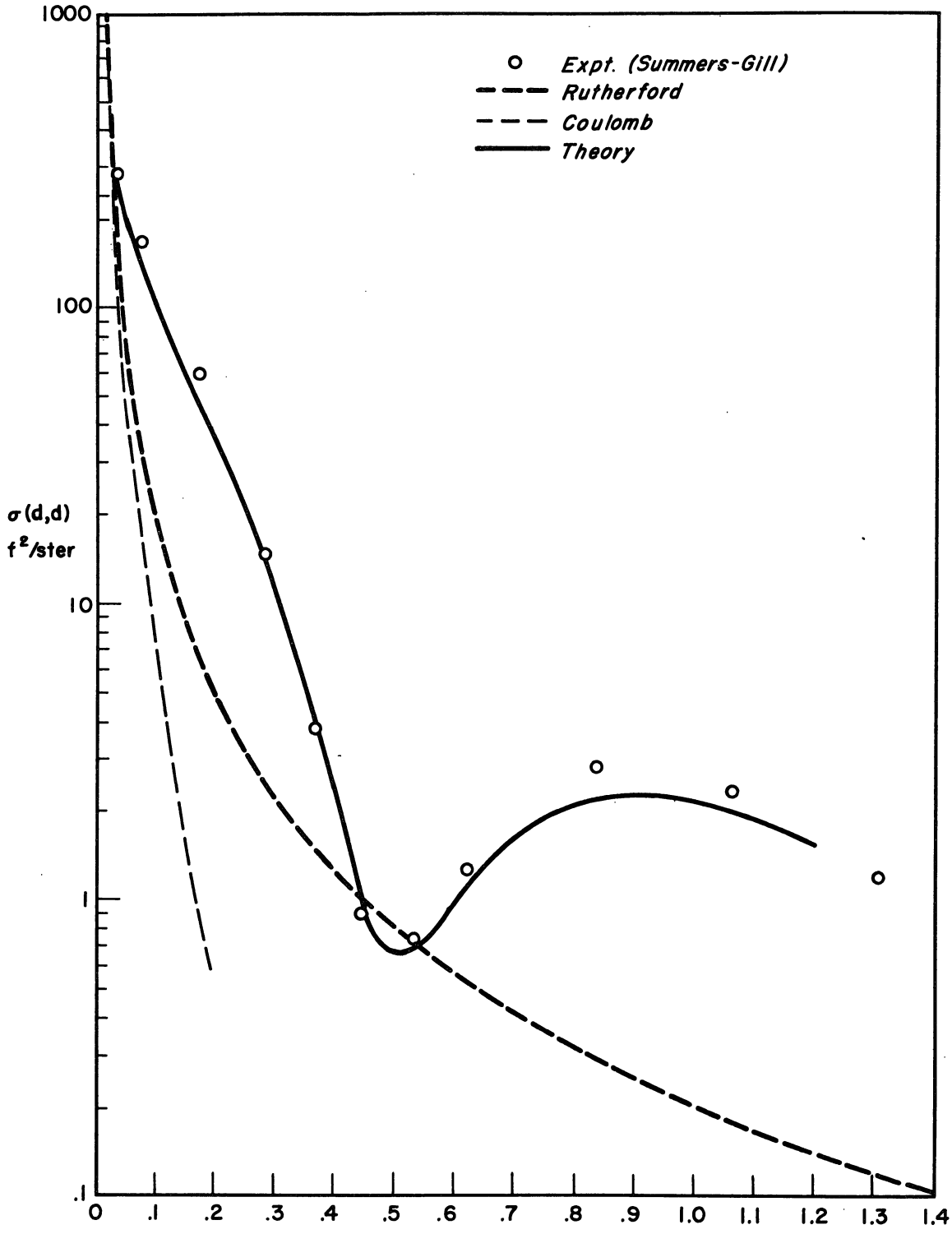


Fig. 5-3. Comparison of theory and experiment for the reaction $Be^9(d,d)$ at 24 Mev. Also shown are the Rutherford cross section and the Coulomb (non-point charge) cross section.

## APPENDIX A

## NUCLEAR UNITS

It is convenient to have a system of units which exploits the fact that nuclear data are primarily given in atomic mass units (amu, $O^{16} = 16$), Mev, and fermis ($10^{-13}$cm). Conversion of units is unnecessary if the fundamental constants are evaluated in this system. Using the values given by Cohen, et al., (67),

(a) proton charge: $\epsilon = 1.20000$ $\epsilon^2 = 1.44000$

(b) velocity of light: $c = 30.5146$ $c^2 = 931.141$

(c) Dirac unit of action: $\hbar = 6.46624$ $\hbar^2 = 41.8123$

Various nuclear units in terms of familiar ones are:

(a) area: $10^{-26}$cm = 10 mb.

(b) time: $1.01786 \times 10^{-22}$ sec.

(c) velocity: $0.982453 \times 10^{9}$ cm/sec.

(d) charge: $4.00257 \times 10^{-10}$ esu.

## APPENDIX B

## PROPERTIES OF THE FUNCTION F(x)

### 1. DEFINITION

$$F(x) = e^{-x^2} \int_0^x e^{t^2} dt. \tag{B.1}$$

In terms of $\phi(x) = \text{erf } x = (2/\pi^{\frac{1}{2}}) \int_0^x e^{-t^2} dt$,

$$F(x) = (\pi^{\frac{1}{2}}/2i)\, e^{-x^2}\, \phi(ix). \tag{B.2}$$

The asymptotic series begins with

$$F(x) \sim \frac{1}{2x} + \frac{1}{4x^3} + \frac{3}{8x^5} + \ldots \tag{B.3}$$

### 2. INTEGRAL EVALUATION

$$I_\ell(a,b,m) = \int_0^b (x^2+m)^{-\ell-\frac{3}{2}} \exp[-\frac{a}{x^2+m}]dx \tag{B.4}$$

Define $c=b^2+m$, $g=b(mc)^{-\frac{1}{2}}$, and $h=c^{-1} + (2a)^{-1} + g^2$, then

$$I_0(a,b,m) = (ma)^{-\frac{1}{2}}\, e^{-a/c} F(ga^{\frac{1}{2}}).$$

$$I_1(a,b,m) = (ma)^{-\frac{1}{2}}\, e^{-a/c} [hF(ga^{\frac{1}{2}}) - \tfrac{1}{2}ga^{-\frac{1}{2}}]$$

$$I_2(a,b,m) = (ma)^{-\frac{1}{2}}\, e^{-a/c} [(h^2+\tfrac{1}{2}a^{-2}) F(ga^{\frac{1}{2}}) + \tfrac{1}{2}ga^{-\frac{1}{2}}(g^2+\tfrac{1}{2}a^{-1})]$$

$$I_3(a,b,m) = (ma)^{-\frac{1}{2}}\, e^{-a/c} [(h^3-\tfrac{1}{2}ha^{-2}-a^{-3}) F(ga^{\frac{1}{2}}) - \tfrac{1}{2}ga^{-\frac{1}{2}}(g^4 + g^2c^{-1}$$

$$+g^2a^{-1}+ 5/4a^2+3/2ac+1/c^2)]$$

Proof: Since $I_\ell = (-d/da)^\ell I_0$, only $I_0$ need be evaluated. If F is expanded in a power series and integrated term-by-term, the result is:

$$x^{-\frac{1}{2}} e^x F(x^{1/2}) = \sum_{n=0}^{\infty} \frac{x^n}{n!\,(2n+1)} \qquad \text{(Lemma)}$$

In $I_0$, expand the exponential and integrate term-by-term,

$$I_0 = \sum_{n=0}^{\infty} \frac{(-a)^n}{n!\,m^{n+1}} \sum_{\nu=0}^{n} \frac{(-1)^\nu}{2\nu+1} \binom{n}{\nu} \left(\frac{b^2}{b^2+m}\right)^{\nu+\frac{1}{2}}$$

Rearranging the series with

$$\sum_{n=0}^{\infty} \sum_{\nu=0}^{n} f(n,\nu) = \sum_{n,\nu=0}^{\infty} f(n+\nu,\nu)$$

gives a product of two series:

$$I_0 = \frac{b}{m}\sqrt{\frac{1}{b^2+m}} \sum_{n=0}^{\infty} \frac{1}{n!}\left(-\frac{a}{m}\right)^n \sum_{\nu=0}^{\infty} \frac{1}{\nu!\,(2\nu+1)} \left(\frac{ab^2}{m\,[b^2+m]}\right)^\nu$$

The first series is an exponential, the second is given by the above lemma. Simplifying the exponent leads to the stated result. In the formulas for $I_1$, $I_2$, and $I_3$, the derivatives of F have been replaced by expressions involving F itself. For example, $F'(x) = 1 - 2x\,F(x)$.

## 3. NUMERICAL TABULATION

The function F(x) is tabulated in Ref. (68) up to x=12, at intervals of 0.01. A part of that table is reproduced here for convenience.

TABLE OF F(x)

| x | F(x) | x | F(x) | x | F(x) |
|---|---|---|---|---|---|
| 0.00 | 0.000 000 | 0.35 | 0.322 770 | 0.70 | 0.510 503 |
| .01 | .009 999 | .36 | .330 451 | .71 | .513 286 |
| .02 | .019 995 | .37 | .338 010 | .72 | .515 926 |
| .03 | .029 981 | .38 | .345 447 | .73 | .518 428 |
| .04 | .039 957 | .39 | .352 759 | .74 | .520 789 |
| .05 | .049 917 | .40 | .359 943 | .75 | .523 013 |
| .06 | .059 857 | .41 | .366 999 | .76 | .525 100 |
| .07 | .069 771 | .42 | .373 924 | .77 | .527 050 |
| .08 | .079 660 | .43 | .380 717 | .78 | .528 866 |
| .09 | .089 516 | .44 | .387 375 | .79 | .530 549 |
| .10 | .099 336 | .45 | .393 899 | .80 | .532 101 |
| .11 | .109 117 | .46 | .400 285 | .81 | .533 523 |
| .12 | .118 854 | .47 | .406 533 | .82 | .534 816 |
| .13 | .128 545 | .48 | .412 641 | .83 | .535 981 |
| .14 | .138 185 | .49 | .418 609 | .84 | .537 021 |
| .15 | .147 769 | .50 | .424 436 | .85 | .537 937 |
| .16 | .157 297 | .51 | .430 120 | .86 | .538 732 |
| .17 | .166 762 | .52 | .435 662 | .87 | .539 406 |
| .18 | .176 162 | .53 | .441 059 | .88 | .539 960 |
| .19 | .185 492 | .54 | .446 311 | .89 | .540 399 |
| .20 | .194 751 | .55 | .451 418 | .90 | .540 724 |
| .21 | .203 933 | .56 | .456 380 | .91 | .540 934 |
| .22 | .213 037 | .57 | .461 195 | .92 | .541 034 |
| .23 | .222 058 | .58 | .465 864 | .93 | .541 025 |
| .24 | .230 993 | .59 | .470 386 | .94 | .540 910 |
| .25 | .239 839 | .60 | .474 763 | .95 | .540 688 |
| .26 | .248 593 | .61 | .478 993 | .96 | .540 363 |
| .27 | .257 253 | .62 | .483 076 | .97 | .539 938 |
| .28 | .265 814 | .63 | .487 013 | .98 | .539 414 |
| .29 | .274 275 | .64 | .490 803 | .99 | .538 793 |
| .30 | .282 631 | .65 | .494 448 | 1.00 | .538 080 |
| .31 | .290 882 | .66 | .497 947 | 1.01 | .537 272 |
| .32 | .299 023 | .67 | .501 303 | 1.02 | .536 375 |
| .33 | .307 054 | .68 | .504 513 | 1.03 | .535 388 |
| 0.34 | 0.314 970 | 0.69 | 0.507 580 | 1.04 | 0.534 317 |

TABLE OF F(x) (concluded)

| x | F(x) | x | F(x) | x | F(x) |
|---|---|---|---|---|---|
| 1.05 | 0.533 162 | 1.40 | 0.456 507 | 1.75 | 0.359 436 |
| 1.06 | .531 925 | 1.41 | .453 718 | 1.76 | .356 865 |
| 1.07 | .530 609 | 1.42 | .450 918 | 1.77 | .354 313 |
| 1.08 | .529 216 | 1.43 | .448 107 | 1.78 | .351 780 |
| 1.09 | .527 748 | 1.44 | .445 286 | 1.79 | .349 266 |
| 1.10 | .526 207 | 1.45 | .442 458 | 1.80 | .346 773 |
| 1.11 | .524 595 | 1.46 | .439 624 | 1.81 | .344 299 |
| 1.12 | .522 915 | 1.47 | .436 785 | 1.82 | .341 846 |
| 1.13 | .521 169 | 1.48 | .433 942 | 1.83 | .339 413 |
| 1.14 | .519 359 | 1.49 | .431 096 | 1.84 | .337 001 |
| 1.15 | .517 487 | 1.50 | .428 249 | 1.85 | .334 609 |
| 1.16 | .515 555 | 1.51 | .425 401 | 1.86 | .332 239 |
| 1.17 | .513 566 | 1.52 | .422 555 | 1.87 | .329 891 |
| 1.18 | .511 521 | 1.53 | .419 710 | 1.88 | .327 563 |
| 1.19 | .509 423 | 1.54 | .416 869 | 1.89 | .325 258 |
| 1.20 | .507 273 | 1.55 | .414 032 | 1.90 | .322 974 |
| 1.21 | .505 075 | 1.56 | .411 199 | 1.91 | .320 712 |
| 1.22 | .502 829 | 1.57 | .408 373 | 1.92 | .318 471 |
| 1.23 | .500 537 | 1.58 | .405 554 | 1.93 | .316 253 |
| 1.24 | .498 202 | 1.59 | .402 742 | 1.94 | .314 057 |
| 1.25 | .495 827 | 1.60 | .399 940 | 1.95 | .311 883 |
| 1.26 | .493 412 | 1.61 | .397 146 | 1.96 | .309 730 |
| 1.27 | .490 960 | 1.62 | .394 364 | 1.97 | .307 600 |
| 1.28 | .488 472 | 1.63 | .391 592 | 1.98 | .305 491 |
| 1.29 | .485 950 | 1.64 | .388 832 | 1.99 | .303 405 |
| 1.30 | .483 397 | 1.65 | .386 085 | 2.00 | .3013 4039 |
| 1.31 | .480 814 | 1.66 | .383 351 | 2.01 | .2992 9770 |
| 1.32 | .478 203 | 1.67 | .380 630 | 2.02 | .2972 7683 |
| 1.33 | .475 566 | 1.68 | .377 925 | 2.03 | .2952 7771 |
| 1.34 | .472 904 | 1.69 | .375 234 | 2.04 | .2933 0025 |
| 1.35 | .470 219 | 1.70 | .372 559 | 2.05 | .2913 4438 |
| 1.36 | .467 513 | 1.71 | .369 900 | 2.06 | .2894 0998 |
| 1.37 | .464 787 | 1.72 | .367 258 | 2.07 | .2874 9696 |
| 1.38 | .462 043 | 1.73 | .364 633 | 2.08 | .2856 0519 |
| 1.39 | 0.459 283 | 1.74 | 0.362 026 | 2.09 | 0.2837 3456 |

## APPENDIX C

## THE APPROXIMATIONS (3.26) AND (3.27)

### 1. THE BESSEL FUNCTION APPROXIMATION (3.26): DERIVATION OF FORMULAS

In order to carry out the integration over the region $r_n < a$ in (3.21) most conveniently, the function $j_\ell(\gamma r_n)\ \exp(-\frac{1}{2}d^2r_n^2)$ is replaced by $Cj_\ell(\beta r_n)$. The problem is to determine the normalization constant C and the effective wave number $\beta$ so as to make this substitution reasonably accurate. (In this section and the following, d stands for any of the quantities $d_{np}$, $d_n$, $d_p$, or $d_o$ defined by (3.17), (3.15), (3.3) and (3.10), while $\beta$ stands for $\gamma_{np}$, $\gamma_n$, $\gamma_p$, or $\gamma_o$. Since $d_o=0$ and $\gamma_o=\gamma$, these will not occur explicitly in the final formulas. The subscript n on $r_n$ will also be dropped.)

Because of the factor $r^2$ in the volume element of (3.21), the region $r \approx a$ will be the most important, so C is chosen to make the two expressions equal at r = a. That is,

$$j_\ell(\gamma r)e^{-\frac{1}{2}d^2r^2} \approx j_\ell(\gamma a)e^{-\frac{1}{2}d^2a^2}\ j_\ell(\beta r)/j_\ell(\beta a). \qquad (C.1)$$

The constant $\beta$ is then chosen so that the outermost extrema of the l.h.s. and r.h.s. of (C.1) have the same height. (The 1s state is an exception and is treated separately.) Since $j_\ell(\gamma r)$ is an inside wave function for a square well it will execute one or more loops inside the

well and be decreasing in absolute magnitude as it approaches r = a. The l.h.s. of (C.1) will have the same qualitative behaviour, as will the r.h.s. The criterion for $\beta$ is that the loops nearest to r = a (of the two sides of (C.1)) shall have the same height. The peak locations will be displaced from each other but this effect is small for the values of d involved here.

The first step is to determine where the l.h.s. of (C.1) has its outermost peak, say r = $\bar{r}$. This can be done by simply plotting it and reading off $\bar{r}$. Alternatively one can set its derivative equal to zero and iterate the resulting transcendental equation. An explicit formula can be obtained by fitting a parabola to $j_\ell(\gamma r)$ at the appropriate peak, a straight line to $\exp(-\frac{1}{2}d^2r^2)$ at the same point, and computing the peak location of their product. The result is the following: Given a straight line, f = A-Br, and a parabola, g = C+Dr+Er$^2$, the extrema of fg are located at r = $\bar{r}$, where

$$3BE\bar{r} = (AE-BD) \pm \sqrt{(AE-BD)^2 + 3BE(AD-BC)} \qquad (C.2)$$

The sign is chosen which gives the smaller value of $\bar{r}$. This will be the plus sign when the parabola opens downward (E < 0), the minus sign when it opens upward (E > 0). (This assumes B > 0, as is the case here.) In the formulas of Section 2 the constants have all been defined as positive numbers, with a suitable change in the signs of (C.2).

The l.h.s. of (C.1) can now be evaluated at its (approximate) peak and the equal peak height condition written as

$$j_\ell(\gamma\bar{r})\, e^{-\frac{1}{2}d^2r^2} = j_\ell(\gamma a)\, e^{-\frac{1}{2}d^2a^2}\; j_\ell(\beta r')/j_\ell(\beta a). \qquad (C.3)$$

Now $\beta r'$ is by definition the $n^{th}$ peak position of $j_\ell(x)$ so that $j_\ell(\beta r')$ is a definite number, the height of $j_\ell$ at this particular peak. Eq. (C.3) involves the unknown $\beta$ only in the argument of $j_\ell(\beta a)$, which is itself determined by (C.3). The quantity $\beta a$ can therefore be found by inverse interpolation in the NBS Tables (69). Since the inverse functions are multiple-valued, it is necessary to select the argument $\beta a$ which corresponds to the state in question. In the formula summary of Section 2 this requirement is incorporated in the form of limits between which $\beta a$ must lie.

The ls-state does not fit the preceding pattern since $j_o(\gamma r)$ and the l.h.s. of (C.1) fall monotonically from unity at $r = 0$ to their values at $r = a$. The point $r = a$ is kept as one point of equality, so that (C.1) still holds, but the other point is taken arbitrarily as $r = a/2$. This gives the equation,

$$j_o(\gamma a/2)\, e^{-\frac{1}{2}d^2(a/2)^2} = j_o(\gamma a)\, e^{-\frac{1}{2}d^2a^2}\; j_o(\beta a/2)/j_o(\beta a) \qquad (C.4)$$

The ratio $j_o(\beta a)/j_o(\beta a/2)$ is determined by (C.4), so that $\beta a$ can be found from a plot of $j_o(x)/j_o(x/2)$, as described in the next section.

## 2. THE BESSEL FUNCTION APPROXIMATION (3.26): SUMMARY OF FORMULAS

The quantum numbers $(n,\ell)$ and the parameters d, a, and $\gamma$ are supposed known. The following formulas determine $\beta$ for the three lowest oscillator shells. Analogous expressions for the higher single-particle states are easily constructed according to the method of Section 1.

(a) n=1, $\ell$=0 (1s).

Evaluate $e^{-3d^2a^2/8} j_0(\gamma a)/j_0(\gamma a/2)$ and with this as the value of $j_0(x)/j_0(x/2)$, enter Fig. C-1 and read out x. Then $\beta = x/a$.

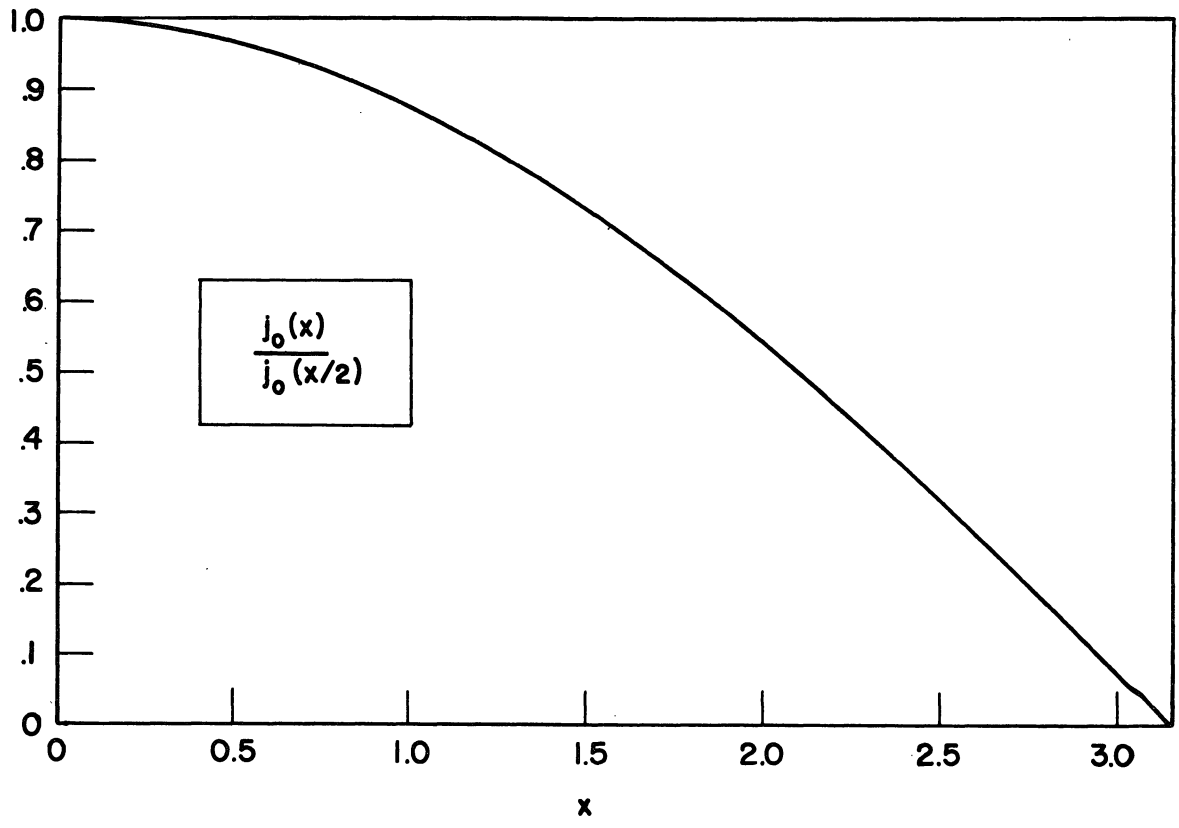


Fig. C-1. Plot of $j_0(x)/j_0(x/2)$.

(b) n=1, $\ell$=1 (1p).

Find $\bar{r}$ from

$$3BE\bar{r} = (AE+BD) - \sqrt{(AE+BD)^2 - 3BE(AD+BC)}$$

where

$$A = (1+4.335d^2/\gamma^2)e^{-2.167a^2/\gamma^2}$$

$$B = 2.082(d^2/\gamma)e^{-2.167a^2/\gamma^2}$$

$$C = 0.07280$$

$$D = 0.4889\gamma$$

$$E = 0.1174\gamma^2$$

Then

$$j_1(\beta a) = 0.4362 j_1(\gamma a) e^{-\frac{1}{2}d^2(a^2-\bar{r}^2)} / j_1(\gamma\bar{r}).$$

From this, $\beta a$ can be found by inverse interpolation in the Bessel function tables (69). The correct value of $\beta a$ lies between 2.08 and 4.49.

(c) n=1, $\ell$=2 (1d).

Find $\bar{r}$ from the expression in the preceding paragraph, using the values

$$A = (1+11.17d^2/\gamma^2)e^{-5.585d^2/\gamma^2}$$

$$B = 3.342(d^2/\gamma)e^{-5.585d^2/\gamma^2}$$

$$C = 0.4861$$

$$D = 0.4745\gamma$$

$$E = 0.07099\gamma^2$$

Then

$$j_2(\beta a) = 0.3068 j_2(\gamma a)\, e^{-\frac{1}{2} d^2(a^2-\bar{r}^2)} / j_2(\gamma \bar{r}).$$

From this, $\beta a$ can be found by inverse interpolation in the Bessel function tables (69). The correct value of $\beta a$ lies between 3.34 and 5.76.

(d) n=2, $\ell$=0 (2s).

Find $\bar{r}$ from the expression in Section 2(b), using the values

$$A = (1+20.19 d^2/\gamma^2)\, e^{-10.10 d^2/\gamma^2}$$

$$B = 4.494 (d^2/\gamma)\, e^{-10.10 d^2/\gamma^2}$$

$$C = 1.976$$

$$D = 0.9761\gamma$$

$$E = 0.1086\gamma^2$$

Then

$$j_o(\beta a) = -0.2172 j_o(\gamma a)\, e^{-\frac{1}{2} d^2(a^2-\bar{r}^2)} / j_o(\gamma \bar{r}).$$

From this, $\beta a$ can be found by inverse interpolation. The correct value is between 4.49 and 6.28.

## 3. THE HANKEL FUNCTION APPROXIMATION (3.27): DERIVATION OF FORMULAS

As in Section 1, d stands for the different $d_{np}$, $d_n$, etc., while $\xi$ stand for $\xi_{np}$, $\xi_n$, etc. The approximation (3.27) replaces $h_\ell(\kappa r) \exp(-\frac{1}{2} d^2 r^2)$ by $C h_\ell(\xi r)$, with C and $\xi$ to be determined. Since the function $h_\ell$ has its maximum value at r = a, C is chosen to make the two expressions equal at that point,

$$h_\ell(\kappa r)\, e^{-\frac{1}{2} d^2 r^2} \approx h_\ell(\kappa a)\, e^{-\frac{1}{2} d^2 a^2}\, h_\ell(\xi r)/h_\ell(\xi a). \qquad (C.5)$$

The constant $\xi$ is then chosen so that (C.5) is an equality also at another point, r = b. This is arbitrarily taken as the point where the l.h.s. of (C.5) has fallen to half its value at r = a.

The first step is to determine where the l.h.s. of (C.5) falls to this 50% point. Since the Hankel functions have the form,

$$h_\ell(x) = x^{-\ell-1} P_\ell(x) e^{-x} , \qquad (C.6)$$

where $P_\ell(x)$ is a polynomial of degree $\ell$, the equation for b is,

$$b^{-\ell-1} P_\ell(\kappa b) e^{-\kappa b - \frac{1}{2}d^2 b^2} = \tfrac{1}{2} a^{-\ell-1} P_\ell(\kappa a) e^{-\kappa a - \frac{1}{2}d^2 a^2} \equiv e^{-\nu} \qquad (C.7)$$

The middle member of (C.7) determines $\nu$ . Taking logarithms,

$$\tfrac{1}{2}d^2 b^2 + \kappa b + \ln \left[ b^{\ell+1} / P_\ell(\kappa b) \right] - \nu = 0. \qquad (C.8)$$

Since the logarithmic term is insensitive to the exact value of b this transcendental equation can be solved iteratively as a quadratic equation for b, assuming the logarithm known:

$$b_{n+1} = -(\kappa/d^2) + \sqrt{(\kappa/d^2)^2 + (2/d^2)\left\{\nu + \ln \left[ b_n^{-\ell-1} P_\ell(\kappa b_n) \right]\right\}} \qquad (C.9)$$

One application of (C.9) using $b_o = a + 0.5$ usually suffices.

Writing (C.5) as an equality at r = b,

$$(\kappa b)^{-\ell-1} P_\ell(\kappa b) e^{-\kappa b - \frac{1}{2}d^2 b^2} = C(\xi b)^{-\ell-1} P_\ell(\xi b) e^{-\xi b} , \qquad (C.10)$$

and dividing this equation into the similar one at r = a, yields

$$e^{\xi(b-a)}P_\ell(\xi a)/P_\ell(\xi b) = e^{\kappa(b-a) + \frac{1}{2}d^2(b^2-a^2)}P_\ell(\kappa a)/P_\ell(\kappa b) \equiv e^{\eta} . \tag{C.11}$$

The middle member determines $\eta$. Taking logarithms and as before, iterating on the slowly varying logarithmic term,

$$\xi_{n+1} = (b-a)^{-1}\{\eta + \ell n\,[P_\ell(\xi b_n)/P_\ell(\xi a)]\} . \tag{C.12}$$

Eq. (C.13) of the following section provides a convenient starting value,

$$\xi_o = \kappa + \tfrac{1}{2}d^2(a+b) .$$

## 4. THE HANKEL FUNCTION APPROXIMATION (3.27): SUMMARY OF FORMULAS

The quantum number $\ell$ and the parameters d, a, and $\kappa$ are supposed known. The following formulas determine $\xi$ for all s, p, and d levels, there being no dependence on the radial quantum number n. The general formulas for higher $\ell$-states have been given in the previous section.

Suitable starting values for the b- and $\xi$-iterations are $b_o = a+0.5$ and $\xi_o = \kappa+\frac{1}{2}d^2(a+b)$.

(a) $\ell=0$. $\quad h_o(x) = x^{-1}e^{-x}. \qquad P_o(x) = 1 .$

$$\nu = \kappa a + \tfrac{1}{2}d^2a^2 + \ell n(2a)$$

$$b_{n+1} = -(\kappa/d^2) + \sqrt{(\kappa/d^2)^2 + (2/d^2)(\nu - \ell n\, b_n)}$$

$$\xi = \kappa + \tfrac{1}{2}d^2(b+a) \tag{C.13}$$

No $\xi$-iteration is required, eq. (C.11) being soluble in this case.

(b) $\ell=1$.

$$h_1(x) = x^{-2}(1+x)e^{-x}. \qquad P_1(x) = 1+x.$$

$$\nu = \kappa a + \tfrac{1}{2}d^2a^2 + \ell n[2a^2/(1+\kappa a)]$$

$$b_{n+1} = -(\kappa/d^2) + \sqrt{(\kappa/d^2)^2 + (2/d^2)\{\nu+\ell n[(1+\kappa b_n)/b_n^2]\}}\ .$$

$$\eta = \kappa(b-a) + \tfrac{1}{2}d^2(b^2-a^2) + \ell n[(1+\kappa a)/(1+\kappa b)].$$

$$\xi_{n+1} = (b-a)^{-1}\{\eta + \ell n[(1+\xi_n b)/(1+\xi_n a)]\}\ .$$

(c) $\ell=2$.

$$h_2(x) = x^{-3}(3+3x+x^2)e^{-x}. \qquad P_2(x) = 3+3x+x^2.$$

$$\nu = \kappa a + \tfrac{1}{2}d^2a^2 + \ell n[2a^3/(3+3\kappa a+\kappa^2a^2)]\ .$$

$$b_{n+1} = -(\kappa/d^2) + \sqrt{(\kappa/d^2)^2 + (2/d^2)\{\nu+\ell n[(3+3\kappa b_n+\kappa^2 b_n^2)/b_n^3]\}}\ .$$

$$\eta = \kappa(b+a) + \tfrac{1}{2}d^2(b^2-a^2) + \ell n[(3+3\kappa a+\kappa^2a^2)/(3+3\kappa b+\kappa^2b^2)].$$

$$\xi_{n+1} = (b-a)^{-1}\{\eta+\ell n[(3+3\xi_n b+\xi_n^2b^2)/(3+3\xi_n a+\xi_n^2a^2)]\}\ .$$

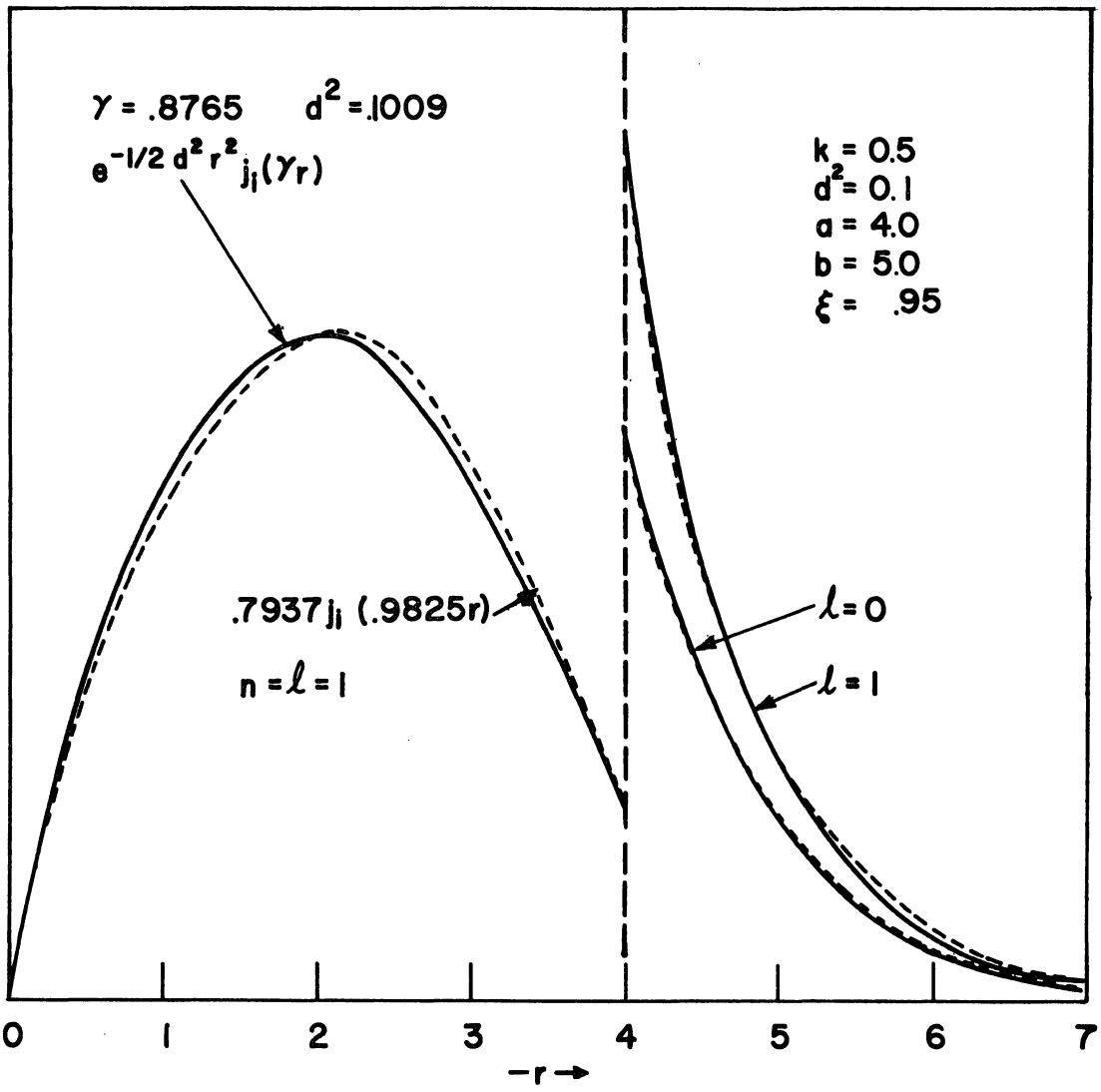


Fig. C-2. Some examples of the Bessel and Hankel function approximations. Solid lines are exact, dotted ones approximate.

## APPENDIX D

## HARMONIC OSCILLATOR WAVE FUNCTIONS

### 1. SUMMARY OF NOTATION

$E_{n\ell}(\omega) = \hbar\omega(2n+\ell-\frac{1}{2})$ = energy eigenvalue in the state $(n,\ell)$.

$\ell$,m = orbital angular momentum and z-projection quantum numbers.

M = reduced mass.

n = radial quantum number. The lowest $\ell$-state is n = 1.

$p = (M\omega/\hbar)^{\frac{1}{2}}$ = oscillator parameter.

$\vec{R}$, $\hat{R}$, r = coordinate vector, unit vector, and radial coordinate, respectively.

$R_{n\ell}(p,r)$ = harmonic oscillator radial wave function.

$V(r) = \frac{1}{2}M\omega^2r^2 = \frac{1}{2}\hbar^2p^4r^2/M$ = potential energy.

$v_{n\ell m}(p,\vec{R}) = R_{n\ell}(p,r)Y_{\ell m}(\hat{R})$ = harmonic oscillator wave function.

$\omega$ = classical frequency.

$Y_{\ell m}(\hat{R})$ = normalized spherical harmonic. $Y^*_{\ell m} = (-1)^m Y_{\ell -m}$ .

### 2. RADIAL WAVE FUNCTIONS

$$R_{1\ell}(p,r) = [p^3 2^{\ell+2}/\pi^{\frac{1}{2}}(2\ell+1)!!]^{\frac{1}{2}}(pr)^{\ell}\exp(-\tfrac{1}{2}p^2r^2).$$

$$R_{2\ell}(p,r) = [p^3 2^{\ell+1}(2\ell+3)/\pi^{\frac{1}{2}}(2\ell+1)!!]^{\frac{1}{2}}(pr)^{\ell}[1-p^2r^2/(\ell+3/2)].$$
$$\cdot \exp(-\tfrac{1}{2}p^2r^2).$$

$$R_{3\ell}(p,r) = [p^3 2^{\ell-1}(2\ell+3)(2\ell+5)/\pi^{\frac{1}{2}}(2\ell+1)!!]^{\frac{1}{2}}(pr)^{\ell}.$$
$$\cdot [1-2p^2r^2/(\ell+3/2)+p^4r^4/(\ell+3/2)(\ell+5/2)]\exp(-\tfrac{1}{2}p^2r^2).$$

$$R_{n\ell}(p,r) = [p^3 2^{\ell-1}(2\ell+2n-1)!!/\pi^{\frac{1}{2}}\{(2\ell+1)!!\}^2]^{\frac{1}{2}} {}_1F_1(1-n;\ell+3/2;p^2r^2)$$
$$(pr)^{\ell}\exp(-\tfrac{1}{2}p^2r^2)$$

The function $R_{1\ell}(p,r)$ starts out at $r = 0$ like $r^{\ell}$ and goes through a single peak at $p^2r^2 = \ell$. $R_{2\ell}$ starts out similarly, goes through a positive peak at $p^2r^2 = \ell+7/4-(2\ell+49/16)^{\frac{1}{2}}$, vanishes at $p^2r^2 = \ell+3/2$, and goes through a negative "peak" at $p^2r^2 = \ell+7/4+(2\ell+49/16)^{\frac{1}{2}}$. $R_{3\ell}$ starts out the same way and has nodes at $p^2r^2 = \ell+5/2\pm(\ell+5/2)^{\frac{1}{2}}$, but its peak positions must be found numerically. An exception is $R_{30}$ which peaks at $p^2r^2 = 0$, 5/2, and 13/2.

The function $r^2R_{1\ell}(p,r)$ (Chapter 4, Section D), peaks at $p^2r^2 = \ell+2$, while $r^2R_{2\ell}(p,r)$ peaks at $p^2r^2 = \ell+11/4\pm[11\ell/4 + 73/16]^{\frac{1}{2}}$. The nodes are unaffected by the factor $r^2$.

## 3. THE GENERALIZED CENTER-OF-MASS TRANSFORMATION

### (a) Derivation

The Schrödinger equation for two particles of equal mass, $M_1=M_2$, moving independently in the same potential well, $\omega_1=\omega_2$,

$$\left[-\frac{\hbar^2\nabla_1^2}{2M_1} - \frac{\hbar^2\nabla_2^2}{2M_2} + \tfrac{1}{2}M_1\omega_1^2r_1^2 + \tfrac{1}{2}M_2\omega_2^2r_2^2 - E\right]\psi = 0 \qquad (D.1)$$

remains separable in the center-of-mass system,

$$\left[-\frac{\hbar^2\nabla^2}{2M} - \frac{\hbar^2\nabla_c^2}{2M_c} + \tfrac{1}{2}M\omega^2r^2 + \tfrac{1}{2}M_c\omega_c^2r_c^2 - E\right]\psi = 0 \qquad (D.2)$$

where $\vec{R} = \vec{R}_1-\vec{R}_2$, $\vec{R}_c = \frac{1}{2}(\vec{R}_1+\vec{R}_2)$, $M = M_1/2$, $M_c = 2M_1$, $\omega_1=\omega_2=\omega=\omega_c$.

If an eigenfunction of (D.1) is expanded in the solutions to (D.2),

$$v_{q_1}(p_1,\vec{R}_1)\,v_{q_2}(p_2,\vec{R}_2) = \sum_{q,q_c} v_q(p,\vec{R})\,v_{q_c}(p_c,\vec{R}_c)(qq_c|q_1q_2), \tag{D.3}$$

then energy and angular momentum conservation make (D.3) a finite sum. (The q's are sets of three quantum numbers, $q_1=n_1\ell_1m_1$, $q=n\ell m$, etc. Also $p^2=M\omega/\hbar$, $p_c^2=M_c\omega_c/\hbar$). That the angular momentum quantum numbers should transform "finitely" is easily seen from the fact that the spherical harmonics are finite polynomials in the cartesian coordinates of the particles, but the corresponding property for the radial quantum numbers is not to be expected, and indeed only holds for the parabolic well. This transformation was first used by Talmi(15) in spectroscopic calculations to replace the conventional Slater method, and has since become standard in such calculations.

It is a trivial step to introduce unequal masses in (D.1) with the definitions $\vec{R}_c=(M_1\vec{R}_1+M_2\vec{R}_2)/(M_1+M_2)$, $M=M_1M_2/(M_1+M_2)$, $M_c=M_1+M_2$. Eq. (D.2) is still separable and (D.3) is still finite. It is essential however that $\omega_1=\omega_2$.

Finally consider the generalization of (D.1) to unequal frequencies. Under the c.m. transformation the kinetic energy separates but the potential energy does not, so there is no analog of (D.2). Expansion (D.3) is still possible but does not terminate. However there is a generalization of the c.m. transformation which will make this expansion finite even in this case. The simplest way to see that such a transformation ought to exist is to observe that the functions in (D.3) depend only on

the products $M_1\omega_1$ and $M_2\omega_2$. Thus already in the case of unequal masses the products are unequal and there ought to be a choice of new frequencies which will preserve the finite structure of (D.3).

The essential element in the finiteness of (D.3) is not the separability of the wave equation, although it was this consideration which led Talmi (15) to the oscillator potential, but the simple way in which the exponentials transform. The desired coordinate transformation must preserve this property but need not separate the wave equation (and indeed does not). The exponential relation which is sought, namely

$$\exp(-\tfrac{1}{2}p_1^2r_1^2)\exp(-\tfrac{1}{2}p_2^2r_2^2) = \exp(-\tfrac{1}{2}p^2r^2)\exp(-\tfrac{1}{2}p_c^2r_c^2), \quad (D.4)$$

demands
$$p_1^2r_1^2+p_2^2r_2^2=p^2r^2+p_c^2r_c^2, \quad (D.5)$$

which can be induced by the generalized center-of-mass transformation,

$$\vec{R} = \vec{R}_1 - \vec{R}_2 \qquad \vec{R}_c = (p_1^2\vec{R}_1 + p_2^2\vec{R}_2)/(p_1^2 + p_2^2)$$

$$p^2 = p_1^2p_2^2/(p_1^2 + p_2^2) \qquad p_c^2 = p_1^2 + p_2^2 \quad (D.6)$$

This transformation is obviously in close analogy to the c.m. transformation. The latter weights the particles according to their masses, putting $\vec{R}_c$ closer to the less mobile (more massive) particle. (D.6) also takes into account the loss of mobility due to the steeper well (higher $\omega$-value). It is therefore a "center-of-rigidity" transformation.

The equation,

$$2n_1 + \ell_1 + 2n_2 + \ell_2 = 2n + \ell + 2n_c + \ell_c , \quad (D.7)$$

which expresses energy conservation when the frequencies are equal, now states that the "number of quanta" is preserved in (D.3). The reason (D.7) holds in the general case is that with the infinite series part of the wave functions split off by (D.4), the remaining finite polynomials transform just as they did before.

Not all the values of n, $\ell$, $n_c$, and $\ell_c$ allowed by (D.7) will actually occur in (D.3), a fact which further simplifies the expansion. The additional restriction is due to conservation of angular momentum. The values $\ell_1$ and $\ell_2$ can couple to total angular momenta from $|\ell_1 - \ell_2|$ to $\ell_1 + \ell_2$. Therefore the admissible values of $\ell$ and $\ell_c$ must be able to couple to some resultant in this same range. (The angular momentum operators implied here are the generators of the infinitesimal rotations in the new coordinates $\vec{R}$ and $\vec{R}_c$.)

The expansion (D.3) conserves parity (the reflection eigenvalue in the new coordinates) as a consequence of (D.7). The latter implies that

$$(-1)^{\ell_1+\ell_2} = (-1)^{\ell+\ell_c} ,$$

so there is no further limitation of the sum on this account.

(b) Summary of Formulas

The following expressions are derived by writing out the l.h.s. of (D.3) in each case in cartesian coordinates, introducing (D.6), and returning to the spherical tensor notation. It is not necessary to treat the different magnetic quantum number combinations $m_1 m_2$ individually (as in Ref. (15)) if the spherical harmonics of degree greater

than one are expressed in terms of vector coupled first degree harmonics. The Clebsch-Gordan coefficients appearing (explicitly or implicitly) in the following formulas arise from this source. (Only the special cases required for eq. (4.18) with $\gamma = 100$ are listed.)

$$\underline{1s}: \quad v^*_{100}(p_1,\vec{R}_1)\,v_{100}(p_2,\vec{R}_2) = v_{100}(p_c,\vec{R}_c)\,v_{100}(p,\vec{R}).$$

$$\underline{1p}: \quad v^*_{11m}(p_1,\vec{R}_1)\,v_{100}(p_2,\vec{R}_2) = (p_1/p_c)\,v^*_{11m}(p_c,\vec{R}_c)\,v_{100}(p,\vec{R})$$
$$+ (p_2/p_c)\,v_{100}(p_c,\vec{R}_c)\,v^*_{11m}(p,\vec{R})$$

$$\underline{1d}: \quad v^*_{12m}(p_1,\vec{R},)\,v_{100}(p_2,\vec{R}_2) = (p_1/p_c)^2 v^*_{12m}(p_c,\vec{R}_c)\,v_{100}(p,\vec{R})$$
$$+ (p_2/p_c)^2 v_{100}(p_c,\vec{R}_c)\,v^*_{12m}(p,\vec{R}) + 2^{\frac{1}{2}}(p/p_c)\sum_k C^{112}_{k.m}\, v^*_{11k}(p_c,\vec{R}_c)$$
$$v^*_{11m-k}\ (p,\vec{R}).$$

$$\underline{2s}: \quad v^*_{200}(p_1,\vec{R}_1)\,v_{100}(p_2,\vec{R}_2) = (p_1/p_c)^2 v_{200}(p_c,\vec{R}_c)\,v_{100}(p,\vec{R})$$
$$+ (p_2/p_c)^2 v_{100}(p_c,\vec{R}_c)\,v_{200}(p,\vec{R}) + 2^{\frac{1}{2}}(p/p_c)\sum_k C^{110}_{k.0} v^*_{11k}(p_c,\vec{R}_c)\,v^*_{1r-k}(p,\vec{R}).$$

The notation used in the previous equations is as follows: $p$, $\vec{R}$, $p_c$, and $\vec{R}_c$ are defined in (D.6); the Clebsch-Gordan coefficient $C^{ABC}_{abc}$ expresses the coupling of A and B to a resultant C, with magnetic quantum numbers written below and a dot indicating a suppressed quantum number whose value is fixed by a + b = c; the asterisk denotes complex conjugate and has been omitted on the real s-functions.

## APPENDIX E

## RADIAL INTEGRALS FOR THE PROTON-TARGET INTERACTION

As mentioned in connection with eqs. (4.20) and (4.21), the radial integrals

$$I^{\nu\lambda}(\tilde{V}_{tp}) = \int_0^\infty j_\lambda(q_3 r_p)\, R_{\nu\lambda}(p, r_p)\, \tilde{V}_{tp}(r_p)\, r_p^2\, dr_p \qquad \text{(E.1)}$$

may be done numerically or by use of Gaussian approximations to $\tilde{V}_{tp}$ and the Weber-Sonine formula (35, p. 35). In this appendix the latter approach will be adopted for the three potentials (5.6a), (5.6b), and (5.7). More general forms can be integrated using the above-mentioned formula specialized to half-integral Bessel functions:

$$\int_0^\infty j_\ell(kr)\, r^{\ell+t} e^{-\frac{1}{2}p^2 r^2}\, dr = \qquad \text{(E.2)}$$

$$\frac{(2^{t-3}\pi)^{1/2}\,\Gamma\left(\ell+\frac{t+1}{2}\right)}{p^{2\ell+t+1}\,\Gamma\left(\ell+\frac{3}{2}\right)}\, {}_1F_1\left(1-\frac{t}{2};\ell+\frac{3}{2};\frac{k^2}{2p^2}\right) k^\ell e^{-k^2/2p^2}$$

For t even, the confluent hypergeometric function in (E.2) is a finite polynomial, while for t odd it can be evaluated in terms of the function F given in Appendix B. Thus,

$${}_1F_1\left(\tfrac{1}{2};\tfrac{3}{2};x^2\right) = \frac{1}{x}\int_0^x e^{t^2} dt \qquad \text{(E.3)}$$

and the functions involving different parameters can be reached by standard contiguity formulas.

The following are some special cases of (E.1), in which it is supposed that

$$V_{tp} = -V_{p0}\, e^{-\frac{1}{2}\tau^2 r_p^2} - \frac{i}{2}\, e\, U_{p0}\, \sigma^2 r_p^2\, e^{-\frac{1}{2}\sigma^2 r_p^2} + \left(\frac{2}{\pi}\right)^{1/2} Z\epsilon^2 \int_0^{\gamma} e^{-\frac{1}{2}x^2 r_p^2}\, dx \qquad \text{(E.4)}$$

Furthermore, because of the short range of the first two terms in (E.4), it is convenient to use the expansion,

$$1 - e^{-\frac{1}{2}\Omega_p^2 r_p^2} \approx \tfrac{1}{2}\Omega_p^2 r_p^2 \qquad \text{(E.5)}$$

Thus, in (E.1) the approximate form is used,

$$\begin{aligned}\tilde{V}_{tp} &\equiv \left(1 - e^{-\frac{1}{2}\Omega_p^2 r_p^2}\right) V_{tp} \\ &\approx \tfrac{1}{2}\Omega_p^2 r_p^2 \left[-V_{p0}\, e^{-\frac{1}{2}\tau^2 r_p^2} - \frac{i}{2}\, e\, U_{p0}\, \sigma^2 r_p^2\, e^{-\frac{1}{2}\sigma^2 r_p^2}\right. \\ &\left. + \left(1 - e^{-\frac{1}{2}\Omega_p^2 r_p^2}\right)\left(\frac{2}{\pi}\right)^{1/2} Z\epsilon^2 \int_0^{\gamma} e^{-\frac{1}{2}x^2 r_p^2}\, dx\right]\end{aligned} \qquad \text{(E.6)}$$

Explicitly,

$$I^{10}\left[\tfrac{1}{2}\Omega_p^2 r_p^2 \left(-V_{p0}\, e^{-\frac{1}{2}\tau^2 r_p^2}\right) =\right.$$

$$= -\tfrac{1}{2}\Omega_p^2 V_{p0}\sqrt{\frac{2\pi^{1/2}p^3}{(p^2+\tau^2)^5}}\left(3-\frac{q_3^2}{p^2+\tau^2}\right)e^{-q_3^2/2(p^2+\tau^2)} \qquad \text{(E.7)}$$

$$I''\left[\tfrac{1}{2}\Omega_p^2 r_p^2\left(-V_{p0}\,e^{-\frac{1}{2}\tau^2 r_p^2}\right)\right]$$

$$= -\Omega_p^2 V_{p0}\sqrt{\frac{\pi^{1/2}p^5}{3(p^2+\tau^2)^7}}\left(5-\frac{q_3^2}{p^2+\tau^2}\right)q_3\,e^{-q_3^2/2(p^2+\tau^2)} \qquad \text{(E.8)}$$

$$I'^0\left[\tfrac{1}{2}\Omega_p^2 r_p^2\left(-\tfrac{i}{2}e U_{p0}\sigma^2 r_p^2 e^{-\frac{1}{2}\sigma^2 r_p^2}\right)\right] \qquad \text{(E.9)}$$

$$= -\tfrac{i}{2}\Omega_p^2 e U_{p0}\sigma^2\sqrt{\frac{\pi^{1/2}p^3}{2(p^2+\sigma^2)^7}}\left(15-\frac{10q_3^2}{p^2+\sigma^2}+\frac{q_3^4}{(p^2+\sigma^2)^2}\right)e^{-\frac{q_3^2}{2(p^2+\sigma^2)}}$$

$$I''\left[\tfrac{1}{2}\Omega_p^2 r_p^2\left(-\tfrac{i}{2}e U_{p0}\sigma^2 r_p^2 e^{-\frac{1}{2}\sigma^2 r_p^2}\right)\right]$$

$$= -\tfrac{i}{2}\Omega_p^2 e U_{p0}\sigma^2\sqrt{\frac{\pi^{1/2}p^5}{3(p^2+\sigma^2)^9}}\left(35-\frac{14q_3^2}{p^2+\sigma^2}+\frac{q_3^4}{(p^2+\sigma^2)^2}\right)\times \qquad \text{(E.10)}$$

$$\times\, q_3\, e^{-q_3^2/2(p^2+\sigma^2)}$$

$$I'^0\left[e^{-\frac{1}{2}\Omega_p^2 r_p^2}\left(\tfrac{2}{\pi}\right)^{1/2} Z\epsilon^2\int_0^\gamma e^{-\frac{1}{2}x^2 r_p^2}dx\right]$$

$$= 2Ze^2\sqrt{p^3/\pi^{1/2}}\,I_0\left(q_3^2/2,\gamma,p^2+\Omega_p^2\right) \qquad \text{(E.11)}$$

$$I''\left[e^{-\frac{1}{2}\Omega_p^2 r_p^2}\left(\tfrac{2}{\pi}\right)^{1/2} Z\epsilon^2\int_0^\gamma e^{-\frac{1}{2}x^2 r_p^2}dx\right]$$

$$= \sqrt{8p^5/3\pi^{1/2}}\,Z\epsilon^2 q_3\,I_1\left(q_3^2/2,\gamma,p^2+\Omega_p^2\right) \qquad \text{(E.12)}$$

By setting $\Omega_p = 0$ in (E.11) and (E.12), the remaining integrals in (E.3) can be obtained. The integrals $I_0$ and $I_1$ are given in Apendix B.

## APPENDIX F

## CURVE FITTING WITH GAUSSIAN-TYPE FUNCTIONS

### 1. THE WOODS-SAXON FORM FACTOR (70)

The Woods-Saxon potential, $V(r) = V_o(1+e^{(r-R)/a})^{-1}$, can be fit as a one-parameter form factor,

$$V(r)/V_o = f(r) = (1+e^{y-Y})^{-1}, \qquad (F.1)$$

with $$y = r/a, \; Y = R/a.$$

The approximation can be started with an exponential,

$$f_A = e^{-\frac{1}{2}g^2y^2} . \qquad (F.2)$$

This agrees with (F.1) at r = 0 neglecting, as will be done throughout, the small quantity $e^{-Y}$ in comparison to unity. The constant g may be determined by arbitrarily equating f and $f_A$ at their 10% points. For f this is found to be at y = Y+2.2, which determines g. The result is,

$$f_A = \exp[-2.146y^2/(Y+2.2)^2]. \qquad (F.3)$$

A plot of the first residual, $f-f_A$, as a function of y/Y for several Y-values shows that its principal maximum is at $y/Y \approx 0.76$, with a half-width which is roughly, $\Delta(y/Y) \approx .64$. If this is to be fitted with $x^n\exp(-\frac{1}{2}x^2)$, using x = hy/Y, then the peak will be located correctly if $h_1 = 1.316$, $h_2 = 1.861$, $h_3 = 2.279$, $h_4 = 2.632$, etc., the subscriptbeing n. The half-widths of these approximating functions are,

when divided by the corresponding $h_n$, $\Delta(y/Y)$ = 1.22, .88, .72, .63, etc. This singles out n = 4.

Finally, if the peak height of $f-f_A$ is plotted against Y it turns out roughly linear. This gives the final form,

$$f-f_A = (1.43Y-2.48)(r/R)^4 \exp[-\tfrac{1}{2}(2.632r/R)^2]. \qquad (F.4)$$

This two-term approximation to f is illustrated in Fig. F-1 for R = 2.8, a = 0.5.

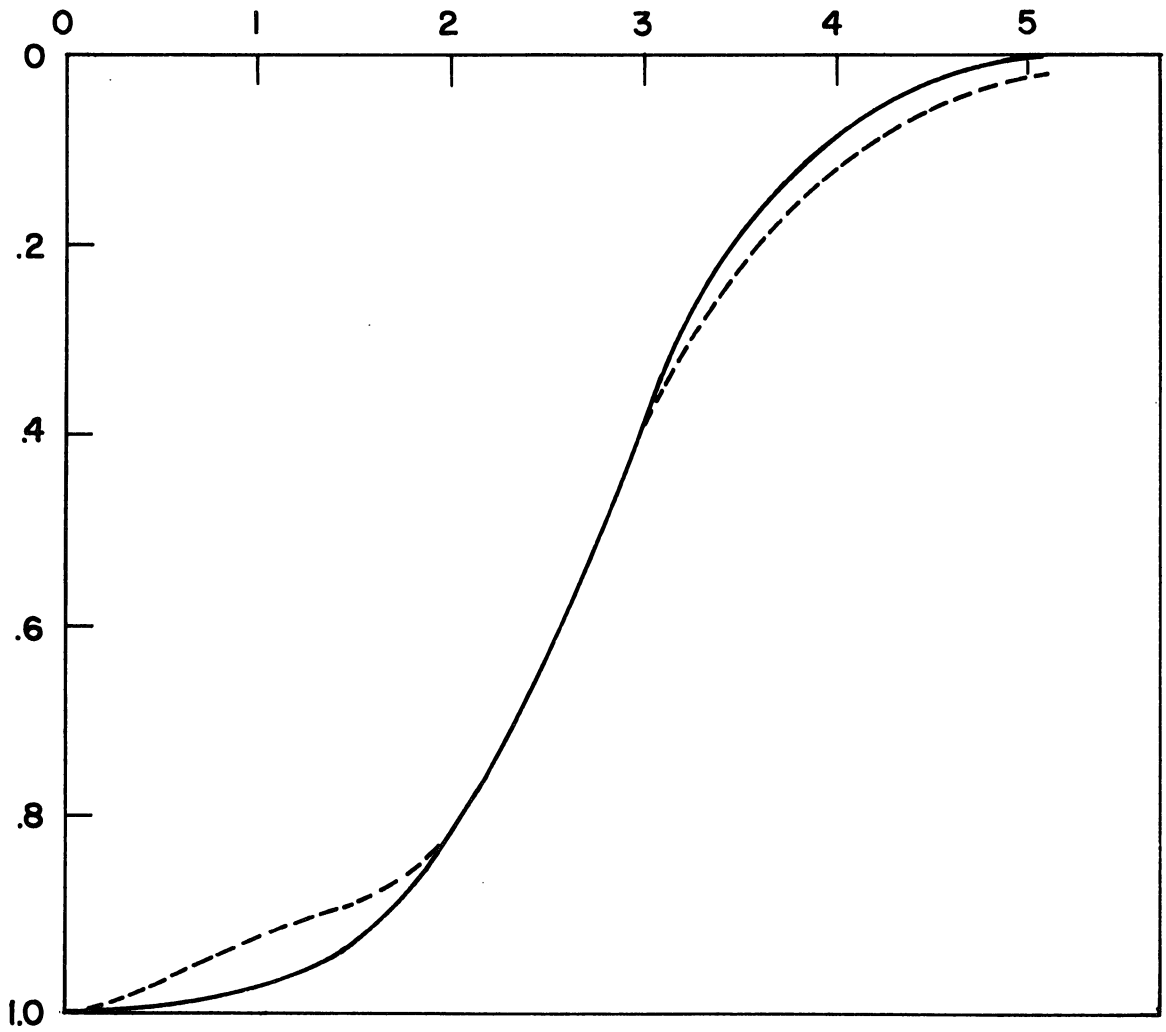


Fig. F-1. Solid curve: Woods-Saxon form factor, R = 2.8, a = 0.5. Dashed curve: Eq. (F-4), $\exp(-.141r^2)+.09r^4 \exp(-.444r^2)$.

2. ALTERNATIVE FORMS FOR THE CUTOFF FUNCTION

(a) If the function f of (3.3) is squared, cubed, etc., it exhibits a sharper rate of decrease, and the new integrals which arise are identical in form to the ones already evaluated. There are merely more terms in the final amplitude, since

$$(1-be^{-\frac{1}{2}\Omega^2r^2})^m = \sum_{k=0}^{m} \binom{m}{k}(-b)^k e^{-\frac{1}{2}k\Omega^2r^2}.$$

(b) If a more rapidly decreasing function g is compared graphically with f of (3.3), the difference is seen to be concentrated principally in two single peak functions.

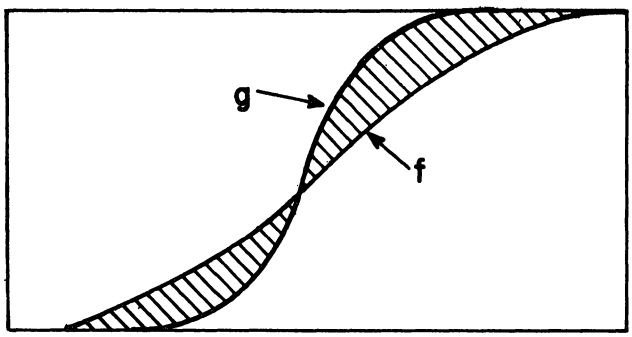


This leads to an expression of the form,

$$g = f + Ar^m e^{-\frac{1}{2}\alpha^2r^2} - Br^n e^{-\frac{1}{2}\beta^2r^2} .$$

The integrals are all obtainable by parametric differentiation from the ones already evaluated, but are rather lengthy to write down.

(c) A fairly simple device is to take b greater than one in (3.3). The unphysical region of negative f in the center of the nucleus must contribute negligibly to the value of the integral.

## 3. THE DEUTERON WAVE FUNCTION

The single Gaussian form for the internal deuteron wave function preceding eq. (4.5), can be improved by using two or more Gaussians. The following figure compares the Hulthén function with a two-term approximation chosen by eye. Using the notation $\psi(r) = (4\pi)^{-\frac{1}{2}} u(r)/r$, the Hulthén function is

$$u_H(r) = [2ab(b+a)/(b-a)^2]^{\frac{1}{2}} (e^{-ar} - e^{-br}), \qquad (F.7)$$

while the "double Gaussian" is

$$u(r) = .33rR_{10}(.83,r) + .78rR_{10}(.32,r). \qquad (F.8)$$

In eq. (F.7), a = .2317, b ≈ 7a, while $R_{10}$ in (F.8) is the oscillator function of Appendix D.

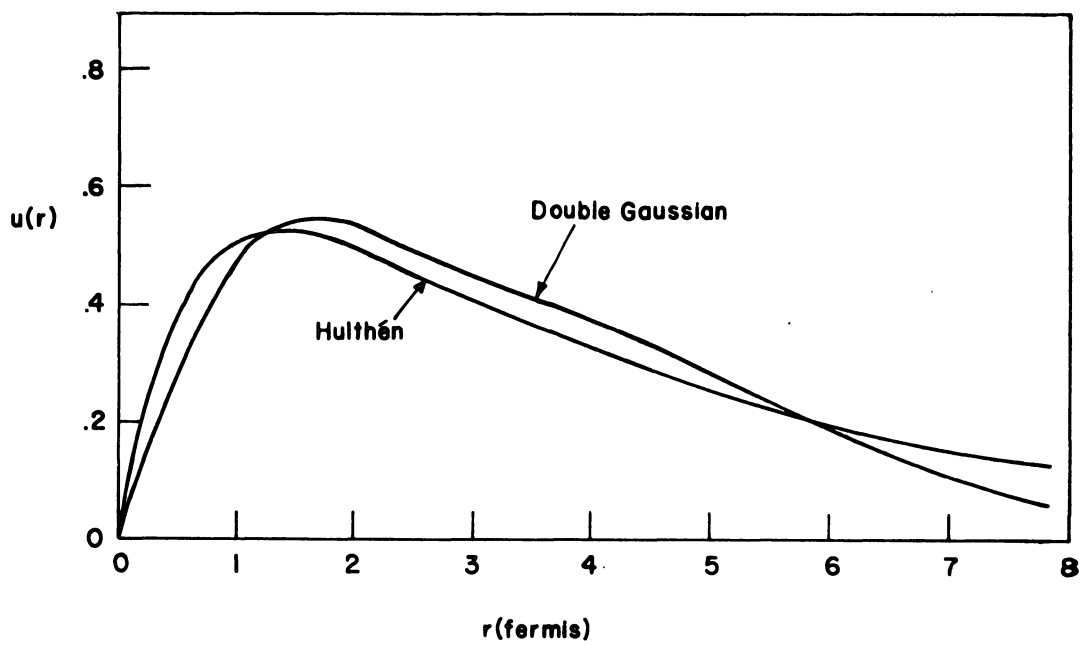


Fig. F-2. A two-term Gaussian approximation to the Hulthén wave function.

## APPENDIX G

## EVALUATION OF THE STRIPPING AMPLITUDES AND THE SQUARE WELL BOUND STATE PROBLEM

### 1. THE BASIC STRIPPING AMPLITUDES

The result of integrating over the region $r_n > a$ in eq. (3.21), as in the original Butler theory, is apart from constants, the "outside" amplitude,

$$O_\ell(x,y) = [G_\ell(y)\, j_\ell(x) + x j_{\ell-1}(x)]/(x^2+y^2) , \qquad (G.1)$$

where

$$G_\ell(y) \equiv -iy\, h^{(1)}_{\ell-1}(iy)/h^{(1)}_\ell(iy) \equiv y\, h_{\ell-1}(y)/h_\ell(y). \qquad (G.2)$$

The quantities x and y define a square well bound state eigenvalue problem. If y is held constant, then the numerator of (G.1) is an oscillatory function of x, similar to a slowly damped sine curve. (The $\ell$=0 curve is an exception, and goes to a positive value at x=0.) Denoting a node position by $x_o$ and y, it is seen that

$$x_o j_{\ell-1}(x_o)/j_\ell(x_o) = -y\, h_{\ell-1}(y)/h_\ell(y), \qquad (G.3)$$

which is just the condition satisfied by the inside and outside wave numbers of a square well bound state of orbital angular momentum $\ell$. The notation is defined in Fig. G-1. The first node (not counting x=0) defines the lowest $\ell$-state, to which the radial quantum number n=1 may be attached. For a given node, n, and given $\ell$-value, the node position

$x = x_o$ is a function of y and can be plotted as a single curve. This is done in Fig. G-2, the square $x_o^2$ being more convenient.

The simplest way to compute the outside amplitude (G.1) is not from its definition but from the stripping tables (14).

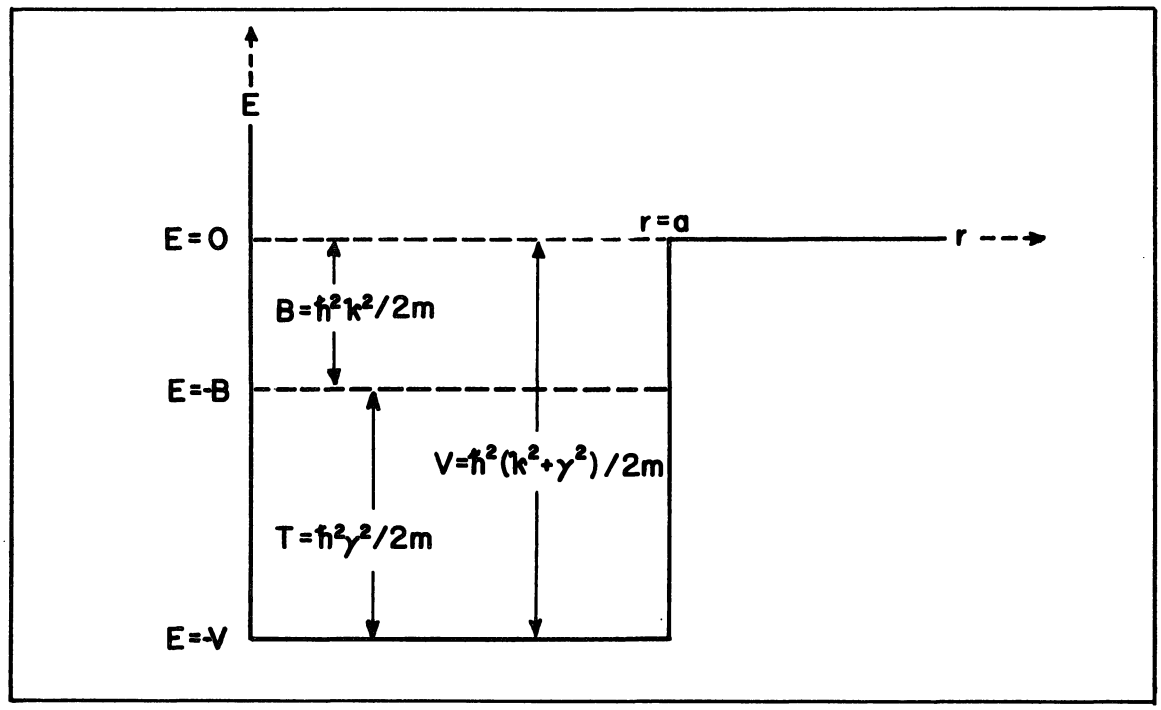


Fig. G-1. Notation for the square well bound state problem. The kinetic, binding, and potential energies are T, B, and -V, respectively. The wave numbers $\gamma$ and $\kappa$ are positive as are $x_o=\gamma a$ and $y=\kappa a$. The reduced mass is m.

$$O_\ell(x,y) = \pm [1+0.008(x^2+y^2)] \sqrt{\sigma^\ell_{TAB}(x,y)} \qquad (G.4)$$

The correct sign in (G.4) can be easily determined, since (G.1) starts out with a positive loop at small x-values and therefore the positive

root in (G.4) is required in this region of x. A sign change in (G.1) occurs as every node, and since these are reflected as minima in $\sigma^{\ell}_{TAB}$, it is only necessary to scan this function briefly to determine when the negative sign should begin to occur in (G.4).

The region $r_n < a$ in (3.21) leads to the "inside" amplitude,

$$I_\ell(x,y) = (x^2+y^2)\ O_\ell(x,y)/(x_o^2-x^2), \qquad (G.5)$$

while the complete integration $r_n \geqslant 0$ gives the Born amplitude,

$$B_\ell(x,y) = (x_o^2+y^2)\ O_\ell(x,y)/(x_o^2-x^2) \qquad (G.6)$$

$$= I_\ell(x,y) + O_\ell(x,y). \qquad (G.7)$$

The quantity $x_o$ is required in order to compute these functions, and since y is known, it is easily found. The spectroscopic designation $(n,\ell)$ is determined by the shell model description of the state in question, the procedure for finding $x_o$ being given in Section 2-(a) of this appendix.

In determining the effective wave number $\gamma_{np}$ (and its variants) in (3.26), the method of approximation (Appendix C) is such that n is the same for $j_\ell(\gamma r_n)$ and $j_\ell(\gamma_{np} r_n)$. Therefore the wave number $\kappa_{np}$ in (3.30) can be found from n, $\ell$, $\gamma_{np}$, and a, as described in Section 2-(b).

The singular point in $I_\ell$ and $B_\ell$ at $x=x_o$ is only apparent, since the numerator vanishes there to the same order and the ratio is finite.

2. SOLVING THE SQUARE WELL EIGENVALUE PROBLEM

If it is assumed that the spectroscopic designation of the state $(n,\ell)$ is known, then there are several forms which the eigenvalue problem can take, depending on which parameters are given. The forms of interest in the present context are the following:

(a). Given the radius a and the binding energy B, find the inside wave number $\gamma$.

Method: Compute $y=\kappa a = (2mBa^2/\hbar^2)^{\frac{1}{2}}$ and enter Fig. G-2 at the bottom. Read up to the $(n,\ell)$ curve and find $x_o^2$ at the left, remembering to correct the ordinate scale as described in the caption. Then the inside wave number is $\gamma=x_o/a$ while the well depth is $V=\hbar^2(x_o^2+y^2)/2ma^2$.

(b). Given the radius a and the inside wave number $\gamma$, find the outside wave number.

Method: Compute $x_o^2 = \gamma^2a^2$ and enter Fig. G-2 at the left, reading out y at the bottom. Then $\kappa = y/a$.

There are other variations of the eigenvalue problem which can be solved in a similar manner. For example, given the radius a and the depth V, find the binding energy B. Or, given the depth V and the binding energy B, find the radius a. For these problems it is more convenient to plot two other quantities as functions of y, namely $(x_o^2+y^2)$ and $y/x_o$. Then the former problem is solved by entering the curve of $(x_o^2+y^2)$ versus y with $x_o^2+y^2 = 2mVa^2/\hbar^2$ and reading out $y = \kappa a$. The

latter is solved by entering the $y/x_o$ curve with $y/x_o = [B/(V-B)]^{\frac{1}{2}}$ and reading out y. The trick here is that $y/x_o = \kappa/\gamma$ is independent of the radius a and can be computed without its knowledge. The same device allows a straight forward determination of the correct radius to use in the Butler formula (Ref. (14), p. 125), eliminating in most cases the need for trial and error.

The functions $x_o^2+y^2$ and $y/x_o$ for the first four s,p, d, f, g, and h states are available from the author on request.

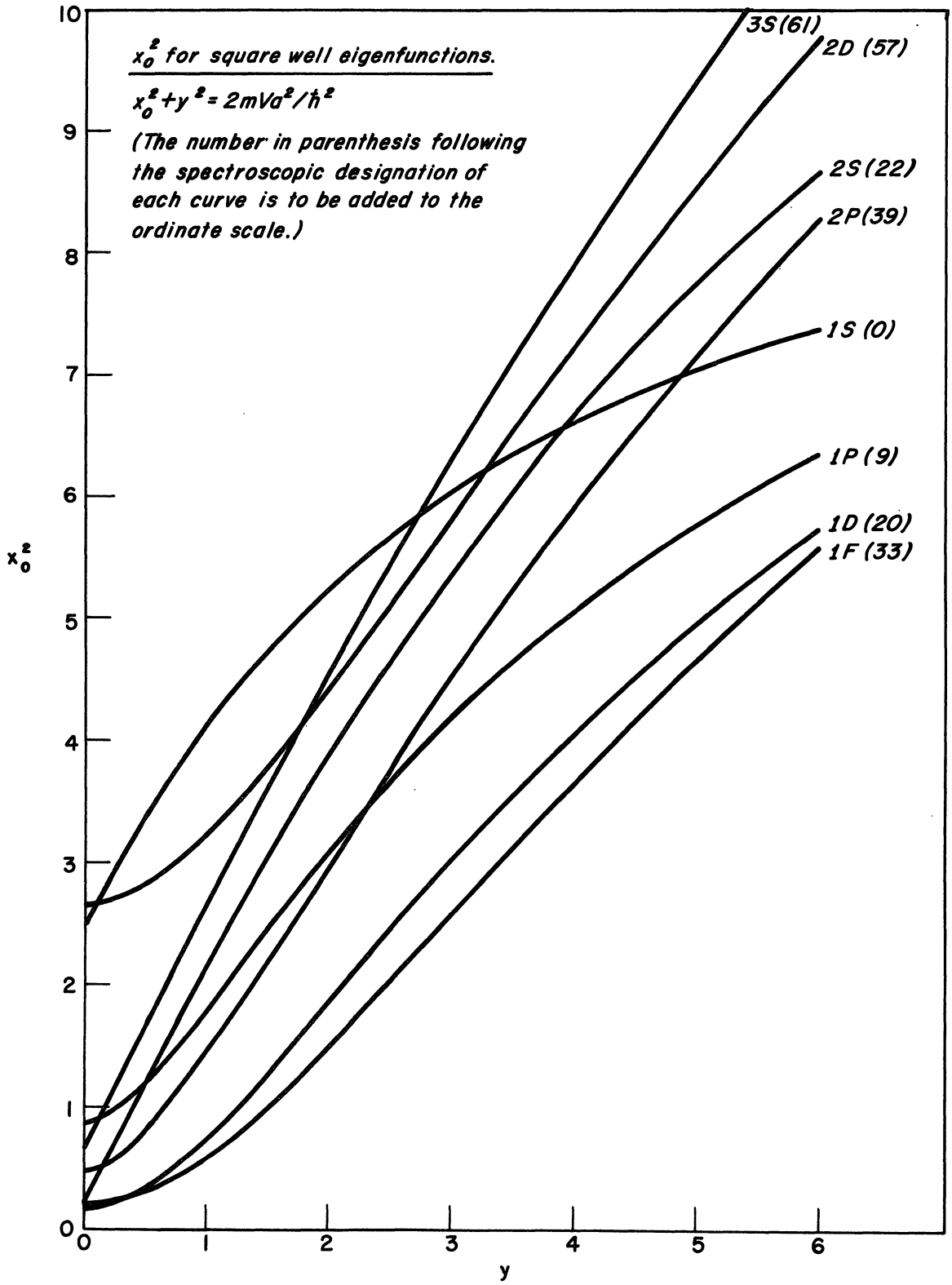


Fig. G-2. Plot of the quantity $x_0^2 = 2mVa^2/\hbar^2 - \kappa^2a^2$ as a function of $y = \kappa a$ for various square well bound states.

REFERENCES


1. S. T. Butler, Proc. Roy. Soc. (London) 208, 559 (1951).

2. A. B. Bhatia, K. Huang, R. Huby, and H. C. Newns, Phil. Mag. 43, 485 (1952).

3. W. Tobocman, Phys. Rev. 115, 98 (1959) and references therein.

4. N. C. Francis and K. M. Watson, Phys. Rev. 93, 313 (1954).

5. P. B. Daitch and J. B. French, Phys. Rev. 87, 900 (1952).

6. R. G. Thomas, Phys. Rev. 100, 25 (1955).

7. A. P. French, Phys. Rev. 107, 1655 (1957).
V. G. Neudachin, Soviet Phys.-JETP 8, 815 (1959).

8. L. Madansky and G. E. Owen, Phys. Rev. 99, 1608 (1955).

9. R. G. Thomas, Phys. Rev. 91, 453 (A)(1953).
Y. Fujimoto, K. Kikuchi, and S. Yoshida, Progr. Theoret. Phys. (Kyoto) 11, 264 (1954).

10. M. H. MacFarlane and J. B. French, Stripping Reactions and the Structure of Light and Intermediate Nuclei, NYO-2846. Oct. 19, 1959. University of Rochester, Rochester, New York. (Unpublished).

11. S. Hayakawa, Proc. Intnl. Conf. of Theoretical Physics. 1953, p. 320. Insatsusha Co., Tokyo.
C. R. Lubitz, (unpublished calculations).

12. J. C. Hensel and W. C. Parkinson, Phys. Rev. 110, 128 (1958) and references therein.

13. H. C. Newns, Proc. Phys. Soc. A66, 477 (1953).
L. F. Chase, Jr., and G. Igo, Phys. Rev. 116, 170 (1959).

14. C. R. Lubitz, Numerical Table of Butler-Born Approximation Stripping Cross Sections, H. M. Randall Laboratory of Physics, Univ. of Mich., Ann Arbor (1957). Available from the department secretary upon request.

15. I. Talmi, Helv. Phys. Acta 25, 185(1952).

16. J. E. Bowcock, Phys. Rev. 112, 923 (1958).

17. E. Gerjuoy, Phys. Rev. 91, 645 (1953).
N. Austern, Phys. Rev. 89, 318 (1953).

18. L. I. Schiff, Quantum Mechanics, (McGraw-Hill Book Co., Inc., New York, 1949) First Edition.

19. L. I. Schiff, Phys. Rev. 103, 443 (1956) and references contained therein.

20. D. C. Peaslee, Ann. Rev. Nuc. Sci. V, 131 (1955).

21. J. S. Blair, Phys. Rev. 108, 827 (1957).

22. A. Elwyn, J. V. Kane, S. Ofer, and D. H. Wilkinson, Phys. Rev. (to be published).

23. S. T. Butler and O. H. Hittmair, Nuclear Stripping Reactions, (John Wiley and Sons, Inc., N. Y., 1957.)

24. R. H. Dalitz, Proc. Phys. Soc. 66A, 28 (1952).

25. W. Tobocman, Review of the Surface Interaction Theory, etc., Tech. Report No. 29, Case Institute of Technology, 1956.

26. J. Horowitz and A. M. L. Messiah, J. Phys. Radium 14, 731 (1953).

27. M. H. MacFarlane and J. B. French, Stripping Reactions and the Structure of Light and Intermediate Nuclei, NYO-2846. Oct. 19, 1959. University of Rochester, Rochester, New York, (Unpublished).

28. J. Horowitz and A. M. L. Messiah, J. Phys. Radium 14, 695 (1953), Phys. Rev. 92, 1326 (1953).

29. N. Austern, "Finite Range Correction in Distorted Waves Calculation," (Unpublished).

30. R. S. Christian and J. L. Gammel, Phys. Rev. 91, 100 (1953).

31. T. Teichmann and E. P. Wigner, Phys. Rev. 87, 123 (1952).

32. F. Ajzenberg and T. Lauritsen, Rev. Mod. Phys. 27, 77 (1955).

33. J. C. Hensel and W. C. Parkinson, Phys. Rev. 110, 128 (1958).
J. A. Green and W. C. Parkinson, Bull. Am. Phys. Soc. Ser. II. 5, 345 (1960).

34. N. F. Mott and H. S. W. Massey, The Theory of Atomic Collisions, (Oxford University Press, London, 1949), 2nd ed., Chap. 6.

35. W. Magnus and F. Oberhettinger, Special Functions of Mathematical Physics (Chelsea Pub. Co., New York. 1949), p. 96.

36. H. C. Newns and M. Y. Refai, Proc. Phys. Soc. A71, 627 (1958).

37. C. R. Lubitz, Bull. Am. Phys. Soc. Ser. II, 5, 18 (1960).

38. R. G. Summers-Gill, Phys. Rev. 109, 1591 (1958).

39. J. B. Reynolds and K. G. Standing, Phys. Rev. 101, 158 (1956).

40. J. Benveniste, R. G. Finke, and E. A. Martinelli, Phys. Rev. 101, 655 (1956).

41. A. M. Lane, Proc. Phys. Soc. 66A, 977 (1953).

42. J. B. French, E. C. Halbert, and S. P. Pandya, Phys. Rev. 99, 1387 (1955).
D. Kurath, Phys. Rev. 101, 216 (1956).

43. E. Feenberg and M. Phillips, Phys. Rev. 51, 597 (1937).

44. H. A. Jahn and H. van Wieringen, Proc. Roy. Soc. (London) 209A, 502 (1951).

45. C. Schwartz and A. de-Shalit, Phys. Rev. 94, 1257 (1954).

46. C. R. Lubitz, Bull. Am. Phys. Soc. Ser II, 5, 346 (1960).

47. F. A. El Bedewi, Proc. Phys. Soc. (London) 65A, 64 (1952).
J. R. Holt and T. N. Marsham, ibid. 66A, 1032 (1953).
T. S. Green and R. Middleton, ibid. 69A, 28 (1956).
B. Zeidman and J. M. Fowler, Phys. Rev. 112, 2020 (1958).

48. H. W. Fulbright, J. A. Bruner, D. A. Bromley, and L. M. Goldman, NYO-3219. University of Rochester, 1952.

49. J. B. French and A. Fujii, Phys. Rev. 105, 652 (1957).

50. S. Glashow and W. Selove, Phys. Rev. 102, 200 (1956).

51. J. Benveniste, R. G. Finke, and E. A. Martinelli, Phys. Rev. 101, 655 (1956).

52. B. Hird, J. A. Cookson, and M. S. Bokhari, Proc. Phys. Soc. (London) 72, 489 (1958).
J. A. Green and W. C. Parkinson, Bull. Am. Phys. Soc. Ser. II, 5, 345 (1960).

53. R. G. Allas and F. B. Shull, Phys. Rev. 116, 996 (1959). This reference summarizes all previous measurements on carbon.

54. W. Tobocman and M. H. Kalos, Phys. Rev. 97, 132 (1955).

55. I. Slaus and W. P. Alford, Report NYO-2173, University of Rochester, Rochester, New York.

56. M. A. Melkanoff, Session IV-A in "Proceedings of the International Conference on the Nuclear Optical Model," Florida State University, Tallahassee, Florida, 1959.

57. S. T. Butler and N. Austern, Phys. Rev. 93, 355 (1954).

58. M. P. Nakada, J. D. Anderson, C. C. Gardner, and C. Wong, Phys. Rev. 110, 1439 (1958).

59. F. Bjorklund and S. Fernbach, University of California Radiation Laboratory Report UCRL-4926T, 1957 (Unpublished).

60. M. H. MacGregor, W. P. Ball, and R. Booth, Phys. Rev. 108, 726 (1957).

61. R. J. Howerton, Tabulated Neutron Cross Sections, Univ. of Calif. Rad. Lab., UCRL-5226.

62. R. W. Hill, Phys. Rev. 109, 2105 (1958).

63. S. Fernbach, Rev. Mod. Phys. 30, 414 (1958).

64. H. Feshbach, C. E. Porter, and V. F. Weisskopf, Phys. Rev. 96, 448 (1954).

65. F. Bjorklund and S. Fernbach, Phys. Rev. 109, 1295 (1958).

66. R. Hofstadter, Rev. Mod. Phys. 28, 214 (1956).

67. E. R. Cohen, J. W. M. Dumond, T. W. Layton, and J. S. Rollett, Rev. Mod. Phys. 27, 363 (1955).

68. W. L. Miller and A. R. Gordon, J. Phys. Chem. 35, 2878 (1931).

69. Tables of Spherical Bessel Functions, Volume 1, Columbia University Press, 1947.

70. R. W. Woods and D. S. Saxon, Phys. Rev. 95, 577 (1954).